IRAQI JOURNAL OF APPLIED PHYSICS

The *Iraqi Journal of Applied Physics (IJAP)* is a peer reviewed journal of high quality devoted to the publication of original research papers from applied physics and their broad range of applications. IJAP publishes quality original research papers, comprehensive review articles, survey articles, book reviews, dissertation abstracts in physics and its applications in the broadest sense. It is intended that the journal may act as an interdisciplinary forum for Physics and its applications. Innovative applications and material that brings together diverse areas of Physics are particularly welcome. Review articles in selected areas are published from time to time. It aims to disseminate knowledge; provide a learned reference in the field; and establish channels of communication between academic and research experts, policy makers and executives in industry, commerce and investment institutions. IJAP is a quarterly specialized periodical dedicated to publishing original papers, letters and reviews in: Applied & Nonlinear Optics, Applied Mechanics & Thermodynamics, Digital & Optical Communications, Electronic Materials & Devices, Laser Physics & Applications, Plasma Physics & Applications, Quantum Physics & Spectroscopy, Semiconductors & Optoelectronics, Solid State Physics & Applications, Alternative and Renewable Energy, and Computers and Networks.

ISSN (Print): 1813-2065, ISSN (Online): 2309-1673, ISSN (Letters): 1999-656X

EDITORIAL BOARD

Raad A. KHAMIS	Asst. Professor	Editor-in-Chief	Plasma Physics	IRAQ
Walid K. HAMOUDI	Professor	Member	Laser Physics	IRAQ
Dayah N. RAOUF	Asst. Professor	Member	Laser and Optics	IRAQ
Raid A. ISMAIL	Professor	Member	Semiconductor Physics	IRAQ
Oday A. HAMMADI	Asst. Professor	Managing Editor	Molecular Physics	IRAQ
Intesar F. RAMLEY	Professor	Member	Communications Eng.	CANADA
Khaled A. AHMED	Professor	Member	Theoretical Physics	IRAQ
Manal J. AL-KINDY	Asst. Professor	Member	Electrical Engineering	IRAQ
Kais A. AL-NAIMEE	Asst. Professor	Member	Quantum Optics	ITALY
Abdulhadi ALKHALILI	Professor	Member	Medical Physics	U.S.A
Abdulmajeed IBRAHIM	Professor	Member	Solid State Physics	IRAQ
Loay E. GEORGE	Asst. Professor	Member	Computers & Networks	IRAQ
Haitham M. MIKHLIF	Lecturer	Member	Molecular Physics	UK

Editorial Office:
P. O. Box 55259, Baghdad 12001, IRAQ
Website: www.iraqiphysicsjournal.com
Emails: info@iraqiphysicsjournal.com, editor_ijap@yahoo.co.uk, editor@ijaponline.com

ADVISORY BOARD

Abdullah M. SUHAIL, Professor, Department of Physics, College of Science, University of Baghdad, IRAQ
Adel K. HAMOUDI, Professor, Department of Physics, College of Science, University of Baghdad, IRAQ
Andrei KASIMOV, Professor, Institute of Material Science, National Academy of Science of Ukraine, Kiev, UKRAINE
Ashok KUMAR, Professor, Harcourt Butler Technological Institute, Nawabganj, Kanpur, Uttar Pradesh 208 002, INDIA
Chang Hee NAM, Professor, Korean Advanced Institute of Science and Technology, 291 Daehak-ro, Daejeon, KOREA
El-Sayed M. FARAG, Professor, Department of Sciences, College of Engineering, Al-Minofiya University, EGYPT
Franko KUEPPERS, Professor, Darmstadt University of Technology, Mornewegstraße 32, Darmstadt, GERMANY
Gang XU, Assistant Professor, Department of Engineering and Physics, University of Central Oklahoma, U.S.A
Heidi ABRAHAMSE, Professor, Faculty of Health Sciences, University of Johannesburg, SOUTH AFRICA
Mansoor SHEIK-BAHAE, Associate Professor, Department of Physics & Astronomy, University of New Mexico, U.S.A
Mazin M. ELIAS, Professor, Laser Institute for Postgraduates, University of Baghdad, Al-Jadiriyah, Baghdad, IRAQ
Mohammad Robi HOSSAN, Assistant Professor, Dept. of Engineering and Physics, Univ. of Central Oklahoma, U.S.A
Mohammed A. HABEEB, Professor, Department of Physics, Faculty of Science, Al-Nahrain University, Baghdad, IRAQ
Morshed KHANDAKER, Associate Professor, Dept. of Engineering and Physics, Univ. of Central Oklahoma, U.S.A
Muhammad A. HUSSAIN, Assistant Professor, Dept. of Laser and Optoelectronics Eng., Al-Nahrain University, IRAQ
Mutaz S. ABDUL-WAHAB, Assistant Professor, Dept. of Electric and Electronic Eng., University of Technology, IRAQ
Nadir F. HABOUBI, Professor, Department of Physics, College of Education, Al-Mustansiriya Univ., Baghdad, IRAQ
Shivaji H. PAWAR, Professor, D.Y. Patil University, Kasaba Bawada, Kolhapur-416 006, INDIA
Xueming LIU, Professor, Department of Electronic Engineering, Tsinghua University, Shuang Qing Lu, Beijing, CHINA
Yanko SAROV, Assistant Professor, Micro- and Nanoelectronic Systems, Technical University Ilmenau, GERMANY
Yushihiro TAGUCHI, Professor, Department of Physics, Chuo University, Higashinakano Hachioji-shi, Tokyo, JAPAN

SPONSORED AND PUBLISHED BY
THE IRAQI SOCIETY FOR ALTERNATIVE AND RENEWABLE ENERGY SOURCES & TECHNIQUES (I.S.A.R.E.S.T.)

IRAQI JOURNAL OF APPLIED PHYSICS

ISSN (Print): 1813-2065, ISSN (Online): 2309-1673, ISSN (Letters): 1999-656X

" INSTRUCTIONS TO AUTHORS "

CONTRIBUTIONS

Contributions to be published in this journal should be original research works, i.e., those not already published or submitted for publication elsewhere, individual papers or letters to editor.
Manuscripts should be submitted to the editor at the mailing address:
Iraqi Journal of Applied Physics, Editorial Board, P. O. Box 55259, Baghdad 12001, IRAQ
Website: www.iraqiphysicsjournal.com
Email: editor@iraqiphysicsjournal.com, editor_ijap@yahoo.co.uk

MANUSCRIPTS

Two hard copies with soft copy on a compact disc (CD) should be submitted to Editor in the following configuration:

- **One-column** Double-spaced one-side A4 size with 2.5 cm margins of all sides
- Times New Roman font (16pt bold for title, 14pt bold for names, 12pt bold for headings, 12pt regular for text)
- Letters should not exceed 10 pages, papers should not exceed 20 pages and reviews are up to author.
- Manuscripts presented in English only are accepted.
- English abstract not exceed 150 words
- 4 keywords (at least) should be maintained on (PACS preferred)
- Author(s) should express all quantities in SI units
- Equations should be written in equation form (*italic* and symbolic)
- Figures and Tables should be separated from text
- Figures and diagrams can be submitted in colors for assessment and they will be returned to authors after provide printable copies
- Charts should be indicated by the software used for
- Only original or high-resolution scanner photos are accepted
- For electronic submission, articles should be formatted with MS-Word software.

AUTHOR NAMES AND AFFILIATIONS

It is IJAP policy that all those who have participated significantly in the technical aspects of a paper be recognized as co-authors or cited in the acknowledgments. In the case of a paper with more than one author, correspondence concerning the paper will be sent to the first author unless staff is advised otherwise.
Author name should consist of first name, middle initial, last name. The author affiliation should consist of the following, as applicable, in the order noted:
- Company or college (with department name or company division), Postal address, City, state, zip code, Country name, contacting telephone, and e-mail

REFERENCES

The references should be brought at the end of the article, and numbered in the order of their appearance in the paper. The reference list should be cited in accordance with the following examples:
[1] X. Ning and M.R. Lovell, "On the Sliding Friction Characteristics of Unidirectional Continuous FRP Composites", *ASME J. Tribol.*, 124(1) (2002) 5-13.
[2] M. Barnes, "Stresses in Solenoids", *J. Appl. Phys.*, 48(5) (2001) 2000–2008.
[3] J. Jones, "Contact Mechanics", Cambridge University Press (Cambridge, UK) (2000), Ch.6, p.56.
[4] Y. Lee, S.A. Korpela and R. Horne, "Structure of Multi-Cellular Natural Convection in a Tall Vertical Annulus", Proc. 7th International Heat Transfer Conference, U. Grigul et al., eds., Hemisphere (Washington DC), 2 (1982) 221–226.
[5] M. Hashish, "Waterjet Technology Development", High Pressure Technology, PVP-Vol. 406 (2000), 135-140.
[6] D.W. Watson, "Thermodynamic Analysis", ASME Paper No. 97-GT-288 (1997).
[7] C.Y. Tung, "Evaporative Heat Transfer in the Contact Line of a Mixture", Ph.D. thesis, Rensselaer Polytechnic Institute, Troy, NY (1982).

PROOFS

Authors will receive proofs of papers and are requested to return one corrected hard copy with a WORD copy on a compact disc (CD). New materials inserted in the original text without Editor permission may cause rejection of paper.

COPYRIGHT FORM

Author(s) will be asked to transfer copyrights of the article to the Journal soon after acceptance of it. This will ensure the widest possible dissemination of information.

OFFPRINTS

Authors will receive offprints free of charge and any additional reprints can be ordered.

SUBSCRIPTION AND ORDERS

Annual fees (4 issues per year) of subscription are:
50 US$ for individuals inside Iraq; **200** US$ for establishments inside Iraq;
100 US$ for individuals abroad; **300** US$ for establishments abroad.
Fees are reduced by 25% for I.S.A.R.E.S.T. members. Orders of issues can be submitted by contacting the editor-in-chief or editorial office at admin@iraqiphysicsjournal.com, or editor_ijap@yahoo.co.uk to maintain the address of issue delivery and payment way.

IRAQI JOURNAL OF APPLIED PHYSICS
Vol. 16, No. 2, April-June 2020, pp. 3-10

J. D. Mansell
T. Rutherford
W. Tulloch
M. Olapinski
M. Fejer
R. L. Byer

Gaussian to Super-Gaussian Laser Beam Intensity Profile Conversion using Glass Micro-Optic Fabricated with Reflowed Photoresist

In this study, we demonstrate a pair of optics for conversion of a Gaussian beam to a super-Gaussian and a super-Gaussian back to a Gaussian Furthermore, we show that beam quality is maintained by super-Gaussian thermal lensing.

Keywords: Profile conversion; Gaussian beam; Micro-optic glass; Profilometry

1. Introduction

Some optical systems require both high laser power and high beam quality. The wavefront distortion induced by illuminating an absorbing transmissive optical material with a Gaussian beam is not parabolic in shape, which causes the laser beam quality to degrade [1]. The thermal lens induced by a high order super-Gaussian or top-hat intensity profile laser beam, however, is parabolic and does not degrade laser beam quality. To avoid laser beam quality degradation when passing through transmissive optics, we create a pair of optics which convert a Gaussian intensity profile into a super-Gaussian profile for transmission through the absorbing optics, and then convert the super-Gaussian profile back into a Gaussian for subsequent use.

We performed ray-optics modeling to determine the spatial phase profile necessary to convert a Gaussian intensity profile into a super-Gaussian intensity profile. We found that we could create a profile very similar to the desired converter profile by reflowing circular pillars of AZ4620 photoresist in an acetone vapor environment. We made a set of converters by reflowing photoresist pillars 1mm in diameter and then etched them into fused silica using a CF4/O2 plasma to form an optic 1.4 microns tall. Figure 1 shows the converter profile measured by a profilometer and the fit to a 4th order polynomial.

By reimaging the plane of the converter optic onto a reflective version of the optic with the same shape, but different amplitude, we found that the phase aberration imposed by the converter could be compensated. To that end, we fabricated another set of optics by adjusting the plasma etch selectivity such that the optic was only 400nm tall. The phase compensators were coated with gold for reflectivity.

Figure 2 shows the optical setup used to test the optics. The 1064nm Nd:YAG laser beam was spatially filtered by a Fabry-Perot ring resonator. The beam after the ring mode cleaner was measured with a beam profiler to have an M2 of 1.02 in X and 1.05 in Y. After going through the converter, the M2 became 2.33 in X and 2.28 in Y. After reflecting from the converter the M2 of the beam was reduced to 1.10 in X and 1.08 in Y. All the laser beam quality was not fully restored due to a slight mismatch in the phase height of the reflective compensator optic and the transmissive converter optic.

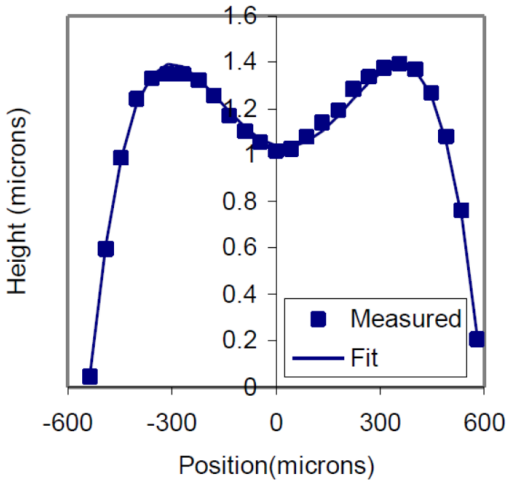

Fig. (1) Surface profile of the converter optic used in the experiments

Figure 3 shows the intensity profile of the super-Gaussian beam measured with a BeamScan and a fit to a super-Gaussian. The fit extracted a beam waist of 480 microns and a super-Gaussian order of 8.75. The laser beam profile fit to a super-Gaussian order above 5 for about 125mm.

The thermal lens shape was measured in a piece of IR absorbing glass heated with 1064nm light and probed by 633nm light on a Shack-Hartmann wavefront sensor with an RMS wavefront accuracy of 1nm. The thermal lens shape was fit to a parabola between the center and the radial point containing 99.9% of the power. The Gaussian intensity profile thermal lens had 49nm of RMS error to the parabolic fit while the super-Gaussian had 0.8nm of error.

 © ALL RIGHTS RESERVED

A higher temperature is desirable for the STI application, since a more dense film that is highly resistant to subsequent wet-etching steps is thus obtained. These applications are discussed in more detail later in the paper.

When tetraethylorthosilicate (TEOS) is used as the silicon source for PECVD oxide deposition, there is less cusping because of the higher surface mobility of the reactants [22]; however, a void still forms if the gap is small enough, because the conformality of the film is not 100%. This means that the amount of deposition on the sidewalls and bottom of the trench portion of a feature is less than on the top of the feature. So, in order to use PECVD films alone for gap-fill applications, they are typically used in conjunction with an argon sputter etch in a multistep PECVD-argon sputter etch-PECVD sequence described previously [23]. Conformal deposition is more typical for thermal (non-plasma) CVD processes such as low-pressure (LP) CVD at high temperatures or for ozone-TEOS atmospheric or subatmospheric pressure (AP or SA) CVD at lower temperatures (less than 600°C). Furthermore, HDP CVD results in a completely different type of profile because of the "bottom-up" deposition from the simultaneous deposition and etching. The resultant topography from any of these CVD processes plays a decisive role in the choice of subsequent planarization techniques. TEOS was the silicon source for the PECVD and the SACVD, and silane for HDP CVD. The typical "bread-loaf" profile of the PECVD oxide film can be adjusted by varying process parameters such as temperature, pressure, and silicon source. The profile of the SACVD oxide film is conformal, and the unique profile of the HDP CVD oxide film is a result of simultaneous etching and deposition. Note that SACVD is a non-plasma process.

Typically, thermal CVD processes such as LPCVD BPSG, APCVD (or SACVD) BPSG, or PSG are used to passivate the polysilicon/metal silicide gate conductor for sub-half-micron devices because of their high-aspect-ratio fill capability compared to plasma CVD processes and because there are no plasma damage concerns with thermal CVD processing. Process-induced IC device damage from plasma processing (in particular at the gate-conductor level, because there is no device protection) is a critical issue for the PECVD passivation dielectrics. Briefly, low process pressure during deposition of the PECVD PSG was identified as the main factor causing gate-oxide charge damage. Increasing the pressure for the PECVD PSG process regardless of dopant source (trimethylphosphite or triethylphosphate) resulted in no charge damage on antenna test sites and device structures. A more recent study describes another technique used to optimize a PECVD PSG process for plasma damage designated as corona oxide semiconductor (COS) charge measurement [24]. The technique, combined with the antenna test structure method of measuring plasma damage, provides a fast and cost-effective way to optimize plasma CVD processes.

Doped silicon oxide films such as PSG or BPSG are preferred for gate-conductor passivation because of their mobile ion barrier properties [25], low reflow temperature for local planarization (applies to BPSG only), high etch selectivity to the underlying barrier layer (e.g., nitride [26]), and faster polishing rate compared to undoped silicon oxide. In this paper, we discuss our recent work with HDP CVD PSG including gap-fill and plasma damage results. We have previously published an overview of our own work and that of others in IBM on relevant thermal CVD processes and applications [27].

The gap-fill requirement for dielectrics in the "back-end-of-line" (BEOL) depends on the interconnect fabrication methods used. Multilevel interconnects usually involve two types of planarization methods: the planarization of interlayer dielectrics and the planarization of metal layers. For the former, for example, an Al(Cu)-based layer is patterned into lines and the insulator is deposited between the spaces and above the lines. Therefore, a critical requirement in this case is the filling of the gaps between the lines without void formation. Void-free filling of high-aspect-ratio features is not a simple matter and requires the use of advanced insulator deposition processes such as HDP CVD. For submicron metal interconnect fabrication, the insulator deposition is generally followed by partial planarization using spin-on-glass (SOG) [28], a resist etch-back [29], or a global planarization using, for example, chemical-mechanical polishing (CMP). For the planarization of metal layers, the damascene technique is most commonly used; several papers reporting its use in IBM have been published [30]. Using this technique, a dielectric such as silicon oxide is deposited on a planar surface and the wiring level is patterned into the dielectric using photolithography and RIE. A thin metal liner and a metal such as tungsten (or aluminum or copper) are then deposited on the patterned dielectric and subsequently planarized by CMP, stopping on the dielectric and leaving metal in the patterned features. Therefore, in the damascene technique, the metal rather than the insulator must fill the high-aspect-ratio features.

A critical film parameter for both interconnect fabrication techniques is the

 ALL RIGHTS RESERVED PRINTED IN IRAQ

dielectric constant (k) of the IMD material. Use of a material having a lower dielectric constant leads to lower total capacitance, decreasing the interconnection delay and power dissipation [31], and thus enhancing performance. To achieve long-range interconnection performance objectives, low-dielectric-constant IMD will be required [32]. The dielectric constant of PECVD silicon oxide is typically 4.1-4.2. By doping the oxide with fluorine, the dielectric constant can be reduced to 3.0-3.7, depending on the fluorine concentration [33]. Si-F replaces the Si-OH and Si-H bonds in the oxide; since fluorine is more electronegative, the polarization changes, lowering the dielectric constant. SOG dielectrics (siloxanes, silsesquioxanes) and organic polymers formed by spin coating (polyimides, fluorinated polyimides, bisbenzocyclobutenes), poly(arylethers), or vapor-phase deposition (parylene N, parylene F, teflon) provide dielectric constants in the range of 1.9-3.0 [34]. Most polymers with a dielectric constant less than 3 are stable to only about 350°C. However, a recent publication on laser-evaporated siloxane thin films reports a dielectric constant of 2.0 and thermal stability to 400°C, although integration results were not published [35]. Also, it has been reported that parylene exhibits a high thermal stability [36], and its successful integration into a metal RIE BEOL has been demonstrated [37]. However, damascene integration may be more difficult to achieve because of the softness of parylene films. Spun-on films of materials such as nanoporous silica and xerogels exhibit a higher thermal stability and low dielectric constants (1.3-2.5), depending on their porosity [38], but associated process integration is challenging. There has been increased development activity in plasma-assisted CVD of amorphous carbon and fluorinated carbon films because of their low dielectric constants (2.3-2.7) and thermal stability up to 400°C [39]. Relevant work on insulators having low dielectric constants has been described elsewhere [40].

In this paper, the plasma-assisted CVD of low-dielectric-constant insulators of potential interest at the ULSI level, including fluorine-doped silicon oxide and amorphous carbon and fluorocarbon, was discussed. To be suitable for the deposition of such insulators, plasma-assisted CVD should be applicable at relatively low substrate temperatures, should not damage underlying layers or devices that may be present on the substrate during deposition, and should produce insulators which, in addition to having low dielectric constants, satisfy etching, annealing, planarization, and stability requirements.

2. Fundamentals of PECVD

In thermal CVD, gas-phase reactive species are generated by heating of initial reactants. In plasma CVD, the plasma energy supplied by an external rf source takes the place of the heating to generate the species that subsequently react and deposit on substrate surfaces. Significantly, excessive heating and degradation on the substrate can be avoided by using plasma electron kinetic energy instead of thermal energy. Besides the aspect of generating reactive species at much lower processing temperatures compared to conventional CVD processing, the ion bombardment can be used to modify film characteristics. Plasma CVD processes can be classified into many sub-processes, such as plasma evaporation deposition, plasma sputtering deposition, plasma ion plating, and plasma nitriding. This classification depends on the conditions of the plasma generated, configuration of the vacuum system, location of the substrate, and type of power supply [19-21]. Plasma-assisted CVD processes for semiconductor processing are generally carried out at pressures of 1mTorr to 20Torr substrate temperatures in the range of 100 to 500°C, rf power densities <0.5 W-cm^{-2}, electron densities of 1.0 x 10^{8} to 1.0x10^{12}cm^{-3}, electron mean free paths of <0.1 cm, and average electron energies of 1eV to 6eV.

When the plasma initiates, energy from the rf electric field is coupled into the reactant gases via the kinetic energy of a few free electrons. These electrons gain energy rapidly through the electric field and lose energy slowly through elastic collisions. The high-energy electrons are capable of inelastic collisions that cause the reactant gas molecules to dissociate and ionize, producing secondary electrons by various electron-impact reactions. Table (1) lists typical electron-impact reactions of silane molecules in an rf plasma discharge. In a steady-state discharge, the electrons generated by electron-impact reactions equal those electrons that are lost to the electrode, walls, and reactive species by attachment and recombination reactions [1].

The two important aspects of a plasma glow discharge are the nonequilibrium low-temperature gas-phase chemical reactions that generate radical and ion reactive species in the plasma discharge, and the flux and energy of these reactive species as they reach and strike the surface of the film being deposited. The bombardment of the ionic species on the surface of the film, which controls the surface mobility of the precursor, is the predominant factor in determining film composition, density, stress, and step coverage or conformality at the relatively low temperatures used in plasma CVD. Reactant gases similar to those used for

© 2008 Iraqi Society for Alternative and Renewable Energy Sources and Techniques (I.S.A.R.E.S.T.)

thermal CVD processes are used for plasma CVD to deposit silicon-based dielectrics at lower deposition temperatures.

Table (1) Typical electron-impact reactions of silane molecules in an rf plasma discharge. The asterisk (*) refers to electronic excited state [1]

Reactant	Reaction products	Enthalpy of formation (eV)
$e^- + SiH_4 \rightarrow$	$SiH_2 + H_2 + e^-$	2.2
	$SiH_3 + H + e^-$	4.0
	$Si + 2H_2 + e^-$	4.2
	$SiH + H_2 + H + e^-$	5.7
	$SiH^* + H_2 + H + e^-$	8.9
	$Si^* + 2H_2 + e^-$	9.5
	$SiH_2 + 2H_2 + 2\ e^-$	11.9
	$SiH_3 + H + 2\ e^-$	12.3
	$Si + 2H_2 + 2\ e^-$	13.6
	$SiH + H_2 + H + e^-$	15.3

2.1 Reaction kinetics

Reactions during plasma deposition are complex and not completely understood. Elementary reactions that occur in plasma have been discussed by various authors [41-43]. The initial reaction between electrons and reactant gas molecules or between reactant gas molecules in plasma can be classified as elastic or inelastic. In the elastic collisions, only minimal translational energy transfer occurs between the gas molecules and reactant gases. For plasma processing, the elastic collisions play a less important role in reactant dissociation. Significantly more translational, rotational, vibrational, and electronically excitational energy transfer occurs in the inelastic collisions. The major inelastic reactions among electrons, reactant gases, and surface that occur during plasma-assisted CVD processing are typically represented in Tables (2-4).

Table (2) Initial electron-impact reactions [1]

Excitation (rotational, vibrational, and electronic)	$e^- + A_2 \rightarrow A_2 + e^-$
Dissociative attachment	$e^- + A_2 \rightarrow A^- + A+ + e^-$
Dissociation	$e^- + A_2 \rightarrow 2A \bullet + e^-$
Ionization	$e^- + A_2 \rightarrow A_2+ + 2e^-$
Dissociative ionization	$e^- + A_2 \rightarrow A+ + A + 2e^-$

Some of the inelastic collisions between inert gases and reactants (such as helium or argon with silane) significantly affect the chemical nature of the discharge and the properties of the deposited films [44-46]. In many plasma deposition processes, inert carrier and diluent gases such as helium and argon have been used to form "cooler" plasma, to create more controlled reaction pathways via Penning reactions between carrier and reactant gases [47], and to suppress gas-phase reactions between reactive species. As a result, a plasma diluted with inert gases such as helium can be used to deposit higher-quality insulators.

Table (3) Inelastic reactions among reactants, inert gases, and substrate. M refers to the inert gas or substrate, and A, B, and C refer to the reactant gases [1]

A	
Penning dissociation	$M^* + A_2 \rightarrow 2A \bullet + M$
Penning ionization	$M^* + A_2 \rightarrow A_2^+ + M + e^-$
Ion-ion recombination	$M^- + A_2^+ \rightarrow A_2 + M$
	or
	$M^- + A_2^+ \rightarrow 2A \bullet + M$
Electron-ion recombination	$e^- + A_2^+ \rightarrow 2A \bullet$
	$e^- + A_2^+ + M \rightarrow A_2 + M$
Charge transfer	$M^+ + A_2 \rightarrow A_2^+ + M$
	$M^- + A_2 \rightarrow A_2^- + M$
B	
Collisional detachment	$M^* + A_2^- \rightarrow A_2 + M + e^-$
Associative detachment	$A^- + A \rightarrow A_2 + e^-$
Atom recombination	$2A + M \rightarrow A_2 + M$
Atom abstraction	$A + BC \rightarrow AB + C$
Atom addition	$A + BC + M \rightarrow ABC + M$

Table (4) Heterogeneous reactions between plasma and surface. S refers to the surface in contact with the plasma, and A and B refer to the reactant gases [1]

Atom recombination	$S - A + A \rightarrow S + A_2$
Metastable de-excitation	$S + M^* \rightarrow S + M$
Atom abstraction	$S - B + A \rightarrow S + AB$
Sputtering	$S - B + M^+ \rightarrow S^+ + B + M$
Surface contact ionization	$S + B^* \rightarrow B^+ + e^- + S$

2.2 Deposition Mechanisms

One of the major advantages of plasma deposition processing is its flexibility for depositing films with desirable properties. For conventional thermal CVD processing, physical and chemical properties of the deposited film pertaining to its stress, conformality, density, moisture resistance, and gap-fill properties can be altered by changing the composition and/or type of reactive species. In plasma-assisted CVD, this can be accomplished by varying deposition parameters such as temperature, rf power, pressure, reactant gas mixture ratio, and type of reactant. For example, silicon oxide films deposited with TEOS generally show higher step coverage or conformality than those deposited

 ALL RIGHTS RESERVED PRINTED IN IRAQ

with silane in a plasma-assisted CVD process. For plasma-assisted CVD of silicon oxide films, properties can be modified not only by changing the type of reactive species, but also by the extent of ion bombardment.

In general, the deposition mechanisms for a plasma CVD process can be qualitatively divided into four major steps, as shown in Fig. (1). Step 1 includes the primary initial electron-impact reactions between electron and reactant gases to form ions and radical reactive species (Tables 1 and 2). Next, in step 2, transport of these reactive species occurs from the plasma to the substrate surface concurrently with the occurrence of many elastic and inelastic collisions in both the plasma and sheath regions, classified as ion and radical generation steps [48]. Step 3 is the absorption and/or reaction of reactive species (radical absorption and ion incorporation) onto the substrate surface. Finally, in step 4, the reactive species and/or reaction products incorporate into the deposited films or re-emit from surface back to the gas phase. Because of their complexity, the latter two steps are the least known and least studied aspects of plasma CVD. Significant roles are played by ion bombardment [49] and various heterogeneous reactions between ions and radicals with the depositing surface in the sheath region. The two steps critically affect film properties such as conformality [50], density, stress [51], and "impurity" incorporation.

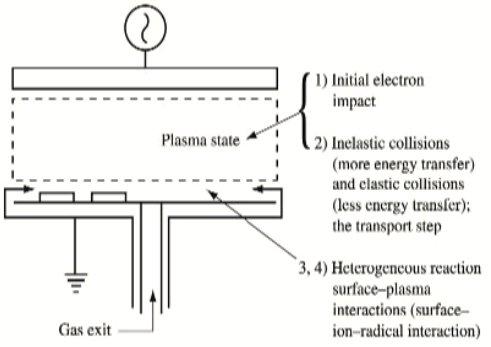

Fig. (1) Four steps that characterize the mechanisms of plasma CVD process [1]

Plasma CVD of amorphous and microcrystalline silicon are the most studied plasma CVD processes, with hundreds of publications on their deposition kinetics and mechanisms. The basic gas-phase chemistry of the silane plasma has been studied by various techniques [49-52]. Different mechanisms have been suggested for the dominant reaction pathway of silicon deposition. One mechanism describes SiH_3 (silyl) radicals playing a dominant role [53], while others describe the decomposition of silane to SiH_2 (silylene) and then SiH_2 insertion into gas-phase SiH_4 to form higher silane species [54] as the main silicon deposition mechanism.

4. Conclusions

We have reviewed the plasma-assisted CVD of dielectric films, with an emphasis on aspects relevant to ULSI semiconductor circuits. In addition, we have indicated that manufacturing needs must be considered early in the process and tool development phase. Obviously, the ultimate goal is to optimize a plasma CVD process for a particular application at the lowest cost of ownership. Future research and development must focus not only on specific technical issues that arise with each new IC generation (such as integration of a stable low-*k* IMD into the BEOL), but also on manufacturability and cost. With 300mm-diameter wafers containing sub-0.25µm semiconductor IC circuits on the horizon, the technical and manufacturing issues are daunting; new challenges are presented to both the semiconductor manufacturers and their equipment suppliers, even for the conventional processes used in IC production.

References

1. S.V. Nguyen, **"Plasma-Assisted Chemical Vapor Deposition",** *Handbook of Thin-Film Deposition Processes and Techniques,* K.K. Schuegraf, Ed., Noyes Publications, Park Ridge, NJ, 1988, pp. 112-141.
2. G.S. Anderson, *J. Appl. Phys.* 33, No. 10, 2991-2992 (1962).
3. L.L. Atl, S.W. Ing, Jr. and K.W. Laendle, *J. Electrochem. Soc.* 110, 465 (1963).
4. S.W. Ing, Jr. and W. Davern, *J. Electrochem. Soc.* 111, 120-122 (1964).
5. A.R. Reinbergh, *Ann. Rev. Mater. Sci.* 9, 341-372 (1979).
6. D.E. Carlson, C.W. Magee and A.R. Triano, *J. Electrochem. Soc.: Solid-State Sci. Technol.* 126, No. 4, 688-691 (1979).
7. S. Sherman et al., *J. Electrochem. Soc.* 144, No. 9, 3198-3204 (1997).
8. H. Randhawa, *Thin Solid Films* 196, 329-349 (1991).
9. J.A. Thornton, *Thin Solid Films* 107, 3-19 (1983).
10. A.T. Bell, *J. Vac. Sci. Technol.* 16, No. 2, 418-419 (1979).
11. R.F. Bunshah, *IEEE Trans. Plasma Sci.* 18, 846-854 (1990).
12. A. Sherman, *Thin Solid Films* 113, 135-149 (1984).
13. S.V. Nguyen, *J. Vac. Sci. Technol. B* 4, No. 5, 1159-1167 (1986).
14. C. Bencher et al., *Solid State Technol.* 40, No. 3, 109-114 (1997).

© 2008 Iraqi Society for Alternative and Renewable Energy Sources and Techniques (I.S.A.R.E.S.T.)

[1] O.A. Hamadi, R.A. Markub and A.A. K. Hadi, "Heat-annealed enhanced-diffusion of silver in gallium arsenide", J. Edu. Al-Mustansiriya Univ., 3 (2001) 35-44.
[2] U.A. Hamadi, M.A.K. Ahmed and R.A. Markub, "Cutting of Ceramic by CW CO_2 Laser", Al-Mustansiriya J. Sci., 12(6) (2001) 307-309.
[3] N.A.K. Al-Rubaiey, O.A. Hamadi and D.N. Raouf, "Effect of gas mixture on output characteristics of a CW CO_2 laser", Iraqi J. Laser, 1(1) (2003) 1-6.
[4] O.A. Hamadi, "Simple arrangement to achieve SHG using a 635nm semiconductor laser", Eng. J. Qatar Univ., 18 (2005) 149-156.
[5] O.A. Hamadi, K.Z. Yahiya and O.N.S. Jassim, "Properties of Silicon Carbide Thin Films Deposited by Vacuum Thermal Evaporation", J. of Semicond. Technol. and Sci., 5(3) (2005) 182-186.
[6] O.A. Hamadi, "Employment some parameters to enhance laser drilling of aluminium", J. Sci. Technol., Sultan Qaboos Univ., 10 (2005) 93-100.
[7] R.A. Ismail, O.A. Abdulrazaq, A.A. Hadi and O.A. Hamadi, "Characterization of Si p-n Photodetectors Produced by Laser-Induced Diffusion", Inter. J. Mod. Phys., 19(31) (2005) 4619-4628.
[8] O.A. Hamadi, "HAZ extent analysis in fiber-reinforced plastic grooving by laser", Iraqi J. Appl. Phys., 1(1) (2005) 1-7.
[9] O.A. Hamadi, "Induced variation of focal length of the lens stimulated in Nd:YAG laser crystal with optical power pumping", Iraqi J. Laser, 2 (2005).
[10] O.A. Hamadi and S.M. Hussain, "Analytical Modelling to Enhance Electric Field Measurement Using Optical Fiber Sensor", Eng. Technol. J., 26 (2006).
[11] O.A. Hamadi and K.S. Khashan, "Effect of Preheating on the Parameters of Laser Keyhole Welding Process: Analytical Study", Iraqi J. Laser, Part A, 5(5) (2006) 11-17.
[12] R.A. Ismail, O.A. Abdulrazaq, A.A. Hadi and O.A. Hamadi, "Full Characterization at 904nm of Si p-n Junction Photodetectors Produced by LID Technique", Euro. Phys. J.: Appl. Phys., 38 (2007) 197-201.
[13] K.S. Khashan and O.A. Hamadi, "Features of spot-matrix surface hardening of low-carbon steel using pulsed laser", J. Eng. Technol., 25(2) (2007).
[14] O.A. Hamadi and K.Z. Yahiya, "Optical and electrical properties of selenium-antimony heterojunction formed on silicon substrate", Sharjah Univ. J. Pure Appl. Sci., 4(2) (2007) 1-11.
[15] B.A. M. Badr, O.A. Hamadi and A.K. Yousif, "Measurement of thermooptic coefficient of semiconductors by single-beam scanning technique", Eng. Technol. J., 27(5) (2007).
[16] O.A. Hamadi, S.M. Hussain, A.A. Hadi and R.O. Mahdi, "Normalized Characteristics of Laser-Induced Diffusion of Arsenic Dopants in Silicon", Eng. Technol. J., 27(4) 2007.
[17] O.A. Hamadi and K.S. Khashan, "Modeling of the Preheating Effect on Keyhole Laser Welding Efficiency", Iraqi J. Appl. Phys. Lett., 1(1) (2008) 10-15.
[18] O.A. Hamadi, B.A.M. Bader and A.K. Yousif, "Electrical Characteristics of Silicon p-n Junction Solar Cells Produced by Plasma-Assisted Matrix Etching Technique", Eng. Technol. J., 28 (2008).
[19] A.A.K. Hadi and O.A. Hamadi, "Optoelectronic Characteristics of As-doped Si Photodetectors Produced by LID Technique", Iraqi J. Appl. Phys. Lett., 1(2) (2008) 23-26.
[20] O.A. Hamadi, "Effect of Annealing on the Electrical Characteristics of CdO-Si Heterostructure Produced by Plasma-Induced Bonding Technique ", Iraqi J. Appl. Phys., 4(3) (2008) 34-37.
[21] O.A. Hamadi, "The Fundamentals of Plasma-Assisted CVD Technique Employed in Thin Films Production", Iraqi J. Appl. Phys. Lett., 1(2) (2008) 3-8.
[22] A.K. Yousif and O.A. Hamadi, "Plasma-Induced Etching of Silicon Surfaces", Bulg. J. Phys., 35(3) (2008) 191-197.
[23] O.A. Hamadi, "Characteristics of CdO-Si Heterostructure Produced by Plasma-Induced Bonding Technique", Proc. IMechE, Part L, J. Mater.: Design and Applications, 222 (2008) 65-71, DOI: 10.1243/14644207JMDA56.
[24] O.A. Hamadi, D.N. Raouf and N.A.-K. Alrubaiey, "Effect of Self-Absorption on the Output Power of CW CO_2 Laser", Iraqi J. Appl. Phys. Lett., 2(1) (2009) 31-34.
[25] O.A. Hamadi, "Profiling of Antimony Diffusivity in Silicon Substrates using Laser-Induced Diffusion Technique", Iraqi J. Appl. Phys. Lett., 3(1) (2010) 23-26.
[26] O.A. Hamadi, N.J. Shakir and F.H. Hussain, "Magnetic Field and Temperature Dependent Measurements of Hall Coefficient in Thermal Evaporated Tin-Doped Cadmium Oxide Thin Films", Bulg. J. Phys., 37(4) (2010) 223-231.
[27] O.A. Hammadi and M.S Edan, "Temperature Dependencies of Refractive Index and Optical Elasticity Coefficient on Lens Induced in Nd:YAG Crystal", Iraqi J. Appl. Phys., 8(1) (2012) 35-41.
[28] O.A. Hammadi, M.K. Khalaf, F.J. Kadhim and B.T. Chiad, "Operation Characteristics of a Closed-Field Unbalanced Dual-Magnetrons Plasma Sputtering System", Bulg. J. Phys., 41(1) (2014) 24-33.

 © ALL RIGHTS RESERVED

[29] O.A. Hammadi and N.I. Naji, "Effect of Acidic Environment on the Spectral Properties of Hibiscus sabdariffa Organic Dye used in Dye-Sensitized Solar Cells", Iraqi J. Appl. Phys., 10(2) (2014) 27-31.
[30] M.K. Khalaf, F.J. Kadhim and O.A. Hammadi, "Effect of Adding Nitrogen to the Gas Mixture on Plasma Characteristics of a Closed-Field Unbalanced DC Magnetron Sputtering System", Iraqi J. Appl. Phys., 10(1) (2014) 27-31.
[31] O.A. Hammadi, "Photovoltaic Properties of Thermally-Grown Selenium-Doped Silicon Photodiodes for Infrared Detection Applications", Phot. Sen., 5(2) (2015) 152-158, DOI: 10.1007/s13320-015-0241-4.
[32] O.A. Hammadi, M.K. Khalaf and F.J. Kadhim, "Fabrication of UV Photodetector from Nickel Oxide Nanoparticles Deposited on Silicon Substrate by Closed-Field Unbalanced Dual Magnetron Sputtering Techniques", Opt. Quant. Electron., 47(12) (2015) 3805-3813, DOI: 10.1007/s11082-015-0247-6
[33] O.A. Hammadi, "Characterization of SiC/Si Heterojunction Fabricated by Plasma-Induced Growth of Nanostructured Silicon Carbide Layer on Silicon Surface", Iraqi J. Appl. Phys., 12(2) (2016) 9-13.
[34] O.A. Hammadi, W.N. Raja, M.A. Saleh and W.A. Altun, "Magnetic Field Distribution of Closed-Field Unbalanced Dual Magnetrons Employed in Plasma Sputtering Systems", Iraqi J. Appl. Phys., 12(3) (2016) 35-42.
[35] O.A. Hammadi, W.N. Raja, M.A. Saleh and W.A. Altun, "Employment of Magnetron to Enhance Langmuir Probe Characteristics of Argon Glow Discharge Plasma in Sputtering System", Iraqi J. Appl. Phys., 12(4) (2016) 19-28.
[36] O.A. Hammadi, M.K. Khalaf and F.J. Kadhim, "Fabrication and Characterization of UV Photodetectors Based on Silicon Nitride Nanostructures Prepared by Magnetron Sputtering", Proc. IMechE, Part N, J. Nanomater. Nanoeng. Nanosys., 230(1) (2016) 32-36, DOI: 10.1177/1740349915610600
[37] O.A. Hammadi and N.E. Naji, "Electrical and spectral characterization of CdS/Si heterojunction prepared by plasma-induced bonding", Opt. Quant. Electron., 48(8) (2016) 375-381, DOI: 10.1007/s11082-016-0647-2
[38] O.A. Hammadi, "Characteristics of Heat-Annealed Silicon Homojunction Infrared Photodetector Fabricated by Plasma-Assisted Technique", Phot. Sen., 6(4) (2016) 345-350, DOI: 10.1007/s13320-016-0338-4
[39] O.A. Hammadi, M.K. Khalaf and F.J. Kadhim, "Silicon Nitride Nanostructures Prepared by Reactive Sputtering Using Closed-Field Unbalanced Dual Magnetrons", Proc. IMechE, Part L, J. Mater.: Design and Applications, 231(5) (2017) 479-487, DOI: 10.1177/1464420715601151
[40] O.A. Hammadi and N.E. Naji, "Fabrication and Characterization of Polycrystalline Nickel Cobaltite Nanostructures Prepared by Plasma Sputtering as Gas Sensor", Phot. Sen., 8(1) (2018) 43-47, DOI: 10.1007/s13320-017-0460-y
[41] O.A. Hammadi, "Production of Nanopowders from Physical Vapor Deposited Films on Nonmetallic Substrates by Conjunctional Freezing-Assisted Ultrasonic Extraction Method", Proc. IMechE, Part N, J. Nanomater. Nanoeng. Nanosys., 232(4) (2018) 135-140, DOI: 10.1177/2397791418807347
[42] O.A. Hammadi, "Nanostructured CdSnSe Thin Films Prepared by DC Plasma Sputtering of Thermally Casted Targets", Iraqi J. Appl. Phys., 14(4) (2018) 33-36.
[43] O.A. Hammadi, "Fabrication of High-Quality Microchannels for Biomedical Applications Using Third-Harmonic Radiation of Nd:YAG Laser", J. Laser Sci. Eng., 10(2) (2018) 61-64.
[44] F.J. Al-Maliki, O.A. Hammadi and E.A. Al-Oubidy, "Optimization of Rutile/Anatase Ratio in Titanium Dioxide Nanostructures prepared by DC Magnetron Sputtering Technique", Iraqi J. Sci., 60 (2019) 91-98.
[45] O.A. Hammadi, "Conjunctional Freezing-Assisted Ultrasonic Extraction of Silicon Dioxide Nanopowders from Thin Films Prepared by Physical Vapor Deposition Technique", Iraqi J. Appl. Phys., 15(4) (2019) 23-28.
[46] O.A. Hammadi, "Synthesis and Characterization of Polycrystalline Carbon Nitride Nanoparticles by Fast Glow Discharge-Induced Reaction of Methane and Ammonia", Adv. in Sci. Eng. Med., 11(5) (2019) 346-350, DOI: https://doi.org/10.1166/asem.2019.2365
[47] O.A. Hammadi, F.J. Kadhim and E.A. Al-Oubidy, "Photocatalytic Activity of Nitrogen-Doped Titanium Dioxide Nanostructures Synthesized by DC Reactive Magnetron Sputtering Technique", Nonlinear Optics, Quantum Optics, 51(1-2) (2019) 67-78.

IRAQI JOURNAL OF APPLIED PHYSICS
Vol. 16, No. 2, April-June 2020, pp. 11-16

R. P. Scott
C. V. Bennett
B. H. Kolner

Simultaneous Amplitude-Modulation and Harmonic Frequency-Modulation Mode Locking of Nd:YAG Laser

Into a fundamentally AM modelocked Nd:YAG laser, we incorporate an electro-optic phase modulator driven at the 22nd harmonic (1.76 GHz). With only 0.6 Watts of RF power we obtain 17 ps pulses at 80 MHz and 8.0 Watts average optical power.

Keywords: Nd:YAG laser; Mode locking; Amplitude modulation; Frequency modulation

1. Introduction

Both AM and FM modelocking have been studied and applied extensively to many different laser systems.1;2 Analysis shows that the optical pulsewidth for either process depends on the modulation depth and frequency according to

$$\tau_p \propto \left(\frac{1}{\delta}\right)^{\frac{1}{4}} \left(\frac{1}{f_m}\right)^{\frac{1}{2}} \quad (1)$$

where _ is the modulation index and fm is the modulation frequency. Clearly, to obtain shorter pulses, raising the frequency fm provides a more rapid rate of return than increasing _. But, for lasers that are limited to constant average output power, the peak power is reduced at a rate / fm −1=2. There are many applications where this tradeo_ is undesirable (e.g. harmonic generation)

However, if two modelocking mechanisms are combined such that one operates at the fundamental frequency and one at a harmonic, the bene_ts of shorter pulses at low repetition rates will be preserved.3;4 Towards this end we report here on simultaneous modelocking; fundamental AM and harmonic FM.

We constructed an electro-optic phase modulator (FM modelocker) with a LiNbO3 crystal in a resonant microwave cavity (fm = 1:76 GHz, QL = 1500, _ = 0:59 rad=p Watt single pass).5 The modulator was placed inside an AM modelocked Nd:YAG laser (Coherent Antares), 15 cm from the output coupler. The 1.76 GHz drive signal was phaselocked to the 40 MHz acousto-optic modelocker signal. This ensured that the phase modulation was synchronized to the AM modelocker.

Simultaneous AM-harmonic FM operation was studied under constant AM modulation conditions. Fig. 1 shows the variation in pulsewidth as a function of phase modulator drive power along with a trend line denoting the −1=8 slope dependence predicted by the theory (cf. Eq. (1) and recall that _ /p Pm). At very low phase modulator drive power, laser operation is dominated by the AM modelocking mechanism. However, with remarkably low power levels, the FM modelocking process begins to dominate. With as little as 15 milliwatts (0.072 radians), the pulsewidth was halved to 40 ps. Raising the modulator power to 0.63 Watts (0.68 radians) reduced the pulsewidth to 17 ps.

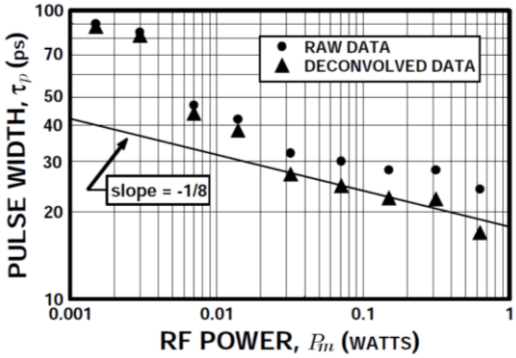

Fig. (1) Optical pulsewidth vs. phase modulator drive power (_ = 0:59 rad= p Watt single pass). Deconvolution applied to data because of photodiode's 17 ps impulse response.

Using AM modelocking alone, we routinely obtain 75 ps pulses with an average optical power of 24 Watts (_4 KW peak). With the phase modulator inserted in the cavity, the average power dropped to about 6 Watts and the laser was somewhat noisy, with occasional self-Q switching. We attribute both the loss and instability to imperfect antireflection coatings and the photorefractive effect in LiNbO3 which may be causing intensity dependent \waveguiding" and spatial mode instability. Nonetheless, we measured a \typical best" pulse of 17 ps at an average optical power of 8 Watts which corresponds to a peak power of 5.9 KW; a 47% increase.

The great utility of simultaneous fundamental and harmonic modelocking is that the pulse repetition rate remains that of the fundamental. Thus, for constant average laser power, the peak power increases linearly with the reduction in pulsewidth. Fig. 2 verifies the fundamental pulse rate when both modelockers are running. Turning o_ the AM modelocker resulted in the repetition rate rising to 1.76 GHz, as expected.

 © ALL RIGHTS RESERVED

A higher temperature is desirable for the STI application, since a more dense film that is highly resistant to subsequent wet-etching steps is thus obtained. These applications are discussed in more detail later in the paper.

When tetraethylorthosilicate (TEOS) is used as the silicon source for PECVD oxide deposition, there is less cusping because of the higher surface mobility of the reactants [22]; however, a void still forms if the gap is small enough, because the conformality of the film is not 100%. This means that the amount of deposition on the sidewalls and bottom of the trench portion of a feature is less than on the top of the feature. So, in order to use PECVD films alone for gap-fill applications, they are typically used in conjunction with an argon sputter etch in a multistep PECVD-argon sputter etch-PECVD sequence described previously [23]. Conformal deposition is more typical for thermal (non-plasma) CVD processes such as low-pressure (LP) CVD at high temperatures or for ozone-TEOS atmospheric or subatmospheric pressure (AP or SA) CVD at lower temperatures (less than 600°C). Furthermore, HDP CVD results in a completely different type of profile because of the "bottom-up" deposition from the simultaneous deposition and etching. The resultant topography from any of these CVD processes plays a decisive role in the choice of subsequent planarization techniques. TEOS was the silicon source for the PECVD and the SACVD, and silane for HDP CVD. The typical "bread-loaf" profile of the PECVD oxide film can be adjusted by varying process parameters such as temperature, pressure, and silicon source. The profile of the SACVD oxide film is conformal, and the unique profile of the HDP CVD oxide film is a result of simultaneous etching and deposition. Note that SACVD is a non-plasma process.

Typically, thermal CVD processes such as LPCVD BPSG, APCVD (or SACVD) BPSG, or PSG are used to passivate the polysilicon/metal silicide gate conductor for sub-half-micron devices because of their high-aspect-ratio fill capability compared to plasma CVD processes and because there are no plasma damage concerns with thermal CVD processing. Process-induced IC device damage from plasma processing (in particular at the gate-conductor level, because there is no device protection) is a critical issue for the PECVD passivation dielectrics. Briefly, low process pressure during deposition of the PECVD PSG was identified as the main factor causing gate-oxide charge damage. Increasing the pressure for the PECVD PSG process regardless of dopant source (trimethylphosphite or triethylphosphate) resulted in no charge damage on antenna test sites and device structures. A more recent study describes another technique used to optimize a PECVD PSG process for plasma damage designated as corona oxide semiconductor (COS) charge measurement [24]. The technique, combined with the antenna test structure method of measuring plasma damage, provides a fast and cost-effective way to optimize plasma CVD processes.

Doped silicon oxide films such as PSG or BPSG are preferred for gate-conductor passivation because of their mobile ion barrier properties [25], low reflow temperature for local planarization (applies to BPSG only), high etch selectivity to the underlying barrier layer (e.g., nitride [26]), and faster polishing rate compared to undoped silicon oxide. In this paper, we discuss our recent work with HDP CVD PSG including gap-fill and plasma damage results. We have previously published an overview of our own work and that of others in IBM on relevant thermal CVD processes and applications [27].

The gap-fill requirement for dielectrics in the "back-end-of-line" (BEOL) depends on the interconnect fabrication methods used. Multilevel interconnects usually involve two types of planarization methods: the planarization of interlayer dielectrics and the planarization of metal layers. For the former, for example, an Al(Cu)-based layer is patterned into lines and the insulator is deposited between the spaces and above the lines. Therefore, a critical requirement in this case is the filling of the gaps between the lines without void formation. Void-free filling of high-aspect-ratio features is not a simple matter and requires the use of advanced insulator deposition processes such as HDP CVD. For submicron metal interconnect fabrication, the insulator deposition is generally followed by partial planarization using spin-on-glass (SOG) [28], a resist etch-back [29], or a global planarization using, for example, chemical-mechanical polishing (CMP). For the planarization of metal layers, the damascene technique is most commonly used; several papers reporting its use in IBM have been published [30]. Using this technique, a dielectric such as silicon oxide is deposited on a planar surface and the wiring level is patterned into the dielectric using photolithography and RIE. A thin metal liner and a metal such as tungsten (or aluminum or copper) are then deposited on the patterned dielectric and subsequently planarized by CMP, stopping on the dielectric and leaving metal in the patterned features. Therefore, in the damascene technique, the metal rather than the insulator must fill the high-aspect-ratio features.

A critical film parameter for both interconnect fabrication techniques is the

 ALL RIGHTS RESERVED PRINTED IN IRAQ

dielectric constant (k) of the IMD material. Use of a material having a lower dielectric constant leads to lower total capacitance, decreasing the interconnection delay and power dissipation [31], and thus enhancing performance. To achieve long-range interconnection performance objectives, low-dielectric-constant IMD will be required [32]. The dielectric constant of PECVD silicon oxide is typically 4.1-4.2. By doping the oxide with fluorine, the dielectric constant can be reduced to 3.0-3.7, depending on the fluorine concentration [33]. Si-F replaces the Si-OH and Si-H bonds in the oxide; since fluorine is more electronegative, the polarization changes, lowering the dielectric constant. SOG dielectrics (siloxanes, silsesquioxanes) and organic polymers formed by spin coating (polyimides, fluorinated polyimides, bisbenzocyclobutenes), poly(arylethers), or vapor-phase deposition (parylene N, parylene F, teflon) provide dielectric constants in the range of 1.9-3.0 [34]. Most polymers with a dielectric constant less than 3 are stable to only about 350°C. However, a recent publication on laser-evaporated siloxane thin films reports a dielectric constant of 2.0 and thermal stability to 400°C, although integration results were not published [35]. Also, it has been reported that parylene exhibits a high thermal stability [36], and its successful integration into a metal RIE BEOL has been demonstrated [37]. However, damascene integration may be more difficult to achieve because of the softness of parylene films. Spun-on films of materials such as nanoporous silica and xerogels exhibit a higher thermal stability and low dielectric constants (1.3-2.5), depending on their porosity [38], but associated process integration is challenging. There has been increased development activity in plasma-assisted CVD of amorphous carbon and fluorinated carbon films because of their low dielectric constants (2.3-2.7) and thermal stability up to 400°C [39]. Relevant work on insulators having low dielectric constants has been described elsewhere [40].

In this paper, the plasma-assisted CVD of low-dielectric-constant insulators of potential interest at the ULSI level, including fluorine-doped silicon oxide and amorphous carbon and fluorocarbon, was discussed. To be suitable for the deposition of such insulators, plasma-assisted CVD should be applicable at relatively low substrate temperatures, should not damage underlying layers or devices that may be present on the substrate during deposition, and should produce insulators which, in addition to having low dielectric constants, satisfy etching, annealing, planarization, and stability requirements.

2. Fundamentals of PECVD

In thermal CVD, gas-phase reactive species are generated by heating of initial reactants. In plasma CVD, the plasma energy supplied by an external rf source takes the place of the heating to generate the species that subsequently react and deposit on substrate surfaces. Significantly, excessive heating and degradation on the substrate can be avoided by using plasma electron kinetic energy instead of thermal energy. Besides the aspect of generating reactive species at much lower processing temperatures compared to conventional CVD processing, the ion bombardment can be used to modify film characteristics. Plasma CVD processes can be classified into many sub-processes, such as plasma evaporation deposition, plasma sputtering deposition, plasma ion plating, and plasma nitriding. This classification depends on the conditions of the plasma generated, configuration of the vacuum system, location of the substrate, and type of power supply [19-21]. Plasma-assisted CVD processes for semiconductor processing are generally carried out at pressures of 1mTorr to 20Torr substrate temperatures in the range of 100 to 500°C, rf power densities <0.5 W-cm^{-2}, electron densities of 1.0 x 10^{8} to 1.0x10^{12}cm^{-3}, electron mean free paths of <0.1 cm, and average electron energies of 1eV to 6eV.

When the plasma initiates, energy from the rf electric field is coupled into the reactant gases via the kinetic energy of a few free electrons. These electrons gain energy rapidly through the electric field and lose energy slowly through elastic collisions. The high-energy electrons are capable of inelastic collisions that cause the reactant gas molecules to dissociate and ionize, producing secondary electrons by various electron-impact reactions. Table (1) lists typical electron-impact reactions of silane molecules in an rf plasma discharge. In a steady-state discharge, the electrons generated by electron-impact reactions equal those electrons that are lost to the electrode, walls, and reactive species by attachment and recombination reactions [1].

The two important aspects of a plasma glow discharge are the nonequilibrium low-temperature gas-phase chemical reactions that generate radical and ion reactive species in the plasma discharge, and the flux and energy of these reactive species as they reach and strike the surface of the film being deposited. The bombardment of the ionic species on the surface of the film, which controls the surface mobility of the precursor, is the predominant factor in determining film composition, density, stress, and step coverage or conformality at the relatively low temperatures used in plasma CVD. Reactant gases similar to those used for

© 2008 Iraqi Society for Alternative and Renewable Energy Sources and Techniques (I.S.A.R.E.S.T.)

thermal CVD processes are used for plasma CVD to deposit silicon-based dielectrics at lower deposition temperatures.

Table (1) Typical electron-impact reactions of silane molecules in an rf plasma discharge. The asterisk (*) refers to electronic excited state [1]

Reactant	Reaction products	Enthalpy of formation (eV)
$e^- + SiH_4 \rightarrow$	$SiH_2 + H_2 + e^-$	2.2
	$SiH_3 + H + e^-$	4.0
	$Si + 2H_2 + e^-$	4.2
	$SiH + H_2 + H + e^-$	5.7
	$SiH^* + H_2 + H + e^-$	8.9
	$Si^* + 2H_2 + e^-$	9.5
	$SiH_2 + 2H_2 + 2\ e^-$	11.9
	$SiH_3 + H + 2\ e^-$	12.3
	$Si + 2H_2 + 2\ e^-$	13.6
	$SiH + H_2 + H + e^-$	15.3

2.1 Reaction kinetics

Reactions during plasma deposition are complex and not completely understood. Elementary reactions that occur in plasma have been discussed by various authors [41-43]. The initial reaction between electrons and reactant gas molecules or between reactant gas molecules in plasma can be classified as elastic or inelastic. In the elastic collisions, only minimal translational energy transfer occurs between the gas molecules and reactant gases. For plasma processing, the elastic collisions play a less important role in reactant dissociation. Significantly more translational, rotational, vibrational, and electronically excitational energy transfer occurs in the inelastic collisions. The major inelastic reactions among electrons, reactant gases, and surface that occur during plasma-assisted CVD processing are typically represented in Tables (2-4).

Table (2) Initial electron-impact reactions [1]

Excitation (rotational, vibrational, and electronic)	$e^- + A_2 \rightarrow A_2 + e^-$
Dissociative attachment	$e^- + A_2 \rightarrow A^- + A+ + e^-$
Dissociation	$e^- + A_2 \rightarrow 2A \bullet + e^-$
Ionization	$e^- + A_2 \rightarrow A_2+ + 2e^-$
Dissociative ionization	$e^- + A_2 \rightarrow A+ + A + 2e^-$

Some of the inelastic collisions between inert gases and reactants (such as helium or argon with silane) significantly affect the chemical nature of the discharge and the properties of the deposited films [44-46]. In many plasma deposition processes, inert carrier and diluent gases such as helium and argon have been used to form "cooler" plasma, to create more controlled reaction pathways via Penning reactions between carrier and reactant gases [47], and to suppress gas-phase reactions between reactive species. As a result, a plasma diluted with inert gases such as helium can be used to deposit higher-quality insulators.

Table (3) Inelastic reactions among reactants, inert gases, and substrate. M refers to the inert gas or substrate, and A, B, and C refer to the reactant gases [1]

A	
Penning dissociation	$M^* + A_2 \rightarrow 2A \bullet + M$
Penning ionization	$M^* + A_2 \rightarrow A_2^+ + M + e^-$
Ion-ion recombination	$M^- + A_2^+ \rightarrow A_2 + M$
	or
	$M^- + A_2^+ \rightarrow 2A \bullet + M$
Electron-ion recombination	$e^- + A_2^+ \rightarrow 2A \bullet$
	$e^- + A_2^+ + M \rightarrow A_2 + M$
Charge transfer	$M^+ + A_2 \rightarrow A_2^+ + M$
	$M^- + A_2 \rightarrow A_2^- + M$
B	
Collisional detachment	$M^* + A_2^- \rightarrow A_2 + M + e^-$
Associative detachment	$A^- + A \rightarrow A_2 + e^-$
Atom recombination	$2A + M \rightarrow A_2 + M$
Atom abstraction	$A + BC \rightarrow AB + C$
Atom addition	$A + BC + M \rightarrow ABC + M$

Table (4) Heterogeneous reactions between plasma and surface. S refers to the surface in contact with the plasma, and A and B refer to the reactant gases [1]

Atom recombination	$S - A + A \rightarrow S + A_2$
Metastable de-excitation	$S + M^* \rightarrow S + M$
Atom abstraction	$S - B + A \rightarrow S + AB$
Sputtering	$S - B + M^+ \rightarrow S^+ + B + M$
Surface contact ionization	$S + B^* \rightarrow B^+ + e^- + S$

2.2 Deposition Mechanisms

One of the major advantages of plasma deposition processing is its flexibility for depositing films with desirable properties. For conventional thermal CVD processing, physical and chemical properties of the deposited film pertaining to its stress, conformality, density, moisture resistance, and gap-fill properties can be altered by changing the composition and/or type of reactive species. In plasma-assisted CVD, this can be accomplished by varying deposition parameters such as temperature, rf power, pressure, reactant gas mixture ratio, and type of reactant. For example, silicon oxide films deposited with TEOS generally show higher step coverage or conformality than those deposited

 ALL RIGHTS RESERVED PRINTED IN IRAQ

with silane in a plasma-assisted CVD process. For plasma-assisted CVD of silicon oxide films, properties can be modified not only by changing the type of reactive species, but also by the extent of ion bombardment.

In general, the deposition mechanisms for a plasma CVD process can be qualitatively divided into four major steps, as shown in Fig. (1). Step 1 includes the primary initial electron-impact reactions between electron and reactant gases to form ions and radical reactive species (Tables 1 and 2). Next, in step 2, transport of these reactive species occurs from the plasma to the substrate surface concurrently with the occurrence of many elastic and inelastic collisions in both the plasma and sheath regions, classified as ion and radical generation steps [48]. Step 3 is the absorption and/or reaction of reactive species (radical absorption and ion incorporation) onto the substrate surface. Finally, in step 4, the reactive species and/or reaction products incorporate into the deposited films or re-emit from surface back to the gas phase. Because of their complexity, the latter two steps are the least known and least studied aspects of plasma CVD. Significant roles are played by ion bombardment [49] and various heterogeneous reactions between ions and radicals with the depositing surface in the sheath region. The two steps critically affect film properties such as conformality [50], density, stress [51], and "impurity" incorporation.

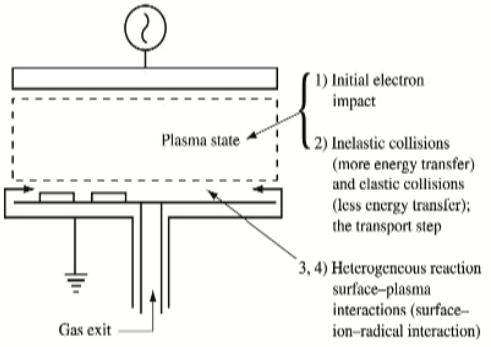

Fig. (1) Four steps that characterize the mechanisms of plasma CVD process [1]

Plasma CVD of amorphous and microcrystalline silicon are the most studied plasma CVD processes, with hundreds of publications on their deposition kinetics and mechanisms. The basic gas-phase chemistry of the silane plasma has been studied by various techniques [49-52]. Different mechanisms have been suggested for the dominant reaction pathway of silicon deposition. One mechanism describes SiH_3 (silyl) radicals playing a dominant role [53], while others describe the decomposition of silane to SiH_2 (silylene) and then SiH_2 insertion into gas-phase SiH_4 to form higher silane species [54] as the main silicon deposition mechanism.

4. Conclusions

We have reviewed the plasma-assisted CVD of dielectric films, with an emphasis on aspects relevant to ULSI semiconductor circuits. In addition, we have indicated that manufacturing needs must be considered early in the process and tool development phase. Obviously, the ultimate goal is to optimize a plasma CVD process for a particular application at the lowest cost of ownership. Future research and development must focus not only on specific technical issues that arise with each new IC generation (such as integration of a stable low-*k* IMD into the BEOL), but also on manufacturability and cost. With 300mm-diameter wafers containing sub-0.25µm semiconductor IC circuits on the horizon, the technical and manufacturing issues are daunting; new challenges are presented to both the semiconductor manufacturers and their equipment suppliers, even for the conventional processes used in IC production.

References

1. S.V. Nguyen, **"Plasma-Assisted Chemical Vapor Deposition",** *Handbook of Thin-Film Deposition Processes and Techniques,* K.K. Schuegraf, Ed., Noyes Publications, Park Ridge, NJ, 1988, pp. 112-141.
2. G.S. Anderson, *J. Appl. Phys.* 33, No. 10, 2991-2992 (1962).
3. L.L. Atl, S.W. Ing, Jr. and K.W. Laendle, *J. Electrochem. Soc.* 110, 465 (1963).
4. S.W. Ing, Jr. and W. Davern, *J. Electrochem. Soc.* 111, 120-122 (1964).
5. A.R. Reinbergh, *Ann. Rev. Mater. Sci.* 9, 341-372 (1979).
6. D.E. Carlson, C.W. Magee and A.R. Triano, *J. Electrochem. Soc.: Solid-State Sci. Technol.* 126, No. 4, 688-691 (1979).
7. S. Sherman et al., *J. Electrochem. Soc.* 144, No. 9, 3198-3204 (1997).
8. H. Randhawa, *Thin Solid Films* 196, 329-349 (1991).
9. J.A. Thornton, *Thin Solid Films* 107, 3-19 (1983).
10. A.T. Bell, *J. Vac. Sci. Technol.* 16, No. 2, 418-419 (1979).
11. R.F. Bunshah, *IEEE Trans. Plasma Sci.* 18, 846-854 (1990).
12. A. Sherman, *Thin Solid Films* 113, 135-149 (1984).
13. S.V. Nguyen, *J. Vac. Sci. Technol. B* 4, No. 5, 1159-1167 (1986).
14. C. Bencher et al., *Solid State Technol.* 40, No. 3, 109-114 (1997).

© 2008 Iraqi Society for Alternative and Renewable Energy Sources and Techniques (I.S.A.R.E.S.T.)

[1] O.A. Hamadi, R.A. Markub and A.A. K. Hadi, "Heat-annealed enhanced-diffusion of silver in gallium arsenide", J. Edu. Al-Mustansiriya Univ., 3 (2001) 35-44.
[2] U.A. Hamadi, M.A.K. Ahmed and R.A. Markub, "Cutting of Ceramic by CW CO_2 Laser", Al-Mustansiriya J. Sci., 12(6) (2001) 307-309.
[3] N.A.K. Al-Rubaiey, O.A. Hamadi and D.N. Raouf, "Effect of gas mixture on output characteristics of a CW CO_2 laser", Iraqi J. Laser, 1(1) (2003) 1-6.
[4] O.A. Hamadi, "Simple arrangement to achieve SHG using a 635nm semiconductor laser", Eng. J. Qatar Univ., 18 (2005) 149-156.
[5] O.A. Hamadi, K.Z. Yahiya and O.N.S. Jassim, "Properties of Silicon Carbide Thin Films Deposited by Vacuum Thermal Evaporation", J. of Semicond. Technol. and Sci., 5(3) (2005) 182-186.
[6] O.A. Hamadi, "Employment some parameters to enhance laser drilling of aluminium", J. Sci. Technol., Sultan Qaboos Univ., 10 (2005) 93-100.
[7] R.A. Ismail, O.A. Abdulrazaq, A.A. Hadi and O.A. Hamadi, "Characterization of Si p-n Photodetectors Produced by Laser-Induced Diffusion", Inter. J. Mod. Phys., 19(31) (2005) 4619-4628.
[8] O.A. Hamadi, "HAZ extent analysis in fiber-reinforced plastic grooving by laser", Iraqi J. Appl. Phys., 1(1) (2005) 1-7.
[9] O.A. Hamadi, "Induced variation of focal length of the lens stimulated in Nd:YAG laser crystal with optical power pumping", Iraqi J. Laser, 2 (2005).
[10] O.A. Hamadi and S.M. Hussain, "Analytical Modelling to Enhance Electric Field Measurement Using Optical Fiber Sensor", Eng. Technol. J., 26 (2006).
[11] O.A. Hamadi and K.S. Khashan, "Effect of Preheating on the Parameters of Laser Keyhole Welding Process: Analytical Study", Iraqi J. Laser, Part A, 5(5) (2006) 11-17.
[12] R.A. Ismail, O.A. Abdulrazaq, A.A. Hadi and O.A. Hamadi, "Full Characterization at 904nm of Si p-n Junction Photodetectors Produced by LID Technique", Euro. Phys. J.: Appl. Phys., 38 (2007) 197-201.
[13] K.S. Khashan and O.A. Hamadi, "Features of spot-matrix surface hardening of low-carbon steel using pulsed laser", J. Eng. Technol., 25(2) (2007).
[14] O.A. Hamadi and K.Z. Yahiya, "Optical and electrical properties of selenium-antimony heterojunction formed on silicon substrate", Sharjah Univ. J. Pure Appl. Sci., 4(2) (2007) 1-11.
[15] B.A. M. Badr, O.A. Hamadi and A.K. Yousif, "Measurement of thermooptic coefficient of semiconductors by single-beam scanning technique", Eng. Technol. J., 27(5) (2007).
[16] O.A. Hamadi, S.M. Hussain, A.A. Hadi and R.O. Mahdi, "Normalized Characteristics of Laser-Induced Diffusion of Arsenic Dopants in Silicon", Eng. Technol. J., 27(4) 2007.
[17] O.A. Hamadi and K.S. Khashan, "Modeling of the Preheating Effect on Keyhole Laser Welding Efficiency", Iraqi J. Appl. Phys. Lett., 1(1) (2008) 10-15.
[18] O.A. Hamadi, B.A.M. Bader and A.K. Yousif, "Electrical Characteristics of Silicon p-n Junction Solar Cells Produced by Plasma-Assisted Matrix Etching Technique", Eng. Technol. J., 28 (2008).
[19] A.A.K. Hadi and O.A. Hamadi, "Optoelectronic Characteristics of As-doped Si Photodetectors Produced by LID Technique", Iraqi J. Appl. Phys. Lett., 1(2) (2008) 23-26.
[20] O.A. Hamadi, "Effect of Annealing on the Electrical Characteristics of CdO-Si Heterostructure Produced by Plasma-Induced Bonding Technique ", Iraqi J. Appl. Phys., 4(3) (2008) 34-37.
[21] O.A. Hamadi, "The Fundamentals of Plasma-Assisted CVD Technique Employed in Thin Films Production", Iraqi J. Appl. Phys. Lett., 1(2) (2008) 3-8.
[22] A.K. Yousif and O.A. Hamadi, "Plasma-Induced Etching of Silicon Surfaces", Bulg. J. Phys., 35(3) (2008) 191-197.
[23] O.A. Hamadi, "Characteristics of CdO-Si Heterostructure Produced by Plasma-Induced Bonding Technique", Proc. IMechE, Part L, J. Mater.: Design and Applications, 222 (2008) 65-71, DOI: 10.1243/14644207JMDA56.
[24] O.A. Hamadi, D.N. Raouf and N.A.-K. Alrubaiey, "Effect of Self-Absorption on the Output Power of CW CO_2 Laser", Iraqi J. Appl. Phys. Lett., 2(1) (2009) 31-34.
[25] O.A. Hamadi, "Profiling of Antimony Diffusivity in Silicon Substrates using Laser-Induced Diffusion Technique", Iraqi J. Appl. Phys. Lett., 3(1) (2010) 23-26.
[26] O.A. Hamadi, N.J. Shakir and F.H. Hussain, "Magnetic Field and Temperature Dependent Measurements of Hall Coefficient in Thermal Evaporated Tin-Doped Cadmium Oxide Thin Films", Bulg. J. Phys., 37(4) (2010) 223-231.
[27] O.A. Hammadi and M.S Edan, "Temperature Dependencies of Refractive Index and Optical Elasticity Coefficient on Lens Induced in Nd:YAG Crystal", Iraqi J. Appl. Phys., 8(1) (2012) 35-41.
[28] O.A. Hammadi, M.K. Khalaf, F.J. Kadhim and B.T. Chiad, "Operation Characteristics of a Closed-Field Unbalanced Dual-Magnetrons Plasma Sputtering System", Bulg. J. Phys., 41(1) (2014) 24-33.

 © ALL RIGHTS RESERVED

[29] O.A. Hammadi and N.I. Naji, "Effect of Acidic Environment on the Spectral Properties of Hibiscus sabdariffa Organic Dye used in Dye-Sensitized Solar Cells", Iraqi J. Appl. Phys., 10(2) (2014) 27-31.
[30] M.K. Khalaf, F.J. Kadhim and O.A. Hammadi, "Effect of Adding Nitrogen to the Gas Mixture on Plasma Characteristics of a Closed-Field Unbalanced DC Magnetron Sputtering System", Iraqi J. Appl. Phys., 10(1) (2014) 27-31.
[31] O.A. Hammadi, "Photovoltaic Properties of Thermally-Grown Selenium-Doped Silicon Photodiodes for Infrared Detection Applications", Phot. Sen., 5(2) (2015) 152-158, DOI: 10.1007/s13320-015-0241-4.
[32] O.A. Hammadi, M.K. Khalaf and F.J. Kadhim, "Fabrication of UV Photodetector from Nickel Oxide Nanoparticles Deposited on Silicon Substrate by Closed-Field Unbalanced Dual Magnetron Sputtering Techniques", Opt. Quant. Electron., 47(12) (2015) 3805-3813, DOI: 10.1007/s11082-015-0247-6
[33] O.A. Hammadi, "Characterization of SiC/Si Heterojunction Fabricated by Plasma-Induced Growth of Nanostructured Silicon Carbide Layer on Silicon Surface", Iraqi J. Appl. Phys., 12(2) (2016) 9-13.
[34] O.A. Hammadi, W.N. Raja, M.A. Saleh and W.A. Altun, "Magnetic Field Distribution of Closed-Field Unbalanced Dual Magnetrons Employed in Plasma Sputtering Systems", Iraqi J. Appl. Phys., 12(3) (2016) 35-42.
[35] O.A. Hammadi, W.N. Raja, M.A. Saleh and W.A. Altun, "Employment of Magnetron to Enhance Langmuir Probe Characteristics of Argon Glow Discharge Plasma in Sputtering System", Iraqi J. Appl. Phys., 12(4) (2016) 19-28.
[36] O.A. Hammadi, M.K. Khalaf and F.J. Kadhim, "Fabrication and Characterization of UV Photodetectors Based on Silicon Nitride Nanostructures Prepared by Magnetron Sputtering", Proc. IMechE, Part N, J. Nanomater. Nanoeng. Nanosys., 230(1) (2016) 32-36, DOI: 10.1177/1740349915610600
[37] O.A. Hammadi and N.E. Naji, "Electrical and spectral characterization of CdS/Si heterojunction prepared by plasma-induced bonding", Opt. Quant. Electron., 48(8) (2016) 375-381, DOI: 10.1007/s11082-016-0647-2
[38] O.A. Hammadi, "Characteristics of Heat-Annealed Silicon Homojunction Infrared Photodetector Fabricated by Plasma-Assisted Technique", Phot. Sen., 6(4) (2016) 345-350, DOI: 10.1007/s13320-016-0338-4
[39] O.A. Hammadi, M.K. Khalaf and F.J. Kadhim, "Silicon Nitride Nanostructures Prepared by Reactive Sputtering Using Closed-Field Unbalanced Dual Magnetrons", Proc. IMechE, Part L, J. Mater.: Design and Applications, 231(5) (2017) 479-487, DOI: 10.1177/1464420715601151
[40] O.A. Hammadi and N.E. Naji, "Fabrication and Characterization of Polycrystalline Nickel Cobaltite Nanostructures Prepared by Plasma Sputtering as Gas Sensor", Phot. Sen., 8(1) (2018) 43-47, DOI: 10.1007/s13320-017-0460-y
[41] O.A. Hammadi, "Production of Nanopowders from Physical Vapor Deposited Films on Nonmetallic Substrates by Conjunctional Freezing-Assisted Ultrasonic Extraction Method", Proc. IMechE, Part N, J. Nanomater. Nanoeng. Nanosys., 232(4) (2018) 135-140, DOI: 10.1177/2397791418807347
[42] O.A. Hammadi, "Nanostructured CdSnSe Thin Films Prepared by DC Plasma Sputtering of Thermally Casted Targets", Iraqi J. Appl. Phys., 14(4) (2018) 33-36.
[43] O.A. Hammadi, "Fabrication of High-Quality Microchannels for Biomedical Applications Using Third-Harmonic Radiation of Nd:YAG Laser", J. Laser Sci. Eng., 10(2) (2018) 61-64.
[44] F.J. Al-Maliki, O.A. Hammadi and E.A. Al-Oubidy, "Optimization of Rutile/Anatase Ratio in Titanium Dioxide Nanostructures prepared by DC Magnetron Sputtering Technique", Iraqi J. Sci., 60 (2019) 91-98.
[45] O.A. Hammadi, "Conjunctional Freezing-Assisted Ultrasonic Extraction of Silicon Dioxide Nanopowders from Thin Films Prepared by Physical Vapor Deposition Technique", Iraqi J. Appl. Phys., 15(4) (2019) 23-28.
[46] O.A. Hammadi, "Synthesis and Characterization of Polycrystalline Carbon Nitride Nanoparticles by Fast Glow Discharge-Induced Reaction of Methane and Ammonia", Adv. in Sci. Eng. Med., 11(5) (2019) 346-350, DOI: https://doi.org/10.1166/asem.2019.2365
[47] O.A. Hammadi, F.J. Kadhim and E.A. Al-Oubidy, "Photocatalytic Activity of Nitrogen-Doped Titanium Dioxide Nanostructures Synthesized by DC Reactive Magnetron Sputtering Technique", Nonlinear Optics, Quantum Optics, 51(1-2) (2019) 67-78.

IRAQI JOURNAL OF APPLIED PHYSICS
Vol. 16, No. 2, April-June 2020, pp. 17-24

Jani Oksanen
Jukka Tulkki

Crosstalk and Noise in Optical Amplifier with Gain Clamping by Vertical Laser Field

We have calculated the transient behavior and noise of a semiconductor optical amplifier with its gain clamped by a vertical cavity laser (VCL). The calculations are based on a numerical stochastic rate equation model including several forward and backward propagating channels that are coupled to the vertical laser field through the active medium. The noise model takes into account randomly amplified spontaneous emission and random gain. Numerical simulations have been carried out to study the relaxation oscillations, cross talk and noise in a system with a strong input signal switched on and off while observing the output signals, VCL photon density and carrier density. Results show that the VCL field captures most of the disturbances, in agreement with available experimental data.

Keywords: Gain clamping; Shot noise; Crosstalk amplifier; Random gain

1. Introduction

Gain clamped semiconductor optical amplifiers (GCSOA) offer many advantages compared with the conventional semiconductor optical amplifiers (SOA). Their response is more linear and they suffer less from cross talk related effects. Conventionally the gain clamping has been achieved by fabricating two distributed Bragg reflector (DBR) mirrors on both ends of the amplifier so that the amplifier forms a cavity for the frequencies selected by the DBRs [1], [2]. However, the fabrication of DBRs makes the amplifier structure more complex and also the amplifier response less ideal. The advantage both the SOA and GCSOA have over the fiber optical amplifiers is their integrability, which in case of the SOA comes with the cost of low performance.

A different approach to gain clamping was introduced

recently by Genoa Corporation [3]. In their amplifier

structure (called linear optical amplifier, LOA) the laser field is perpendicular, rather than parallel, to the signal and vertical in the actual amplifier structure (see Fig. 1). The physics of the LOA differs from that of the parallel approach, because the steady state power density of the vertical laser field has a distinctive, monotonously decreasing, position dependence.

This paper presents a position dependent stochastic rate equation model allowing for the analysis of the propagation of several signal and noise channels in forward and backward directions in the amplifier. The stabilizing laser field and the carrier density in the system are taken into account with the standard rate equations that are modified to include the effect of the propagating signals. The model is then used to evaluate the cross talk, switching transients, amplified spontaneous emission (ASE), noise intensity and noise figure of the amplifier. Examples of the carrier density fluctuations and vertical laser field intensities are also given for selected cases.

2. LOA Model

The gain clamping by vertical laser can be realized by combining a vertical microcavity laser (VCL) with a build-in waveguide in a direction perpendicular to the cavity (Fig. 1). The stochastic rate equation model describing the behavior of the carrier density □_____and the photon densities of the vertical laser field _____ , the signal ___ _____ and the noise ____ _____ can be written in the form

$$\frac{\partial n}{\partial t} = \frac{I}{qhwl} - vG_L L - v\sum_{i,\rho}\left\{G_i\left(S_i^\rho + N_i^\rho\right)\right\}_r - \frac{n}{\tau} \quad (1)$$

$$\frac{\partial L}{\partial t} = v\left(G_L - \alpha_L\right)L + \eta_L\frac{n}{\tau_r} \quad (2)$$

$$\frac{\partial S_i^\rho}{\partial t} = -\rho v\frac{\partial S_i^\rho}{\partial x} + vG_iS_i^\rho \quad (3)$$

$$\frac{\partial N_i^\rho}{\partial t} = -\rho v\frac{\partial N_i^\rho}{\partial x} + v\left\{G_iN_i^\rho\right\}_r + \left\{\eta_i\frac{n}{\tau_r}\right\}_r + v\left\{G_iS_i^\rho\right\}_r - vG_iS_i^\rho, \quad (4)$$

where curly brackets with subindex ?denote that the effect of the enclosed entity is considered to be random

For a list of physical quantities appearing in Eqs. (1)-(4), see Table I. Equation (1) states that the carrier density increases by injection and reduces by the stimulated emission to the vertical laser field and signal (and noise), and the combined effect of spontaneous emission and nonradiative recombination. The vertical laser mode is described by the standard rate equation model (2), where the photon density changes due to the effects of the gain and the losses of the cavity (single mode operation

 © ALL RIGHTS RESERVED

A higher temperature is desirable for the STI application, since a more dense film that is highly resistant to subsequent wet-etching steps is thus obtained. These applications are discussed in more detail later in the paper.

When tetraethylorthosilicate (TEOS) is used as the silicon source for PECVD oxide deposition, there is less cusping because of the higher surface mobility of the reactants [22]; however, a void still forms if the gap is small enough, because the conformality of the film is not 100%. This means that the amount of deposition on the sidewalls and bottom of the trench portion of a feature is less than on the top of the feature. So, in order to use PECVD films alone for gap-fill applications, they are typically used in conjunction with an argon sputter etch in a multistep PECVD-argon sputter etch-PECVD sequence described previously [23]. Conformal deposition is more typical for thermal (non-plasma) CVD processes such as low-pressure (LP) CVD at high temperatures or for ozone-TEOS atmospheric or subatmospheric pressure (AP or SA) CVD at lower temperatures (less than 600°C). Furthermore, HDP CVD results in a completely different type of profile because of the "bottom-up" deposition from the simultaneous deposition and etching. The resultant topography from any of these CVD processes plays a decisive role in the choice of subsequent planarization techniques. TEOS was the silicon source for the PECVD and the SACVD, and silane for HDP CVD. The typical "bread-loaf" profile of the PECVD oxide film can be adjusted by varying process parameters such as temperature, pressure, and silicon source. The profile of the SACVD oxide film is conformal, and the unique profile of the HDP CVD oxide film is a result of simultaneous etching and deposition. Note that SACVD is a non-plasma process.

Typically, thermal CVD processes such as LPCVD BPSG, APCVD (or SACVD) BPSG, or PSG are used to passivate the polysilicon/metal silicide gate conductor for sub-half-micron devices because of their high-aspect-ratio fill capability compared to plasma CVD processes and because there are no plasma damage concerns with thermal CVD processing. Process-induced IC device damage from plasma processing (in particular at the gate-conductor level, because there is no device protection) is a critical issue for the PECVD passivation dielectrics. Briefly, low process pressure during deposition of the PECVD PSG was identified as the main factor causing gate-oxide charge damage. Increasing the pressure for the PECVD PSG process regardless of dopant source (trimethylphosphite or triethylphosphate) resulted in no charge damage on antenna test sites and device structures. A more recent study describes another technique used to optimize a PECVD PSG process for plasma damage designated as corona oxide semiconductor (COS) charge measurement [24]. The technique, combined with the antenna test structure method of measuring plasma damage, provides a fast and cost-effective way to optimize plasma CVD processes.

Doped silicon oxide films such as PSG or BPSG are preferred for gate-conductor passivation because of their mobile ion barrier properties [25], low reflow temperature for local planarization (applies to BPSG only), high etch selectivity to the underlying barrier layer (e.g., nitride [26]), and faster polishing rate compared to undoped silicon oxide. In this paper, we discuss our recent work with HDP CVD PSG including gap-fill and plasma damage results. We have previously published an overview of our own work and that of others in IBM on relevant thermal CVD processes and applications [27].

The gap-fill requirement for dielectrics in the "back-end-of-line" (BEOL) depends on the interconnect fabrication methods used. Multilevel interconnects usually involve two types of planarization methods: the planarization of interlayer dielectrics and the planarization of metal layers. For the former, for example, an Al(Cu)-based layer is patterned into lines and the insulator is deposited between the spaces and above the lines. Therefore, a critical requirement in this case is the filling of the gaps between the lines without void formation. Void-free filling of high-aspect-ratio features is not a simple matter and requires the use of advanced insulator deposition processes such as HDP CVD. For submicron metal interconnect fabrication, the insulator deposition is generally followed by partial planarization using spin-on-glass (SOG) [28], a resist etch-back [29], or a global planarization using, for example, chemical-mechanical polishing (CMP). For the planarization of metal layers, the damascene technique is most commonly used; several papers reporting its use in IBM have been published [30]. Using this technique, a dielectric such as silicon oxide is deposited on a planar surface and the wiring level is patterned into the dielectric using photolithography and RIE. A thin metal liner and a metal such as tungsten (or aluminum or copper) are then deposited on the patterned dielectric and subsequently planarized by CMP, stopping on the dielectric and leaving metal in the patterned features. Therefore, in the damascene technique, the metal rather than the insulator must fill the high-aspect-ratio features.

A critical film parameter for both interconnect fabrication techniques is the

 ALL RIGHTS RESERVED PRINTED IN IRAQ

dielectric constant (k) of the IMD material. Use of a material having a lower dielectric constant leads to lower total capacitance, decreasing the interconnection delay and power dissipation [31], and thus enhancing performance. To achieve long-range interconnection performance objectives, low-dielectric-constant IMD will be required [32]. The dielectric constant of PECVD silicon oxide is typically 4.1-4.2. By doping the oxide with fluorine, the dielectric constant can be reduced to 3.0-3.7, depending on the fluorine concentration [33]. Si-F replaces the Si-OH and Si-H bonds in the oxide; since fluorine is more electronegative, the polarization changes, lowering the dielectric constant. SOG dielectrics (siloxanes, silsesquioxanes) and organic polymers formed by spin coating (polyimides, fluorinated polyimides, bisbenzocyclobutenes), poly(arylethers), or vapor-phase deposition (parylene N, parylene F, teflon) provide dielectric constants in the range of 1.9-3.0 [34]. Most polymers with a dielectric constant less than 3 are stable to only about 350°C. However, a recent publication on laser-evaporated siloxane thin films reports a dielectric constant of 2.0 and thermal stability to 400°C, although integration results were not published [35]. Also, it has been reported that parylene exhibits a high thermal stability [36], and its successful integration into a metal RIE BEOL has been demonstrated [37]. However, damascene integration may be more difficult to achieve because of the softness of parylene films. Spun-on films of materials such as nanoporous silica and xerogels exhibit a higher thermal stability and low dielectric constants (1.3-2.5), depending on their porosity [38], but associated process integration is challenging. There has been increased development activity in plasma-assisted CVD of amorphous carbon and fluorinated carbon films because of their low dielectric constants (2.3-2.7) and thermal stability up to 400°C [39]. Relevant work on insulators having low dielectric constants has been described elsewhere [40].

In this paper, the plasma-assisted CVD of low-dielectric-constant insulators of potential interest at the ULSI level, including fluorine-doped silicon oxide and amorphous carbon and fluorocarbon, was discussed. To be suitable for the deposition of such insulators, plasma-assisted CVD should be applicable at relatively low substrate temperatures, should not damage underlying layers or devices that may be present on the substrate during deposition, and should produce insulators which, in addition to having low dielectric constants, satisfy etching, annealing, planarization, and stability requirements.

2. Fundamentals of PECVD

In thermal CVD, gas-phase reactive species are generated by heating of initial reactants. In plasma CVD, the plasma energy supplied by an external rf source takes the place of the heating to generate the species that subsequently react and deposit on substrate surfaces. Significantly, excessive heating and degradation on the substrate can be avoided by using plasma electron kinetic energy instead of thermal energy. Besides the aspect of generating reactive species at much lower processing temperatures compared to conventional CVD processing, the ion bombardment can be used to modify film characteristics. Plasma CVD processes can be classified into many sub-processes, such as plasma evaporation deposition, plasma sputtering deposition, plasma ion plating, and plasma nitriding. This classification depends on the conditions of the plasma generated, configuration of the vacuum system, location of the substrate, and type of power supply [19-21]. Plasma-assisted CVD processes for semiconductor processing are generally carried out at pressures of 1mTorr to 20Torr substrate temperatures in the range of 100 to 500°C, rf power densities <0.5 W-cm^{-2}, electron densities of 1.0 x 10^{8} to 1.0x10^{12}cm^{-3}, electron mean free paths of <0.1 cm, and average electron energies of 1eV to 6eV.

When the plasma initiates, energy from the rf electric field is coupled into the reactant gases via the kinetic energy of a few free electrons. These electrons gain energy rapidly through the electric field and lose energy slowly through elastic collisions. The high-energy electrons are capable of inelastic collisions that cause the reactant gas molecules to dissociate and ionize, producing secondary electrons by various electron-impact reactions. Table (1) lists typical electron-impact reactions of silane molecules in an rf plasma discharge. In a steady-state discharge, the electrons generated by electron-impact reactions equal those electrons that are lost to the electrode, walls, and reactive species by attachment and recombination reactions [1].

The two important aspects of a plasma glow discharge are the nonequilibrium low-temperature gas-phase chemical reactions that generate radical and ion reactive species in the plasma discharge, and the flux and energy of these reactive species as they reach and strike the surface of the film being deposited. The bombardment of the ionic species on the surface of the film, which controls the surface mobility of the precursor, is the predominant factor in determining film composition, density, stress, and step coverage or conformality at the relatively low temperatures used in plasma CVD. Reactant gases similar to those used for

© 2008 Iraqi Society for Alternative and Renewable Energy Sources and Techniques (I.S.A.R.E.S.T.)

thermal CVD processes are used for plasma CVD to deposit silicon-based dielectrics at lower deposition temperatures.

Table (1) Typical electron-impact reactions of silane molecules in an rf plasma discharge. The asterisk (*) refers to electronic excited state [1]

Reactant	Reaction products	Enthalpy of formation (eV)
$e^- + SiH_4 \rightarrow$	$SiH_2 + H_2 + e^-$	2.2
	$SiH_3 + H + e^-$	4.0
	$Si + 2H_2 + e^-$	4.2
	$SiH + H_2 + H + e^-$	5.7
	$SiH^* + H_2 + H + e^-$	8.9
	$Si^* + 2H_2 + e^-$	9.5
	$SiH_2 + 2H_2 + 2\ e^-$	11.9
	$SiH_3 + H + 2\ e^-$	12.3
	$Si + 2H_2 + 2\ e^-$	13.6
	$SiH + H_2 + H + e^-$	15.3

2.1 Reaction kinetics

Reactions during plasma deposition are complex and not completely understood. Elementary reactions that occur in plasma have been discussed by various authors [41-43]. The initial reaction between electrons and reactant gas molecules or between reactant gas molecules in plasma can be classified as elastic or inelastic. In the elastic collisions, only minimal translational energy transfer occurs between the gas molecules and reactant gases. For plasma processing, the elastic collisions play a less important role in reactant dissociation. Significantly more translational, rotational, vibrational, and electronically excitational energy transfer occurs in the inelastic collisions. The major inelastic reactions among electrons, reactant gases, and surface that occur during plasma-assisted CVD processing are typically represented in Tables (2-4).

Table (2) Initial electron-impact reactions [1]

Excitation (rotational, vibrational, and electronic)	$e^- + A_2 \rightarrow A_2 + e^-$
Dissociative attachment	$e^- + A_2 \rightarrow A^- + A+ + e^-$
Dissociation	$e^- + A_2 \rightarrow 2A \bullet + e^-$
Ionization	$e^- + A_2 \rightarrow A_2+ + 2e^-$
Dissociative ionization	$e^- + A_2 \rightarrow A+ + A + 2e^-$

Some of the inelastic collisions between inert gases and reactants (such as helium or argon with silane) significantly affect the chemical nature of the discharge and the properties of the deposited films [44-46]. In many plasma deposition processes, inert carrier and diluent gases such as helium and argon have been used to form "cooler" plasma, to create more controlled reaction pathways via Penning reactions between carrier and reactant gases [47], and to suppress gas-phase reactions between reactive species. As a result, a plasma diluted with inert gases such as helium can be used to deposit higher-quality insulators.

Table (3) Inelastic reactions among reactants, inert gases, and substrate. M refers to the inert gas or substrate, and A, B, and C refer to the reactant gases [1]

A	
Penning dissociation	$M^* + A_2 \rightarrow 2A \bullet + M$
Penning ionization	$M^* + A_2 \rightarrow A_2^+ + M + e^-$
Ion-ion recombination	$M^- + A_2^+ \rightarrow A_2 + M$
	or
	$M^- + A_2^+ \rightarrow 2A \bullet + M$
Electron-ion recombination	$e^- + A_2^+ \rightarrow 2A \bullet$
	$e^- + A_2^+ + M \rightarrow A_2 + M$
Charge transfer	$M^+ + A_2 \rightarrow A_2^+ + M$
	$M^- + A_2 \rightarrow A_2^- + M$
B	
Collisional detachment	$M^* + A_2^- \rightarrow A_2 + M + e^-$
Associative detachment	$A^- + A \rightarrow A_2 + e^-$
Atom recombination	$2A + M \rightarrow A_2 + M$
Atom abstraction	$A + BC \rightarrow AB + C$
Atom addition	$A + BC + M \rightarrow ABC + M$

Table (4) Heterogeneous reactions between plasma and surface. S refers to the surface in contact with the plasma, and A and B refer to the reactant gases [1]

Atom recombination	$S - A + A \rightarrow S + A_2$
Metastable de-excitation	$S + M^* \rightarrow S + M$
Atom abstraction	$S - B + A \rightarrow S + AB$
Sputtering	$S - B + M^+ \rightarrow S^+ + B + M$
Surface contact ionization	$S + B^* \rightarrow B^+ + e^- + S$

2.2 Deposition Mechanisms

One of the major advantages of plasma deposition processing is its flexibility for depositing films with desirable properties. For conventional thermal CVD processing, physical and chemical properties of the deposited film pertaining to its stress, conformality, density, moisture resistance, and gap-fill properties can be altered by changing the composition and/or type of reactive species. In plasma-assisted CVD, this can be accomplished by varying deposition parameters such as temperature, rf power, pressure, reactant gas mixture ratio, and type of reactant. For example, silicon oxide films deposited with TEOS generally show higher step coverage or conformality than those deposited

 ALL RIGHTS RESERVED PRINTED IN IRAQ

with silane in a plasma-assisted CVD process. For plasma-assisted CVD of silicon oxide films, properties can be modified not only by changing the type of reactive species, but also by the extent of ion bombardment.

In general, the deposition mechanisms for a plasma CVD process can be qualitatively divided into four major steps, as shown in Fig. (1). Step 1 includes the primary initial electron-impact reactions between electron and reactant gases to form ions and radical reactive species (Tables 1 and 2). Next, in step 2, transport of these reactive species occurs from the plasma to the substrate surface concurrently with the occurrence of many elastic and inelastic collisions in both the plasma and sheath regions, classified as ion and radical generation steps [48]. Step 3 is the absorption and/or reaction of reactive species (radical absorption and ion incorporation) onto the substrate surface. Finally, in step 4, the reactive species and/or reaction products incorporate into the deposited films or re-emit from surface back to the gas phase. Because of their complexity, the latter two steps are the least known and least studied aspects of plasma CVD. Significant roles are played by ion bombardment [49] and various heterogeneous reactions between ions and radicals with the depositing surface in the sheath region. The two steps critically affect film properties such as conformality [50], density, stress [51], and "impurity" incorporation.

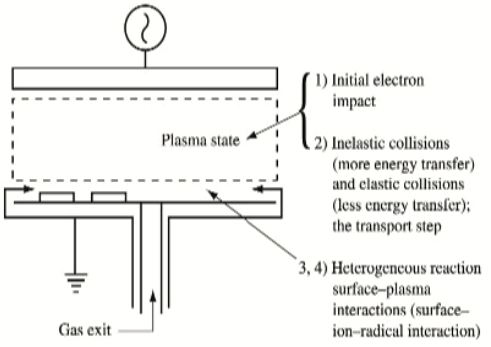

Fig. (1) Four steps that characterize the mechanisms of plasma CVD process [1]

Plasma CVD of amorphous and microcrystalline silicon are the most studied plasma CVD processes, with hundreds of publications on their deposition kinetics and mechanisms. The basic gas-phase chemistry of the silane plasma has been studied by various techniques [49-52]. Different mechanisms have been suggested for the dominant reaction pathway of silicon deposition. One mechanism describes SiH_3 (silyl) radicals playing a dominant role [53], while others describe the decomposition of silane to SiH_2 (silylene) and then SiH_2 insertion into gas-phase SiH_4 to form higher silane species [54] as the main silicon deposition mechanism.

4. Conclusions

We have reviewed the plasma-assisted CVD of dielectric films, with an emphasis on aspects relevant to ULSI semiconductor circuits. In addition, we have indicated that manufacturing needs must be considered early in the process and tool development phase. Obviously, the ultimate goal is to optimize a plasma CVD process for a particular application at the lowest cost of ownership. Future research and development must focus not only on specific technical issues that arise with each new IC generation (such as integration of a stable low-*k* IMD into the BEOL), but also on manufacturability and cost. With 300mm-diameter wafers containing sub-0.25µm semiconductor IC circuits on the horizon, the technical and manufacturing issues are daunting; new challenges are presented to both the semiconductor manufacturers and their equipment suppliers, even for the conventional processes used in IC production.

References

1. S.V. Nguyen, **"Plasma-Assisted Chemical Vapor Deposition",** *Handbook of Thin-Film Deposition Processes and Techniques,* K.K. Schuegraf, Ed., Noyes Publications, Park Ridge, NJ, 1988, pp. 112-141.
2. G.S. Anderson, *J. Appl. Phys.* 33, No. 10, 2991-2992 (1962).
3. L.L. Atl, S.W. Ing, Jr. and K.W. Laendle, *J. Electrochem. Soc.* 110, 465 (1963).
4. S.W. Ing, Jr. and W. Davern, *J. Electrochem. Soc.* 111, 120-122 (1964).
5. A.R. Reinbergh, *Ann. Rev. Mater. Sci.* 9, 341-372 (1979).
6. D.E. Carlson, C.W. Magee and A.R. Triano, *J. Electrochem. Soc.: Solid-State Sci. Technol.* 126, No. 4, 688-691 (1979).
7. S. Sherman et al., *J. Electrochem. Soc.* 144, No. 9, 3198-3204 (1997).
8. H. Randhawa, *Thin Solid Films* 196, 329-349 (1991).
9. J.A. Thornton, *Thin Solid Films* 107, 3-19 (1983).
10. A.T. Bell, *J. Vac. Sci. Technol.* 16, No. 2, 418-419 (1979).
11. R.F. Bunshah, *IEEE Trans. Plasma Sci.* 18, 846-854 (1990).
12. A. Sherman, *Thin Solid Films* 113, 135-149 (1984).
13. S.V. Nguyen, *J. Vac. Sci. Technol. B* 4, No. 5, 1159-1167 (1986).
14. C. Bencher et al., *Solid State Technol.* 40, No. 3, 109-114 (1997).

© 2008 Iraqi Society for Alternative and Renewable Energy Sources and Techniques (I.S.A.R.E.S.T.)

[1] O.A. Hamadi, R.A. Markub and A.A. K. Hadi, "Heat-annealed enhanced-diffusion of silver in gallium arsenide", J. Edu. Al-Mustansiriya Univ., 3 (2001) 35-44.
[2] U.A. Hamadi, M.A.K. Ahmed and R.A. Markub, "Cutting of Ceramic by CW CO_2 Laser", Al-Mustansiriya J. Sci., 12(6) (2001) 307-309.
[3] N.A.K. Al-Rubaiey, O.A. Hamadi and D.N. Raouf, "Effect of gas mixture on output characteristics of a CW CO_2 laser", Iraqi J. Laser, 1(1) (2003) 1-6.
[4] O.A. Hamadi, "Simple arrangement to achieve SHG using a 635nm semiconductor laser", Eng. J. Qatar Univ., 18 (2005) 149-156.
[5] O.A. Hamadi, K.Z. Yahiya and O.N.S. Jassim, "Properties of Silicon Carbide Thin Films Deposited by Vacuum Thermal Evaporation", J. of Semicond. Technol. and Sci., 5(3) (2005) 182-186.
[6] O.A. Hamadi, "Employment some parameters to enhance laser drilling of aluminium", J. Sci. Technol., Sultan Qaboos Univ., 10 (2005) 93-100.
[7] R.A. Ismail, O.A. Abdulrazaq, A.A. Hadi and O.A. Hamadi, "Characterization of Si p-n Photodetectors Produced by Laser-Induced Diffusion", Inter. J. Mod. Phys., 19(31) (2005) 4619-4628.
[8] O.A. Hamadi, "HAZ extent analysis in fiber-reinforced plastic grooving by laser", Iraqi J. Appl. Phys., 1(1) (2005) 1-7.
[9] O.A. Hamadi, "Induced variation of focal length of the lens stimulated in Nd:YAG laser crystal with optical power pumping", Iraqi J. Laser, 2 (2005).
[10] O.A. Hamadi and S.M. Hussain, "Analytical Modelling to Enhance Electric Field Measurement Using Optical Fiber Sensor", Eng. Technol. J., 26 (2006).
[11] O.A. Hamadi and K.S. Khashan, "Effect of Preheating on the Parameters of Laser Keyhole Welding Process: Analytical Study", Iraqi J. Laser, Part A, 5(5) (2006) 11-17.
[12] R.A. Ismail, O.A. Abdulrazaq, A.A. Hadi and O.A. Hamadi, "Full Characterization at 904nm of Si p-n Junction Photodetectors Produced by LID Technique", Euro. Phys. J.: Appl. Phys., 38 (2007) 197-201.
[13] K.S. Khashan and O.A. Hamadi, "Features of spot-matrix surface hardening of low-carbon steel using pulsed laser", J. Eng. Technol., 25(2) (2007).
[14] O.A. Hamadi and K.Z. Yahiya, "Optical and electrical properties of selenium-antimony heterojunction formed on silicon substrate", Sharjah Univ. J. Pure Appl. Sci., 4(2) (2007) 1-11.
[15] B.A. M. Badr, O.A. Hamadi and A.K. Yousif, "Measurement of thermooptic coefficient of semiconductors by single-beam scanning technique", Eng. Technol. J., 27(5) (2007).
[16] O.A. Hamadi, S.M. Hussain, A.A. Hadi and R.O. Mahdi, "Normalized Characteristics of Laser-Induced Diffusion of Arsenic Dopants in Silicon", Eng. Technol. J., 27(4) 2007.
[17] O.A. Hamadi and K.S. Khashan, "Modeling of the Preheating Effect on Keyhole Laser Welding Efficiency", Iraqi J. Appl. Phys. Lett., 1(1) (2008) 10-15.
[18] O.A. Hamadi, B.A.M. Bader and A.K. Yousif, "Electrical Characteristics of Silicon p-n Junction Solar Cells Produced by Plasma-Assisted Matrix Etching Technique", Eng. Technol. J., 28 (2008).
[19] A.A.K. Hadi and O.A. Hamadi, "Optoelectronic Characteristics of As-doped Si Photodetectors Produced by LID Technique", Iraqi J. Appl. Phys. Lett., 1(2) (2008) 23-26.
[20] O.A. Hamadi, "Effect of Annealing on the Electrical Characteristics of CdO-Si Heterostructure Produced by Plasma-Induced Bonding Technique ", Iraqi J. Appl. Phys., 4(3) (2008) 34-37.
[21] O.A. Hamadi, "The Fundamentals of Plasma-Assisted CVD Technique Employed in Thin Films Production", Iraqi J. Appl. Phys. Lett., 1(2) (2008) 3-8.
[22] A.K. Yousif and O.A. Hamadi, "Plasma-Induced Etching of Silicon Surfaces", Bulg. J. Phys., 35(3) (2008) 191-197.
[23] O.A. Hamadi, "Characteristics of CdO-Si Heterostructure Produced by Plasma-Induced Bonding Technique", Proc. IMechE, Part L, J. Mater.: Design and Applications, 222 (2008) 65-71, DOI: 10.1243/14644207JMDA56.
[24] O.A. Hamadi, D.N. Raouf and N.A.-K. Alrubaiey, "Effect of Self-Absorption on the Output Power of CW CO_2 Laser", Iraqi J. Appl. Phys. Lett., 2(1) (2009) 31-34.
[25] O.A. Hamadi, "Profiling of Antimony Diffusivity in Silicon Substrates using Laser-Induced Diffusion Technique", Iraqi J. Appl. Phys. Lett., 3(1) (2010) 23-26.
[26] O.A. Hamadi, N.J. Shakir and F.H. Hussain, "Magnetic Field and Temperature Dependent Measurements of Hall Coefficient in Thermal Evaporated Tin-Doped Cadmium Oxide Thin Films", Bulg. J. Phys., 37(4) (2010) 223-231.
[27] O.A. Hammadi and M.S Edan, "Temperature Dependencies of Refractive Index and Optical Elasticity Coefficient on Lens Induced in Nd:YAG Crystal", Iraqi J. Appl. Phys., 8(1) (2012) 35-41.
[28] O.A. Hammadi, M.K. Khalaf, F.J. Kadhim and B.T. Chiad, "Operation Characteristics of a Closed-Field Unbalanced Dual-Magnetrons Plasma Sputtering System", Bulg. J. Phys., 41(1) (2014) 24-33.

 © ALL RIGHTS RESERVED

[29] O.A. Hammadi and N.I. Naji, "Effect of Acidic Environment on the Spectral Properties of Hibiscus sabdariffa Organic Dye used in Dye-Sensitized Solar Cells", Iraqi J. Appl. Phys., 10(2) (2014) 27-31.
[30] M.K. Khalaf, F.J. Kadhim and O.A. Hammadi, "Effect of Adding Nitrogen to the Gas Mixture on Plasma Characteristics of a Closed-Field Unbalanced DC Magnetron Sputtering System", Iraqi J. Appl. Phys., 10(1) (2014) 27-31.
[31] O.A. Hammadi, "Photovoltaic Properties of Thermally-Grown Selenium-Doped Silicon Photodiodes for Infrared Detection Applications", Phot. Sen., 5(2) (2015) 152-158, DOI: 10.1007/s13320-015-0241-4.
[32] O.A. Hammadi, M.K. Khalaf and F.J. Kadhim, "Fabrication of UV Photodetector from Nickel Oxide Nanoparticles Deposited on Silicon Substrate by Closed-Field Unbalanced Dual Magnetron Sputtering Techniques", Opt. Quant. Electron., 47(12) (2015) 3805-3813, DOI: 10.1007/s11082-015-0247-6
[33] O.A. Hammadi, "Characterization of SiC/Si Heterojunction Fabricated by Plasma-Induced Growth of Nanostructured Silicon Carbide Layer on Silicon Surface", Iraqi J. Appl. Phys., 12(2) (2016) 9-13.
[34] O.A. Hammadi, W.N. Raja, M.A. Saleh and W.A. Altun, "Magnetic Field Distribution of Closed-Field Unbalanced Dual Magnetrons Employed in Plasma Sputtering Systems", Iraqi J. Appl. Phys., 12(3) (2016) 35-42.
[35] O.A. Hammadi, W.N. Raja, M.A. Saleh and W.A. Altun, "Employment of Magnetron to Enhance Langmuir Probe Characteristics of Argon Glow Discharge Plasma in Sputtering System", Iraqi J. Appl. Phys., 12(4) (2016) 19-28.
[36] O.A. Hammadi, M.K. Khalaf and F.J. Kadhim, "Fabrication and Characterization of UV Photodetectors Based on Silicon Nitride Nanostructures Prepared by Magnetron Sputtering", Proc. IMechE, Part N, J. Nanomater. Nanoeng. Nanosys., 230(1) (2016) 32-36, DOI: 10.1177/1740349915610600
[37] O.A. Hammadi and N.E. Naji, "Electrical and spectral characterization of CdS/Si heterojunction prepared by plasma-induced bonding", Opt. Quant. Electron., 48(8) (2016) 375-381, DOI: 10.1007/s11082-016-0647-2
[38] O.A. Hammadi, "Characteristics of Heat-Annealed Silicon Homojunction Infrared Photodetector Fabricated by Plasma-Assisted Technique", Phot. Sen., 6(4) (2016) 345-350, DOI: 10.1007/s13320-016-0338-4
[39] O.A. Hammadi, M.K. Khalaf and F.J. Kadhim, "Silicon Nitride Nanostructures Prepared by Reactive Sputtering Using Closed-Field Unbalanced Dual Magnetrons", Proc. IMechE, Part L, J. Mater.: Design and Applications, 231(5) (2017) 479-487, DOI: 10.1177/1464420715601151
[40] O.A. Hammadi and N.E. Naji, "Fabrication and Characterization of Polycrystalline Nickel Cobaltite Nanostructures Prepared by Plasma Sputtering as Gas Sensor", Phot. Sen., 8(1) (2018) 43-47, DOI: 10.1007/s13320-017-0460-y
[41] O.A. Hammadi, "Production of Nanopowders from Physical Vapor Deposited Films on Nonmetallic Substrates by Conjunctional Freezing-Assisted Ultrasonic Extraction Method", Proc. IMechE, Part N, J. Nanomater. Nanoeng. Nanosys., 232(4) (2018) 135-140, DOI: 10.1177/2397791418807347
[42] O.A. Hammadi, "Nanostructured CdSnSe Thin Films Prepared by DC Plasma Sputtering of Thermally Casted Targets", Iraqi J. Appl. Phys., 14(4) (2018) 33-36.
[43] O.A. Hammadi, "Fabrication of High-Quality Microchannels for Biomedical Applications Using Third-Harmonic Radiation of Nd:YAG Laser", J. Laser Sci. Eng., 10(2) (2018) 61-64.
[44] F.J. Al-Maliki, O.A. Hammadi and E.A. Al-Oubidy, "Optimization of Rutile/Anatase Ratio in Titanium Dioxide Nanostructures prepared by DC Magnetron Sputtering Technique", Iraqi J. Sci., 60 (2019) 91-98.
[45] O.A. Hammadi, "Conjunctional Freezing-Assisted Ultrasonic Extraction of Silicon Dioxide Nanopowders from Thin Films Prepared by Physical Vapor Deposition Technique", Iraqi J. Appl. Phys., 15(4) (2019) 23-28.
[46] O.A. Hammadi, "Synthesis and Characterization of Polycrystalline Carbon Nitride Nanoparticles by Fast Glow Discharge-Induced Reaction of Methane and Ammonia", Adv. in Sci. Eng. Med., 11(5) (2019) 346-350, DOI: https://doi.org/10.1166/asem.2019.2365
[47] O.A. Hammadi, F.J. Kadhim and E.A. Al-Oubidy, "Photocatalytic Activity of Nitrogen-Doped Titanium Dioxide Nanostructures Synthesized by DC Reactive Magnetron Sputtering Technique", Nonlinear Optics, Quantum Optics, 51(1-2) (2019) 67-78.

IRAQI JOURNAL OF APPLIED PHYSICS
Vol. 16, No. 2, April-June 2020, pp. 25-30

Diomar Cesar Lobão
Alex Povitsky

Modeling of Plume Dynamics in Laser Ablation with Application to Nanotubes Synthesis

The aim of this study is to find optimal conditions for the formation of carbon nanotubes in a laser furnace. This paper describe our mathematical model and numerical algorithm, and discuss some of the fluid physics underlying this crucial technology. An axisymmetric unsteady computational gas dynamic model of plume expansion into ambiance has been developed. In the present work the vapor gas phase is modeled using the Relaxing TVD scheme in generalized coordinates. A numerical model of pulsed ablated gas is proposed based on the mass, momentum, and energy conservation laws. The proposed model implements a multi-species formulation for concentration of chemical components combined with the compressible Euler equations. To advance the solution in time, this set of equations is integrated numerically by second order Runge-Kutta scheme.

Keywords: Carbon nanotubes; Laser ablation; Plume dynamics; Runge-Kutta modeling

1. Introduction

Known processes of production of carbon nanotubes include laser ablation (LA), chemical vapor deposition (CVD), and decomposition of high-pressure carbon oxide (HiPco). The practical choice of the process is a trade-off between product quality and quantity. All these processes are controlled by metal catalyst particles that initiate synthesis of carbon nanotubes from feed-stock gas or ejected plume. Similar to the HiPco modeling [7], the LA CFD model is based on the combined Eulerian and Lagrangian approach applied to the tracking of the trajectories of catalyst particles. The Lagrangian approach to track temperature of the catalyst particles in the plume is implemented to evaluate the efficiency of the process. In the laser vaporization process, the feedstock plume loaded with catalyst particles expands explosively into the background gas. The thermal behavior of catalyst particles is critical for nanotubes synthesis.

Available experimental data [1,2] include average plume temperature at a given time moment and the plume geometric shape. Our computational results are in good agreement with these computational and experimental results. There is no available experimental data about temperature of individual catalyst particles. The present code perform very well in very low ambient pressure, pressure of order of 10^6 atm as well as up to 10 atm has been tested.

Shock waves were formed in the ambient gas in the case of the explosive ablation. The propagation of incident and reflected shock waves affects the plume behind it. The plume mixing is caused by the Raleigh–Taylor instability at the plume to gas interface and the baroclinic deposition of vorticity while the reflected shock wave interacts with the plume [7]. For the assessment of the proposed mathematical model and numerical method, numerical results are compared with those obtained in the experiments found in [1,2] where the ambient gas was the inert Argon and the substrate target material was the Carbon Trimmer C3.

2. Governing Equations

The compressible Euler equations written in general curvilinear coordinates x;h for unsteady flows take the following form:

$$\frac{\partial \tilde{Q}}{\partial \tilde{t}} + \frac{\partial \tilde{F}}{\partial \xi} + \frac{\partial \tilde{G}}{\partial \eta} = \tilde{S} \qquad (1)$$

For generality all variables will be non–dimensionalized. Although the parameters used in the non–dimensionalization process are arbitrary, freestream quantities are usually used. Applying a non-dimensionalization to the Euler equations leaves all equations in the same form as before, so they can be viewed as equations in the new non–dimensional variables. The conserved variable vector and fluxes are given as,

$$Q = \frac{\delta}{J}\begin{bmatrix} \rho \\ \rho u \\ \rho v \\ E \\ \rho C_1 \\ \rho C_2 \end{bmatrix} \qquad F = \frac{\delta}{J}\begin{bmatrix} \rho U \\ \rho uU + \xi_x p \\ \rho vU + \xi_y p \\ (E+p)U \\ \rho C_1 U \\ \rho C_2 U \end{bmatrix} \qquad (2)$$

$$G = \frac{\delta}{J}\begin{bmatrix} \rho V \\ \rho uV + \eta_x p \\ \rho vV + \eta_y p \\ (E+p)V \\ \rho C_1 V \\ \rho C_2 V \end{bmatrix} \qquad S = \frac{1}{J}\begin{bmatrix} 0 \\ 0 \\ p \\ 0 \\ 0 \\ 0 \end{bmatrix} \qquad (3)$$

where ρ is the density, m $\rho U \rho V \rho C_1 \rho C_2 T$ is mass, E is total energy per unit volume, p pressure, and $C_1 C_2$ are mass fraction of two species being considered respectively. UV are the contravariant velocities [8] which are in directions normal to constant $\xi\eta$ surfaces respectively, and J $1 x_\xi y_\eta x_\eta y_\xi$ is the Jacobian of

 © ALL RIGHTS RESERVED

A higher temperature is desirable for the STI application, since a more dense film that is highly resistant to subsequent wet-etching steps is thus obtained. These applications are discussed in more detail later in the paper.

When tetraethylorthosilicate (TEOS) is used as the silicon source for PECVD oxide deposition, there is less cusping because of the higher surface mobility of the reactants [22]; however, a void still forms if the gap is small enough, because the conformality of the film is not 100%. This means that the amount of deposition on the sidewalls and bottom of the trench portion of a feature is less than on the top of the feature. So, in order to use PECVD films alone for gap-fill applications, they are typically used in conjunction with an argon sputter etch in a multistep PECVD-argon sputter etch-PECVD sequence described previously [23]. Conformal deposition is more typical for thermal (non-plasma) CVD processes such as low-pressure (LP) CVD at high temperatures or for ozone-TEOS atmospheric or subatmospheric pressure (AP or SA) CVD at lower temperatures (less than 600°C). Furthermore, HDP CVD results in a completely different type of profile because of the "bottom-up" deposition from the simultaneous deposition and etching. The resultant topography from any of these CVD processes plays a decisive role in the choice of subsequent planarization techniques. TEOS was the silicon source for the PECVD and the SACVD, and silane for HDP CVD. The typical "bread-loaf" profile of the PECVD oxide film can be adjusted by varying process parameters such as temperature, pressure, and silicon source. The profile of the SACVD oxide film is conformal, and the unique profile of the HDP CVD oxide film is a result of simultaneous etching and deposition. Note that SACVD is a non-plasma process.

Typically, thermal CVD processes such as LPCVD BPSG, APCVD (or SACVD) BPSG, or PSG are used to passivate the polysilicon/metal silicide gate conductor for sub-half-micron devices because of their high-aspect-ratio fill capability compared to plasma CVD processes and because there are no plasma damage concerns with thermal CVD processing. Process-induced IC device damage from plasma processing (in particular at the gate-conductor level, because there is no device protection) is a critical issue for the PECVD passivation dielectrics. Briefly, low process pressure during deposition of the PECVD PSG was identified as the main factor causing gate-oxide charge damage. Increasing the pressure for the PECVD PSG process regardless of dopant source (trimethylphosphite or triethylphosphate) resulted in no charge damage on antenna test sites and device structures. A more recent study describes another technique used to optimize a PECVD PSG process for plasma damage designated as corona oxide semiconductor (COS) charge measurement [24]. The technique, combined with the antenna test structure method of measuring plasma damage, provides a fast and cost-effective way to optimize plasma CVD processes.

Doped silicon oxide films such as PSG or BPSG are preferred for gate-conductor passivation because of their mobile ion barrier properties [25], low reflow temperature for local planarization (applies to BPSG only), high etch selectivity to the underlying barrier layer (e.g., nitride [26]), and faster polishing rate compared to undoped silicon oxide. In this paper, we discuss our recent work with HDP CVD PSG including gap-fill and plasma damage results. We have previously published an overview of our own work and that of others in IBM on relevant thermal CVD processes and applications [27].

The gap-fill requirement for dielectrics in the "back-end-of-line" (BEOL) depends on the interconnect fabrication methods used. Multilevel interconnects usually involve two types of planarization methods: the planarization of interlayer dielectrics and the planarization of metal layers. For the former, for example, an Al(Cu)-based layer is patterned into lines and the insulator is deposited between the spaces and above the lines. Therefore, a critical requirement in this case is the filling of the gaps between the lines without void formation. Void-free filling of high-aspect-ratio features is not a simple matter and requires the use of advanced insulator deposition processes such as HDP CVD. For submicron metal interconnect fabrication, the insulator deposition is generally followed by partial planarization using spin-on-glass (SOG) [28], a resist etch-back [29], or a global planarization using, for example, chemical-mechanical polishing (CMP). For the planarization of metal layers, the damascene technique is most commonly used; several papers reporting its use in IBM have been published [30]. Using this technique, a dielectric such as silicon oxide is deposited on a planar surface and the wiring level is patterned into the dielectric using photolithography and RIE. A thin metal liner and a metal such as tungsten (or aluminum or copper) are then deposited on the patterned dielectric and subsequently planarized by CMP, stopping on the dielectric and leaving metal in the patterned features. Therefore, in the damascene technique, the metal rather than the insulator must fill the high-aspect-ratio features.

A critical film parameter for both interconnect fabrication techniques is the

 ALL RIGHTS RESERVED PRINTED IN IRAQ

dielectric constant (k) of the IMD material. Use of a material having a lower dielectric constant leads to lower total capacitance, decreasing the interconnection delay and power dissipation [31], and thus enhancing performance. To achieve long-range interconnection performance objectives, low-dielectric-constant IMD will be required [32]. The dielectric constant of PECVD silicon oxide is typically 4.1-4.2. By doping the oxide with fluorine, the dielectric constant can be reduced to 3.0-3.7, depending on the fluorine concentration [33]. Si-F replaces the Si-OH and Si-H bonds in the oxide; since fluorine is more electronegative, the polarization changes, lowering the dielectric constant. SOG dielectrics (siloxanes, silsesquioxanes) and organic polymers formed by spin coating (polyimides, fluorinated polyimides, bisbenzocyclobutenes), poly(arylethers), or vapor-phase deposition (parylene N, parylene F, teflon) provide dielectric constants in the range of 1.9-3.0 [34]. Most polymers with a dielectric constant less than 3 are stable to only about 350°C. However, a recent publication on laser-evaporated siloxane thin films reports a dielectric constant of 2.0 and thermal stability to 400°C, although integration results were not published [35]. Also, it has been reported that parylene exhibits a high thermal stability [36], and its successful integration into a metal RIE BEOL has been demonstrated [37]. However, damascene integration may be more difficult to achieve because of the softness of parylene films. Spun-on films of materials such as nanoporous silica and xerogels exhibit a higher thermal stability and low dielectric constants (1.3-2.5), depending on their porosity [38], but associated process integration is challenging. There has been increased development activity in plasma-assisted CVD of amorphous carbon and fluorinated carbon films because of their low dielectric constants (2.3-2.7) and thermal stability up to 400°C [39]. Relevant work on insulators having low dielectric constants has been described elsewhere [40].

In this paper, the plasma-assisted CVD of low-dielectric-constant insulators of potential interest at the ULSI level, including fluorine-doped silicon oxide and amorphous carbon and fluorocarbon, was discussed. To be suitable for the deposition of such insulators, plasma-assisted CVD should be applicable at relatively low substrate temperatures, should not damage underlying layers or devices that may be present on the substrate during deposition, and should produce insulators which, in addition to having low dielectric constants, satisfy etching, annealing, planarization, and stability requirements.

2. Fundamentals of PECVD

In thermal CVD, gas-phase reactive species are generated by heating of initial reactants. In plasma CVD, the plasma energy supplied by an external rf source takes the place of the heating to generate the species that subsequently react and deposit on substrate surfaces. Significantly, excessive heating and degradation on the substrate can be avoided by using plasma electron kinetic energy instead of thermal energy. Besides the aspect of generating reactive species at much lower processing temperatures compared to conventional CVD processing, the ion bombardment can be used to modify film characteristics. Plasma CVD processes can be classified into many sub-processes, such as plasma evaporation deposition, plasma sputtering deposition, plasma ion plating, and plasma nitriding. This classification depends on the conditions of the plasma generated, configuration of the vacuum system, location of the substrate, and type of power supply [19-21]. Plasma-assisted CVD processes for semiconductor processing are generally carried out at pressures of 1mTorr to 20Torr substrate temperatures in the range of 100 to 500°C, rf power densities <0.5 W-cm^{-2}, electron densities of 1.0 x 10^{8} to 1.0x10^{12}cm^{-3}, electron mean free paths of <0.1 cm, and average electron energies of 1eV to 6eV.

When the plasma initiates, energy from the rf electric field is coupled into the reactant gases via the kinetic energy of a few free electrons. These electrons gain energy rapidly through the electric field and lose energy slowly through elastic collisions. The high-energy electrons are capable of inelastic collisions that cause the reactant gas molecules to dissociate and ionize, producing secondary electrons by various electron-impact reactions. Table (1) lists typical electron-impact reactions of silane molecules in an rf plasma discharge. In a steady-state discharge, the electrons generated by electron-impact reactions equal those electrons that are lost to the electrode, walls, and reactive species by attachment and recombination reactions [1].

The two important aspects of a plasma glow discharge are the nonequilibrium low-temperature gas-phase chemical reactions that generate radical and ion reactive species in the plasma discharge, and the flux and energy of these reactive species as they reach and strike the surface of the film being deposited. The bombardment of the ionic species on the surface of the film, which controls the surface mobility of the precursor, is the predominant factor in determining film composition, density, stress, and step coverage or conformality at the relatively low temperatures used in plasma CVD. Reactant gases similar to those used for

© 2008 Iraqi Society for Alternative and Renewable Energy Sources and Techniques (I.S.A.R.E.S.T.)

thermal CVD processes are used for plasma CVD to deposit silicon-based dielectrics at lower deposition temperatures.

Table (1) Typical electron-impact reactions of silane molecules in an rf plasma discharge. The asterisk (*) refers to electronic excited state [1]

Reactant	Reaction products	Enthalpy of formation (eV)
$e^- + SiH_4 \rightarrow$	$SiH_2 + H_2 + e^-$	2.2
	$SiH_3 + H + e^-$	4.0
	$Si + 2H_2 + e^-$	4.2
	$SiH + H_2 + H + e^-$	5.7
	$SiH^* + H_2 + H + e^-$	8.9
	$Si^* + 2H_2 + e^-$	9.5
	$SiH_2 + 2H_2 + 2\ e^-$	11.9
	$SiH_3 + H + 2\ e^-$	12.3
	$Si + 2H_2 + 2\ e^-$	13.6
	$SiH + H_2 + H + e^-$	15.3

2.1 Reaction kinetics

Reactions during plasma deposition are complex and not completely understood. Elementary reactions that occur in plasma have been discussed by various authors [41-43]. The initial reaction between electrons and reactant gas molecules or between reactant gas molecules in plasma can be classified as elastic or inelastic. In the elastic collisions, only minimal translational energy transfer occurs between the gas molecules and reactant gases. For plasma processing, the elastic collisions play a less important role in reactant dissociation. Significantly more translational, rotational, vibrational, and electronically excitational energy transfer occurs in the inelastic collisions. The major inelastic reactions among electrons, reactant gases, and surface that occur during plasma-assisted CVD processing are typically represented in Tables (2-4).

Table (2) Initial electron-impact reactions [1]

Excitation (rotational, vibrational, and electronic)	$e^- + A_2 \rightarrow A_2 + e^-$
Dissociative attachment	$e^- + A_2 \rightarrow A^- + A+ + e^-$
Dissociation	$e^- + A_2 \rightarrow 2A \bullet + e^-$
Ionization	$e^- + A_2 \rightarrow A_2+ + 2e^-$
Dissociative ionization	$e^- + A_2 \rightarrow A+ + A + 2e^-$

Some of the inelastic collisions between inert gases and reactants (such as helium or argon with silane) significantly affect the chemical nature of the discharge and the properties of the deposited films [44-46]. In many plasma deposition processes, inert carrier and diluent gases such as helium and argon have been used to form "cooler" plasma, to create more controlled reaction pathways via Penning reactions between carrier and reactant gases [47], and to suppress gas-phase reactions between reactive species. As a result, a plasma diluted with inert gases such as helium can be used to deposit higher-quality insulators.

Table (3) Inelastic reactions among reactants, inert gases, and substrate. M refers to the inert gas or substrate, and A, B, and C refer to the reactant gases [1]

A	
Penning dissociation	$M^* + A_2 \rightarrow 2A \bullet + M$
Penning ionization	$M^* + A_2 \rightarrow A_2^+ + M + e^-$
Ion-ion recombination	$M^- + A_2^+ \rightarrow A_2 + M$
	or
	$M^- + A_2^+ \rightarrow 2A \bullet + M$
Electron-ion recombination	$e^- + A_2^+ \rightarrow 2A \bullet$
	$e^- + A_2^+ + M \rightarrow A_2 + M$
Charge transfer	$M^+ + A_2 \rightarrow A_2^+ + M$
	$M^- + A_2 \rightarrow A_2^- + M$
B	
Collisional detachment	$M^* + A_2^- \rightarrow A_2 + M + e^-$
Associative detachment	$A^- + A \rightarrow A_2 + e^-$
Atom recombination	$2A + M \rightarrow A_2 + M$
Atom abstraction	$A + BC \rightarrow AB + C$
Atom addition	$A + BC + M \rightarrow ABC + M$

Table (4) Heterogeneous reactions between plasma and surface. S refers to the surface in contact with the plasma, and A and B refer to the reactant gases [1]

Atom recombination	$S - A + A \rightarrow S + A_2$
Metastable de-excitation	$S + M^* \rightarrow S + M$
Atom abstraction	$S - B + A \rightarrow S + AB$
Sputtering	$S - B + M^+ \rightarrow S^+ + B + M$
Surface contact ionization	$S + B^* \rightarrow B^+ + e^- + S$

2.2 Deposition Mechanisms

One of the major advantages of plasma deposition processing is its flexibility for depositing films with desirable properties. For conventional thermal CVD processing, physical and chemical properties of the deposited film pertaining to its stress, conformality, density, moisture resistance, and gap-fill properties can be altered by changing the composition and/or type of reactive species. In plasma-assisted CVD, this can be accomplished by varying deposition parameters such as temperature, rf power, pressure, reactant gas mixture ratio, and type of reactant. For example, silicon oxide films deposited with TEOS generally show higher step coverage or conformality than those deposited

 ALL RIGHTS RESERVED PRINTED IN IRAQ

with silane in a plasma-assisted CVD process. For plasma-assisted CVD of silicon oxide films, properties can be modified not only by changing the type of reactive species, but also by the extent of ion bombardment.

In general, the deposition mechanisms for a plasma CVD process can be qualitatively divided into four major steps, as shown in Fig. (1). Step 1 includes the primary initial electron-impact reactions between electron and reactant gases to form ions and radical reactive species (Tables 1 and 2). Next, in step 2, transport of these reactive species occurs from the plasma to the substrate surface concurrently with the occurrence of many elastic and inelastic collisions in both the plasma and sheath regions, classified as ion and radical generation steps [48]. Step 3 is the absorption and/or reaction of reactive species (radical absorption and ion incorporation) onto the substrate surface. Finally, in step 4, the reactive species and/or reaction products incorporate into the deposited films or re-emit from surface back to the gas phase. Because of their complexity, the latter two steps are the least known and least studied aspects of plasma CVD. Significant roles are played by ion bombardment [49] and various heterogeneous reactions between ions and radicals with the depositing surface in the sheath region. The two steps critically affect film properties such as conformality [50], density, stress [51], and "impurity" incorporation.

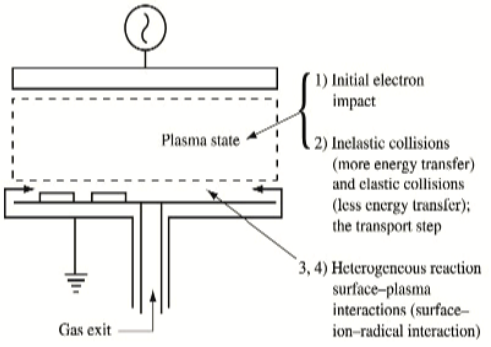

Fig. (1) Four steps that characterize the mechanisms of plasma CVD process [1]

Plasma CVD of amorphous and microcrystalline silicon are the most studied plasma CVD processes, with hundreds of publications on their deposition kinetics and mechanisms. The basic gas-phase chemistry of the silane plasma has been studied by various techniques [49-52]. Different mechanisms have been suggested for the dominant reaction pathway of silicon deposition. One mechanism describes SiH_3 (silyl) radicals playing a dominant role [53], while others describe the decomposition of silane to SiH_2 (silylene) and then SiH_2 insertion into gas-phase SiH_4 to form higher silane species [54] as the main silicon deposition mechanism.

4. Conclusions

We have reviewed the plasma-assisted CVD of dielectric films, with an emphasis on aspects relevant to ULSI semiconductor circuits. In addition, we have indicated that manufacturing needs must be considered early in the process and tool development phase. Obviously, the ultimate goal is to optimize a plasma CVD process for a particular application at the lowest cost of ownership. Future research and development must focus not only on specific technical issues that arise with each new IC generation (such as integration of a stable low-*k* IMD into the BEOL), but also on manufacturability and cost. With 300mm-diameter wafers containing sub-0.25µm semiconductor IC circuits on the horizon, the technical and manufacturing issues are daunting; new challenges are presented to both the semiconductor manufacturers and their equipment suppliers, even for the conventional processes used in IC production.

References

1. S.V. Nguyen, **"Plasma-Assisted Chemical Vapor Deposition",** *Handbook of Thin-Film Deposition Processes and Techniques,* K.K. Schuegraf, Ed., Noyes Publications, Park Ridge, NJ, 1988, pp. 112-141.
2. G.S. Anderson, *J. Appl. Phys.* 33, No. 10, 2991-2992 (1962).
3. L.L. Atl, S.W. Ing, Jr. and K.W. Laendle, *J. Electrochem. Soc.* 110, 465 (1963).
4. S.W. Ing, Jr. and W. Davern, *J. Electrochem. Soc.* 111, 120-122 (1964).
5. A.R. Reinbergh, *Ann. Rev. Mater. Sci.* 9, 341-372 (1979).
6. D.E. Carlson, C.W. Magee and A.R. Triano, *J. Electrochem. Soc.: Solid-State Sci. Technol.* 126, No. 4, 688-691 (1979).
7. S. Sherman et al., *J. Electrochem. Soc.* 144, No. 9, 3198-3204 (1997).
8. H. Randhawa, *Thin Solid Films* 196, 329-349 (1991).
9. J.A. Thornton, *Thin Solid Films* 107, 3-19 (1983).
10. A.T. Bell, *J. Vac. Sci. Technol.* 16, No. 2, 418-419 (1979).
11. R.F. Bunshah, *IEEE Trans. Plasma Sci.* 18, 846-854 (1990).
12. A. Sherman, *Thin Solid Films* 113, 135-149 (1984).
13. S.V. Nguyen, *J. Vac. Sci. Technol. B* 4, No. 5, 1159-1167 (1986).
14. C. Bencher et al., *Solid State Technol.* 40, No. 3, 109-114 (1997).

© 2008 Iraqi Society for Alternative and Renewable Energy Sources and Techniques (I.S.A.R.E.S.T.)

[1] O.A. Hamadi, R.A. Markub and A.A. K. Hadi, "Heat-annealed enhanced-diffusion of silver in gallium arsenide", J. Edu. Al-Mustansiriya Univ., 3 (2001) 35-44.
[2] U.A. Hamadi, M.A.K. Ahmed and R.A. Markub, "Cutting of Ceramic by CW CO_2 Laser", Al-Mustansiriya J. Sci., 12(6) (2001) 307-309.
[3] N.A.K. Al-Rubaiey, O.A. Hamadi and D.N. Raouf, "Effect of gas mixture on output characteristics of a CW CO_2 laser", Iraqi J. Laser, 1(1) (2003) 1-6.
[4] O.A. Hamadi, "Simple arrangement to achieve SHG using a 635nm semiconductor laser", Eng. J. Qatar Univ., 18 (2005) 149-156.
[5] O.A. Hamadi, K.Z. Yahiya and O.N.S. Jassim, "Properties of Silicon Carbide Thin Films Deposited by Vacuum Thermal Evaporation", J. of Semicond. Technol. and Sci., 5(3) (2005) 182-186.
[6] O.A. Hamadi, "Employment some parameters to enhance laser drilling of aluminium", J. Sci. Technol., Sultan Qaboos Univ., 10 (2005) 93-100.
[7] R.A. Ismail, O.A. Abdulrazaq, A.A. Hadi and O.A. Hamadi, "Characterization of Si p-n Photodetectors Produced by Laser-Induced Diffusion", Inter. J. Mod. Phys., 19(31) (2005) 4619-4628.
[8] O.A. Hamadi, "HAZ extent analysis in fiber-reinforced plastic grooving by laser", Iraqi J. Appl. Phys., 1(1) (2005) 1-7.
[9] O.A. Hamadi, "Induced variation of focal length of the lens stimulated in Nd:YAG laser crystal with optical power pumping", Iraqi J. Laser, 2 (2005).
[10] O.A. Hamadi and S.M. Hussain, "Analytical Modelling to Enhance Electric Field Measurement Using Optical Fiber Sensor", Eng. Technol. J., 26 (2006).
[11] O.A. Hamadi and K.S. Khashan, "Effect of Preheating on the Parameters of Laser Keyhole Welding Process: Analytical Study", Iraqi J. Laser, Part A, 5(5) (2006) 11-17.
[12] R.A. Ismail, O.A. Abdulrazaq, A.A. Hadi and O.A. Hamadi, "Full Characterization at 904nm of Si p-n Junction Photodetectors Produced by LID Technique", Euro. Phys. J.: Appl. Phys., 38 (2007) 197-201.
[13] K.S. Khashan and O.A. Hamadi, "Features of spot-matrix surface hardening of low-carbon steel using pulsed laser", J. Eng. Technol., 25(2) (2007).
[14] O.A. Hamadi and K.Z. Yahiya, "Optical and electrical properties of selenium-antimony heterojunction formed on silicon substrate", Sharjah Univ. J. Pure Appl. Sci., 4(2) (2007) 1-11.
[15] B.A. M. Badr, O.A. Hamadi and A.K. Yousif, "Measurement of thermooptic coefficient of semiconductors by single-beam scanning technique", Eng. Technol. J., 27(5) (2007).
[16] O.A. Hamadi, S.M. Hussain, A.A. Hadi and R.O. Mahdi, "Normalized Characteristics of Laser-Induced Diffusion of Arsenic Dopants in Silicon", Eng. Technol. J., 27(4) 2007.
[17] O.A. Hamadi and K.S. Khashan, "Modeling of the Preheating Effect on Keyhole Laser Welding Efficiency", Iraqi J. Appl. Phys. Lett., 1(1) (2008) 10-15.
[18] O.A. Hamadi, B.A.M. Bader and A.K. Yousif, "Electrical Characteristics of Silicon p-n Junction Solar Cells Produced by Plasma-Assisted Matrix Etching Technique", Eng. Technol. J., 28 (2008).
[19] A.A.K. Hadi and O.A. Hamadi, "Optoelectronic Characteristics of As-doped Si Photodetectors Produced by LID Technique", Iraqi J. Appl. Phys. Lett., 1(2) (2008) 23-26.
[20] O.A. Hamadi, "Effect of Annealing on the Electrical Characteristics of CdO-Si Heterostructure Produced by Plasma-Induced Bonding Technique ", Iraqi J. Appl. Phys., 4(3) (2008) 34-37.
[21] O.A. Hamadi, "The Fundamentals of Plasma-Assisted CVD Technique Employed in Thin Films Production", Iraqi J. Appl. Phys. Lett., 1(2) (2008) 3-8.
[22] A.K. Yousif and O.A. Hamadi, "Plasma-Induced Etching of Silicon Surfaces", Bulg. J. Phys., 35(3) (2008) 191-197.
[23] O.A. Hamadi, "Characteristics of CdO-Si Heterostructure Produced by Plasma-Induced Bonding Technique", Proc. IMechE, Part L, J. Mater.: Design and Applications, 222 (2008) 65-71, DOI: 10.1243/14644207JMDA56.
[24] O.A. Hamadi, D.N. Raouf and N.A.-K. Alrubaiey, "Effect of Self-Absorption on the Output Power of CW CO_2 Laser", Iraqi J. Appl. Phys. Lett., 2(1) (2009) 31-34.
[25] O.A. Hamadi, "Profiling of Antimony Diffusivity in Silicon Substrates using Laser-Induced Diffusion Technique", Iraqi J. Appl. Phys. Lett., 3(1) (2010) 23-26.
[26] O.A. Hamadi, N.J. Shakir and F.H. Hussain, "Magnetic Field and Temperature Dependent Measurements of Hall Coefficient in Thermal Evaporated Tin-Doped Cadmium Oxide Thin Films", Bulg. J. Phys., 37(4) (2010) 223-231.
[27] O.A. Hammadi and M.S Edan, "Temperature Dependencies of Refractive Index and Optical Elasticity Coefficient on Lens Induced in Nd:YAG Crystal", Iraqi J. Appl. Phys., 8(1) (2012) 35-41.
[28] O.A. Hammadi, M.K. Khalaf, F.J. Kadhim and B.T. Chiad, "Operation Characteristics of a Closed-Field Unbalanced Dual-Magnetrons Plasma Sputtering System", Bulg. J. Phys., 41(1) (2014) 24-33.

 © ALL RIGHTS RESERVED

[29] O.A. Hammadi and N.I. Naji, "Effect of Acidic Environment on the Spectral Properties of Hibiscus sabdariffa Organic Dye used in Dye-Sensitized Solar Cells", Iraqi J. Appl. Phys., 10(2) (2014) 27-31.
[30] M.K. Khalaf, F.J. Kadhim and O.A. Hammadi, "Effect of Adding Nitrogen to the Gas Mixture on Plasma Characteristics of a Closed-Field Unbalanced DC Magnetron Sputtering System", Iraqi J. Appl. Phys., 10(1) (2014) 27-31.
[31] O.A. Hammadi, "Photovoltaic Properties of Thermally-Grown Selenium-Doped Silicon Photodiodes for Infrared Detection Applications", Phot. Sen., 5(2) (2015) 152-158, DOI: 10.1007/s13320-015-0241-4.
[32] O.A. Hammadi, M.K. Khalaf and F.J. Kadhim, "Fabrication of UV Photodetector from Nickel Oxide Nanoparticles Deposited on Silicon Substrate by Closed-Field Unbalanced Dual Magnetron Sputtering Techniques", Opt. Quant. Electron., 47(12) (2015) 3805-3813, DOI: 10.1007/s11082-015-0247-6
[33] O.A. Hammadi, "Characterization of SiC/Si Heterojunction Fabricated by Plasma-Induced Growth of Nanostructured Silicon Carbide Layer on Silicon Surface", Iraqi J. Appl. Phys., 12(2) (2016) 9-13.
[34] O.A. Hammadi, W.N. Raja, M.A. Saleh and W.A. Altun, "Magnetic Field Distribution of Closed-Field Unbalanced Dual Magnetrons Employed in Plasma Sputtering Systems", Iraqi J. Appl. Phys., 12(3) (2016) 35-42.
[35] O.A. Hammadi, W.N. Raja, M.A. Saleh and W.A. Altun, "Employment of Magnetron to Enhance Langmuir Probe Characteristics of Argon Glow Discharge Plasma in Sputtering System", Iraqi J. Appl. Phys., 12(4) (2016) 19-28.
[36] O.A. Hammadi, M.K. Khalaf and F.J. Kadhim, "Fabrication and Characterization of UV Photodetectors Based on Silicon Nitride Nanostructures Prepared by Magnetron Sputtering", Proc. IMechE, Part N, J. Nanomater. Nanoeng. Nanosys., 230(1) (2016) 32-36, DOI: 10.1177/1740349915610600
[37] O.A. Hammadi and N.E. Naji, "Electrical and spectral characterization of CdS/Si heterojunction prepared by plasma-induced bonding", Opt. Quant. Electron., 48(8) (2016) 375-381, DOI: 10.1007/s11082-016-0647-2
[38] O.A. Hammadi, "Characteristics of Heat-Annealed Silicon Homojunction Infrared Photodetector Fabricated by Plasma-Assisted Technique", Phot. Sen., 6(4) (2016) 345-350, DOI: 10.1007/s13320-016-0338-4
[39] O.A. Hammadi, M.K. Khalaf and F.J. Kadhim, "Silicon Nitride Nanostructures Prepared by Reactive Sputtering Using Closed-Field Unbalanced Dual Magnetrons", Proc. IMechE, Part L, J. Mater.: Design and Applications, 231(5) (2017) 479-487, DOI: 10.1177/1464420715601151
[40] O.A. Hammadi and N.E. Naji, "Fabrication and Characterization of Polycrystalline Nickel Cobaltite Nanostructures Prepared by Plasma Sputtering as Gas Sensor", Phot. Sen., 8(1) (2018) 43-47, DOI: 10.1007/s13320-017-0460-y
[41] O.A. Hammadi, "Production of Nanopowders from Physical Vapor Deposited Films on Nonmetallic Substrates by Conjunctional Freezing-Assisted Ultrasonic Extraction Method", Proc. IMechE, Part N, J. Nanomater. Nanoeng. Nanosys., 232(4) (2018) 135-140, DOI: 10.1177/2397791418807347
[42] O.A. Hammadi, "Nanostructured CdSnSe Thin Films Prepared by DC Plasma Sputtering of Thermally Casted Targets", Iraqi J. Appl. Phys., 14(4) (2018) 33-36.
[43] O.A. Hammadi, "Fabrication of High-Quality Microchannels for Biomedical Applications Using Third-Harmonic Radiation of Nd:YAG Laser", J. Laser Sci. Eng., 10(2) (2018) 61-64.
[44] F.J. Al-Maliki, O.A. Hammadi and E.A. Al-Oubidy, "Optimization of Rutile/Anatase Ratio in Titanium Dioxide Nanostructures prepared by DC Magnetron Sputtering Technique", Iraqi J. Sci., 60 (2019) 91-98.
[45] O.A. Hammadi, "Conjunctional Freezing-Assisted Ultrasonic Extraction of Silicon Dioxide Nanopowders from Thin Films Prepared by Physical Vapor Deposition Technique", Iraqi J. Appl. Phys., 15(4) (2019) 23-28.
[46] O.A. Hammadi, "Synthesis and Characterization of Polycrystalline Carbon Nitride Nanoparticles by Fast Glow Discharge-Induced Reaction of Methane and Ammonia", Adv. in Sci. Eng. Med., 11(5) (2019) 346-350, DOI: https://doi.org/10.1166/asem.2019.2365
[47] O.A. Hammadi, F.J. Kadhim and E.A. Al-Oubidy, "Photocatalytic Activity of Nitrogen-Doped Titanium Dioxide Nanostructures Synthesized by DC Reactive Magnetron Sputtering Technique", Nonlinear Optics, Quantum Optics, 51(1-2) (2019) 67-78.

IRAQI JOURNAL OF APPLIED PHYSICS
Vol. 16, No. 2, April-June 2020, pp. 31-36

Th. Schwarz-Selinger
David G. Cahill
S.-C. Chen
S.-J. Moon
C. P. Grigoropoulos

Micron-Scale Modifications of Silicon Surface Morphology by Pulsed-Laser Texturing

The morphologies of Si surfaces are modified with single, tightly-focused nanosecond laser pulses and characterized by atomic force microscopy (AFM). Dimple-shaped features with diameters 1–4 μm and depths 1–300 nm are produced by varying the laser-spot diameter and the peak energy densities F0 in the range 0.4 < F0 < 1.3 J cm−2. Greater control of the depth of shallow dimples and quantitative comparison of theory and experiment is enabled by first removing the native oxide of Si with dilute HF acid. We develop approximate analytical solutions for two-dimensional fluid-flow driven by gradients in the surface tension; these solutions provide fundamental insight on how the morphology depends on laser parameters and the thermophysical properties of the melt and its surface. Quantitative comparisons between theory and experiment are enabled by using numerical simulations of heat flow in one-dimension as inputs to the analytical fluid-flow equations; we find good agreement with AFM data for the dimple shape and depth.

Keywords: Pulsed-laser texturing; Surface modification; Morphology; Silicon surface

1. Introduction

Micron-scale modifications of NiP_x hard-disk substrates by laser processing was demonstrated nearly 10 years ago [1]. Since that time, the process of "laser zone texturing" has become established as a standard manufacturing tool for controlling friction in the landing zone of the disk. Laser texturing does not rely on material removal—as, for example, is the case for laser-drilling or laser-ablation—but on hydrodynamic redistribution of the molten region produced by inhomogeneous heating. Temperature gradients at the surface of the melt produce gradients in the surface tension that, in most cases, drive fluid from the hot center of the melt to the cold periphery. A dimple-shaped feature is typically observed after resolidification [2,3]. Laser texturing is a particularly powerful method for creating subtle changes in morphology with good control over the lateral and vertical dimensions of the surface feature [4].

Although laser texturing of NiP_x has significant technological relevance, a quantitative understanding of the process is hampered by the lack of key data for the high temperature thermophysical properties of NiP_x and the complexity of the surface properties of this metastable amorphous alloy. Our study of laser texturing of Si is motivated by the opportunity for greater scientific understanding: most of the thermophysical and surface properties of Si are known and therefore we can more critically confront theory with the results of experiment. Using Si, we can remove the native oxide and produce hydrogen termination of the surface by treatment with hydrofluoric (HF) acid; this surface preparation allows us to isolate the role of desorption of surface contaminants in laser texturing.

We have found that laser texturing provides a convenient and flexible method for modifying the morphology of Si substrates and we are applying laser textured Si wafers in other experiments on the physics of epitaxial crystal growth and mass-transport on clean crystal surfaces; laser texturing avoids the contamination and substrate damage that is sometimes produced by lithographic processing and plasma etching. Our analytical model for the dimple shape and depth, see Sec. IV, allows us to quantitatively understand how the geometry of the surface feature is controlled by the lateral distribution of energy density in the focused laser beam.

2. Experimental Details

Our apparatus (at U. Illinois) for laser texturing uses a diode-pumped, passively Q-switched and frequency doubled (532 nm) neodymium yttrium aluminum garnet (Nd:YAG) laser that generates nanosecond pulses (full width-half-maximum FWHM _ 1 ns) with a repetition rate of 17 kHz. We select a single pulse from the pulse train with an acousto-optic modulator; only the first order diffracted beam passes through a first aperture. Our standard configuration uses a ×5 beam expansion that produces a $1/e^2$ intensity radius at the back-focal plane of the objective lens of w_0 = 4.1 mm. We truncate this beam with a second aperture of radius a _ 1.5mm to control the energy density at the surface of the sample. In most cases, the focal length of the objective lens is f = 10 mm; this combination of beam expansion, truncation, and f produces a $1/e^2$ beam diameter on the surface of 2w _ 3 μm. For selected experiments, we use other combinations of the beam expansion and objective lenses to create laser spots of diameter 1, 2, and 4 μm; in these cases, the energy of the pulse is attenuated by neutral density filters.

 © ALL RIGHTS RESERVED

A higher temperature is desirable for the STI application, since a more dense film that is highly resistant to subsequent wet-etching steps is thus obtained. These applications are discussed in more detail later in the paper.

When tetraethylorthosilicate (TEOS) is used as the silicon source for PECVD oxide deposition, there is less cusping because of the higher surface mobility of the reactants [22]; however, a void still forms if the gap is small enough, because the conformality of the film is not 100%. This means that the amount of deposition on the sidewalls and bottom of the trench portion of a feature is less than on the top of the feature. So, in order to use PECVD films alone for gap-fill applications, they are typically used in conjunction with an argon sputter etch in a multistep PECVD-argon sputter etch-PECVD sequence described previously [23]. Conformal deposition is more typical for thermal (non-plasma) CVD processes such as low-pressure (LP) CVD at high temperatures or for ozone-TEOS atmospheric or subatmospheric pressure (AP or SA) CVD at lower temperatures (less than 600°C). Furthermore, HDP CVD results in a completely different type of profile because of the "bottom-up" deposition from the simultaneous deposition and etching. The resultant topography from any of these CVD processes plays a decisive role in the choice of subsequent planarization techniques. TEOS was the silicon source for the PECVD and the SACVD, and silane for HDP CVD. The typical "bread-loaf" profile of the PECVD oxide film can be adjusted by varying process parameters such as temperature, pressure, and silicon source. The profile of the SACVD oxide film is conformal, and the unique profile of the HDP CVD oxide film is a result of simultaneous etching and deposition. Note that SACVD is a non-plasma process.

Typically, thermal CVD processes such as LPCVD BPSG, APCVD (or SACVD) BPSG, or PSG are used to passivate the polysilicon/metal silicide gate conductor for sub-half-micron devices because of their high-aspect-ratio fill capability compared to plasma CVD processes and because there are no plasma damage concerns with thermal CVD processing. Process-induced IC device damage from plasma processing (in particular at the gate-conductor level, because there is no device protection) is a critical issue for the PECVD passivation dielectrics. Briefly, low process pressure during deposition of the PECVD PSG was identified as the main factor causing gate-oxide charge damage. Increasing the pressure for the PECVD PSG process regardless of dopant source (trimethylphosphite or triethylphosphate) resulted in no charge damage on antenna test sites and device structures. A more recent study describes another technique used to optimize a PECVD PSG process for plasma damage designated as corona oxide semiconductor (COS) charge measurement [24]. The technique, combined with the antenna test structure method of measuring plasma damage, provides a fast and cost-effective way to optimize plasma CVD processes.

Doped silicon oxide films such as PSG or BPSG are preferred for gate-conductor passivation because of their mobile ion barrier properties [25], low reflow temperature for local planarization (applies to BPSG only), high etch selectivity to the underlying barrier layer (e.g., nitride [26]), and faster polishing rate compared to undoped silicon oxide. In this paper, we discuss our recent work with HDP CVD PSG including gap-fill and plasma damage results. We have previously published an overview of our own work and that of others in IBM on relevant thermal CVD processes and applications [27].

The gap-fill requirement for dielectrics in the "back-end-of-line" (BEOL) depends on the interconnect fabrication methods used. Multilevel interconnects usually involve two types of planarization methods: the planarization of interlayer dielectrics and the planarization of metal layers. For the former, for example, an Al(Cu)-based layer is patterned into lines and the insulator is deposited between the spaces and above the lines. Therefore, a critical requirement in this case is the filling of the gaps between the lines without void formation. Void-free filling of high-aspect-ratio features is not a simple matter and requires the use of advanced insulator deposition processes such as HDP CVD. For submicron metal interconnect fabrication, the insulator deposition is generally followed by partial planarization using spin-on-glass (SOG) [28], a resist etch-back [29], or a global planarization using, for example, chemical-mechanical polishing (CMP). For the planarization of metal layers, the damascene technique is most commonly used; several papers reporting its use in IBM have been published [30]. Using this technique, a dielectric such as silicon oxide is deposited on a planar surface and the wiring level is patterned into the dielectric using photolithography and RIE. A thin metal liner and a metal such as tungsten (or aluminum or copper) are then deposited on the patterned dielectric and subsequently planarized by CMP, stopping on the dielectric and leaving metal in the patterned features. Therefore, in the damascene technique, the metal rather than the insulator must fill the high-aspect-ratio features.

A critical film parameter for both interconnect fabrication techniques is the

 ALL RIGHTS RESERVED PRINTED IN IRAQ

dielectric constant (k) of the IMD material. Use of a material having a lower dielectric constant leads to lower total capacitance, decreasing the interconnection delay and power dissipation [31], and thus enhancing performance. To achieve long-range interconnection performance objectives, low-dielectric-constant IMD will be required [32]. The dielectric constant of PECVD silicon oxide is typically 4.1-4.2. By doping the oxide with fluorine, the dielectric constant can be reduced to 3.0-3.7, depending on the fluorine concentration [33]. Si-F replaces the Si-OH and Si-H bonds in the oxide; since fluorine is more electronegative, the polarization changes, lowering the dielectric constant. SOG dielectrics (siloxanes, silsesquioxanes) and organic polymers formed by spin coating (polyimides, fluorinated polyimides, bisbenzocyclobutenes), poly(arylethers), or vapor-phase deposition (parylene N, parylene F, teflon) provide dielectric constants in the range of 1.9-3.0 [34]. Most polymers with a dielectric constant less than 3 are stable to only about 350°C. However, a recent publication on laser-evaporated siloxane thin films reports a dielectric constant of 2.0 and thermal stability to 400°C, although integration results were not published [35]. Also, it has been reported that parylene exhibits a high thermal stability [36], and its successful integration into a metal RIE BEOL has been demonstrated [37]. However, damascene integration may be more difficult to achieve because of the softness of parylene films. Spun-on films of materials such as nanoporous silica and xerogels exhibit a higher thermal stability and low dielectric constants (1.3-2.5), depending on their porosity [38], but associated process integration is challenging. There has been increased development activity in plasma-assisted CVD of amorphous carbon and fluorinated carbon films because of their low dielectric constants (2.3-2.7) and thermal stability up to 400°C [39]. Relevant work on insulators having low dielectric constants has been described elsewhere [40].

In this paper, the plasma-assisted CVD of low-dielectric-constant insulators of potential interest at the ULSI level, including fluorine-doped silicon oxide and amorphous carbon and fluorocarbon, was discussed. To be suitable for the deposition of such insulators, plasma-assisted CVD should be applicable at relatively low substrate temperatures, should not damage underlying layers or devices that may be present on the substrate during deposition, and should produce insulators which, in addition to having low dielectric constants, satisfy etching, annealing, planarization, and stability requirements.

2. Fundamentals of PECVD

In thermal CVD, gas-phase reactive species are generated by heating of initial reactants. In plasma CVD, the plasma energy supplied by an external rf source takes the place of the heating to generate the species that subsequently react and deposit on substrate surfaces. Significantly, excessive heating and degradation on the substrate can be avoided by using plasma electron kinetic energy instead of thermal energy. Besides the aspect of generating reactive species at much lower processing temperatures compared to conventional CVD processing, the ion bombardment can be used to modify film characteristics. Plasma CVD processes can be classified into many sub-processes, such as plasma evaporation deposition, plasma sputtering deposition, plasma ion plating, and plasma nitriding. This classification depends on the conditions of the plasma generated, configuration of the vacuum system, location of the substrate, and type of power supply [19-21]. Plasma-assisted CVD processes for semiconductor processing are generally carried out at pressures of 1mTorr to 20Torr substrate temperatures in the range of 100 to 500°C, rf power densities <0.5 W-cm^{-2}, electron densities of 1.0 x 10^{8} to 1.0x10^{12}cm^{-3}, electron mean free paths of <0.1 cm, and average electron energies of 1eV to 6eV.

When the plasma initiates, energy from the rf electric field is coupled into the reactant gases via the kinetic energy of a few free electrons. These electrons gain energy rapidly through the electric field and lose energy slowly through elastic collisions. The high-energy electrons are capable of inelastic collisions that cause the reactant gas molecules to dissociate and ionize, producing secondary electrons by various electron-impact reactions. Table (1) lists typical electron-impact reactions of silane molecules in an rf plasma discharge. In a steady-state discharge, the electrons generated by electron-impact reactions equal those electrons that are lost to the electrode, walls, and reactive species by attachment and recombination reactions [1].

The two important aspects of a plasma glow discharge are the nonequilibrium low-temperature gas-phase chemical reactions that generate radical and ion reactive species in the plasma discharge, and the flux and energy of these reactive species as they reach and strike the surface of the film being deposited. The bombardment of the ionic species on the surface of the film, which controls the surface mobility of the precursor, is the predominant factor in determining film composition, density, stress, and step coverage or conformality at the relatively low temperatures used in plasma CVD. Reactant gases similar to those used for

© 2008 Iraqi Society for Alternative and Renewable Energy Sources and Techniques (I.S.A.R.E.S.T.)

thermal CVD processes are used for plasma CVD to deposit silicon-based dielectrics at lower deposition temperatures.

Table (1) Typical electron-impact reactions of silane molecules in an rf plasma discharge. The asterisk (*) refers to electronic excited state [1]

Reactant	Reaction products	Enthalpy of formation (eV)
$e^- + SiH_4 \rightarrow$	$SiH_2 + H_2 + e^-$	2.2
	$SiH_3 + H + e^-$	4.0
	$Si + 2H_2 + e^-$	4.2
	$SiH + H_2 + H + e^-$	5.7
	$SiH^* + H_2 + H + e^-$	8.9
	$Si^* + 2H_2 + e^-$	9.5
	$SiH_2 + 2H_2 + 2\ e^-$	11.9
	$SiH_3 + H + 2\ e^-$	12.3
	$Si + 2H_2 + 2\ e^-$	13.6
	$SiH + H_2 + H + e^-$	15.3

2.1 Reaction kinetics

Reactions during plasma deposition are complex and not completely understood. Elementary reactions that occur in plasma have been discussed by various authors [41-43]. The initial reaction between electrons and reactant gas molecules or between reactant gas molecules in plasma can be classified as elastic or inelastic. In the elastic collisions, only minimal translational energy transfer occurs between the gas molecules and reactant gases. For plasma processing, the elastic collisions play a less important role in reactant dissociation. Significantly more translational, rotational, vibrational, and electronically excitational energy transfer occurs in the inelastic collisions. The major inelastic reactions among electrons, reactant gases, and surface that occur during plasma-assisted CVD processing are typically represented in Tables (2-4).

Table (2) Initial electron-impact reactions [1]

Excitation (rotational, vibrational, and electronic)	$e^- + A_2 \rightarrow A_2 + e^-$
Dissociative attachment	$e^- + A_2 \rightarrow A^- + A+ + e^-$
Dissociation	$e^- + A_2 \rightarrow 2A \bullet + e^-$
Ionization	$e^- + A_2 \rightarrow A_2+ + 2e^-$
Dissociative ionization	$e^- + A_2 \rightarrow A+ + A + 2e^-$

Some of the inelastic collisions between inert gases and reactants (such as helium or argon with silane) significantly affect the chemical nature of the discharge and the properties of the deposited films [44-46]. In many plasma deposition processes, inert carrier and diluent gases such as helium and argon have been used to form "cooler" plasma, to create more controlled reaction pathways via Penning reactions between carrier and reactant gases [47], and to suppress gas-phase reactions between reactive species. As a result, a plasma diluted with inert gases such as helium can be used to deposit higher-quality insulators.

Table (3) Inelastic reactions among reactants, inert gases, and substrate. M refers to the inert gas or substrate, and A, B, and C refer to the reactant gases [1]

A	
Penning dissociation	$M^* + A_2 \rightarrow 2A \bullet + M$
Penning ionization	$M^* + A_2 \rightarrow A_2^+ + M + e^-$
Ion-ion recombination	$M^- + A_2^+ \rightarrow A_2 + M$
	or
	$M^- + A_2^+ \rightarrow 2A \bullet + M$
Electron-ion recombination	$e^- + A_2^+ \rightarrow 2A \bullet$
	$e^- + A_2^+ + M \rightarrow A_2 + M$
Charge transfer	$M^+ + A_2 \rightarrow A_2^+ + M$
	$M^- + A_2 \rightarrow A_2^- + M$
B	
Collisional detachment	$M^* + A_2^- \rightarrow A_2 + M + e^-$
Associative detachment	$A^- + A \rightarrow A_2 + e^-$
Atom recombination	$2A + M \rightarrow A_2 + M$
Atom abstraction	$A + BC \rightarrow AB + C$
Atom addition	$A + BC + M \rightarrow ABC + M$

Table (4) Heterogeneous reactions between plasma and surface. S refers to the surface in contact with the plasma, and A and B refer to the reactant gases [1]

Atom recombination	$S - A + A \rightarrow S + A_2$
Metastable de-excitation	$S + M^* \rightarrow S + M$
Atom abstraction	$S - B + A \rightarrow S + AB$
Sputtering	$S - B + M^+ \rightarrow S^+ + B + M$
Surface contact ionization	$S + B^* \rightarrow B^+ + e^- + S$

2.2 Deposition Mechanisms

One of the major advantages of plasma deposition processing is its flexibility for depositing films with desirable properties. For conventional thermal CVD processing, physical and chemical properties of the deposited film pertaining to its stress, conformality, density, moisture resistance, and gap-fill properties can be altered by changing the composition and/or type of reactive species. In plasma-assisted CVD, this can be accomplished by varying deposition parameters such as temperature, rf power, pressure, reactant gas mixture ratio, and type of reactant. For example, silicon oxide films deposited with TEOS generally show higher step coverage or conformality than those deposited

 ALL RIGHTS RESERVED PRINTED IN IRAQ

with silane in a plasma-assisted CVD process. For plasma-assisted CVD of silicon oxide films, properties can be modified not only by changing the type of reactive species, but also by the extent of ion bombardment.

In general, the deposition mechanisms for a plasma CVD process can be qualitatively divided into four major steps, as shown in Fig. (1). Step 1 includes the primary initial electron-impact reactions between electron and reactant gases to form ions and radical reactive species (Tables 1 and 2). Next, in step 2, transport of these reactive species occurs from the plasma to the substrate surface concurrently with the occurrence of many elastic and inelastic collisions in both the plasma and sheath regions, classified as ion and radical generation steps [48]. Step 3 is the absorption and/or reaction of reactive species (radical absorption and ion incorporation) onto the substrate surface. Finally, in step 4, the reactive species and/or reaction products incorporate into the deposited films or re-emit from surface back to the gas phase. Because of their complexity, the latter two steps are the least known and least studied aspects of plasma CVD. Significant roles are played by ion bombardment [49] and various heterogeneous reactions between ions and radicals with the depositing surface in the sheath region. The two steps critically affect film properties such as conformality [50], density, stress [51], and "impurity" incorporation.

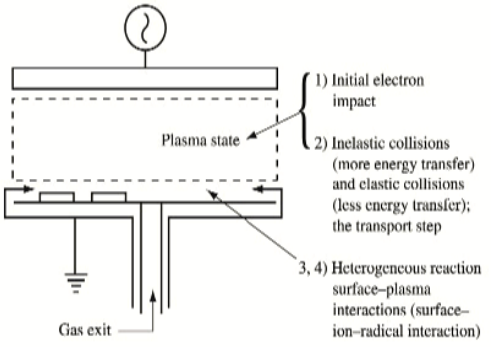

Fig. (1) Four steps that characterize the mechanisms of plasma CVD process [1]

Plasma CVD of amorphous and microcrystalline silicon are the most studied plasma CVD processes, with hundreds of publications on their deposition kinetics and mechanisms. The basic gas-phase chemistry of the silane plasma has been studied by various techniques [49-52]. Different mechanisms have been suggested for the dominant reaction pathway of silicon deposition. One mechanism describes SiH_3 (silyl) radicals playing a dominant role [53], while others describe the decomposition of silane to SiH_2 (silylene) and then SiH_2 insertion into gas-phase SiH_4 to form higher silane species [54] as the main silicon deposition mechanism.

4. Conclusions

We have reviewed the plasma-assisted CVD of dielectric films, with an emphasis on aspects relevant to ULSI semiconductor circuits. In addition, we have indicated that manufacturing needs must be considered early in the process and tool development phase. Obviously, the ultimate goal is to optimize a plasma CVD process for a particular application at the lowest cost of ownership. Future research and development must focus not only on specific technical issues that arise with each new IC generation (such as integration of a stable low-*k* IMD into the BEOL), but also on manufacturability and cost. With 300mm-diameter wafers containing sub-0.25µm semiconductor IC circuits on the horizon, the technical and manufacturing issues are daunting; new challenges are presented to both the semiconductor manufacturers and their equipment suppliers, even for the conventional processes used in IC production.

References

1. S.V. Nguyen, **"Plasma-Assisted Chemical Vapor Deposition",** *Handbook of Thin-Film Deposition Processes and Techniques,* K.K. Schuegraf, Ed., Noyes Publications, Park Ridge, NJ, 1988, pp. 112-141.
2. G.S. Anderson, *J. Appl. Phys.* 33, No. 10, 2991-2992 (1962).
3. L.L. Atl, S.W. Ing, Jr. and K.W. Laendle, *J. Electrochem. Soc.* 110, 465 (1963).
4. S.W. Ing, Jr. and W. Davern, *J. Electrochem. Soc.* 111, 120-122 (1964).
5. A.R. Reinbergh, *Ann. Rev. Mater. Sci.* 9, 341-372 (1979).
6. D.E. Carlson, C.W. Magee and A.R. Triano, *J. Electrochem. Soc.: Solid-State Sci. Technol.* 126, No. 4, 688-691 (1979).
7. S. Sherman et al., *J. Electrochem. Soc.* 144, No. 9, 3198-3204 (1997).
8. H. Randhawa, *Thin Solid Films* 196, 329-349 (1991).
9. J.A. Thornton, *Thin Solid Films* 107, 3-19 (1983).
10. A.T. Bell, *J. Vac. Sci. Technol.* 16, No. 2, 418-419 (1979).
11. R.F. Bunshah, *IEEE Trans. Plasma Sci.* 18, 846-854 (1990).
12. A. Sherman, *Thin Solid Films* 113, 135-149 (1984).
13. S.V. Nguyen, *J. Vac. Sci. Technol. B* 4, No. 5, 1159-1167 (1986).
14. C. Bencher et al., *Solid State Technol.* 40, No. 3, 109-114 (1997).

© 2008 Iraqi Society for Alternative and Renewable Energy Sources and Techniques (I.S.A.R.E.S.T.)

[1] O.A. Hamadi, R.A. Markub and A.A. K. Hadi, "Heat-annealed enhanced-diffusion of silver in gallium arsenide", J. Edu. Al-Mustansiriya Univ., 3 (2001) 35-44.
[2] U.A. Hamadi, M.A.K. Ahmed and R.A. Markub, "Cutting of Ceramic by CW CO_2 Laser", Al-Mustansiriya J. Sci., 12(6) (2001) 307-309.
[3] N.A.K. Al-Rubaiey, O.A. Hamadi and D.N. Raouf, "Effect of gas mixture on output characteristics of a CW CO_2 laser", Iraqi J. Laser, 1(1) (2003) 1-6.
[4] O.A. Hamadi, "Simple arrangement to achieve SHG using a 635nm semiconductor laser", Eng. J. Qatar Univ., 18 (2005) 149-156.
[5] O.A. Hamadi, K.Z. Yahiya and O.N.S. Jassim, "Properties of Silicon Carbide Thin Films Deposited by Vacuum Thermal Evaporation", J. of Semicond. Technol. and Sci., 5(3) (2005) 182-186.
[6] O.A. Hamadi, "Employment some parameters to enhance laser drilling of aluminium", J. Sci. Technol., Sultan Qaboos Univ., 10 (2005) 93-100.
[7] R.A. Ismail, O.A. Abdulrazaq, A.A. Hadi and O.A. Hamadi, "Characterization of Si p-n Photodetectors Produced by Laser-Induced Diffusion", Inter. J. Mod. Phys., 19(31) (2005) 4619-4628.
[8] O.A. Hamadi, "HAZ extent analysis in fiber-reinforced plastic grooving by laser", Iraqi J. Appl. Phys., 1(1) (2005) 1-7.
[9] O.A. Hamadi, "Induced variation of focal length of the lens stimulated in Nd:YAG laser crystal with optical power pumping", Iraqi J. Laser, 2 (2005).
[10] O.A. Hamadi and S.M. Hussain, "Analytical Modelling to Enhance Electric Field Measurement Using Optical Fiber Sensor", Eng. Technol. J., 26 (2006).
[11] O.A. Hamadi and K.S. Khashan, "Effect of Preheating on the Parameters of Laser Keyhole Welding Process: Analytical Study", Iraqi J. Laser, Part A, 5(5) (2006) 11-17.
[12] R.A. Ismail, O.A. Abdulrazaq, A.A. Hadi and O.A. Hamadi, "Full Characterization at 904nm of Si p-n Junction Photodetectors Produced by LID Technique", Euro. Phys. J.: Appl. Phys., 38 (2007) 197-201.
[13] K.S. Khashan and O.A. Hamadi, "Features of spot-matrix surface hardening of low-carbon steel using pulsed laser", J. Eng. Technol., 25(2) (2007).
[14] O.A. Hamadi and K.Z. Yahiya, "Optical and electrical properties of selenium-antimony heterojunction formed on silicon substrate", Sharjah Univ. J. Pure Appl. Sci., 4(2) (2007) 1-11.
[15] B.A. M. Badr, O.A. Hamadi and A.K. Yousif, "Measurement of thermooptic coefficient of semiconductors by single-beam scanning technique", Eng. Technol. J., 27(5) (2007).
[16] O.A. Hamadi, S.M. Hussain, A.A. Hadi and R.O. Mahdi, "Normalized Characteristics of Laser-Induced Diffusion of Arsenic Dopants in Silicon", Eng. Technol. J., 27(4) 2007.
[17] O.A. Hamadi and K.S. Khashan, "Modeling of the Preheating Effect on Keyhole Laser Welding Efficiency", Iraqi J. Appl. Phys. Lett., 1(1) (2008) 10-15.
[18] O.A. Hamadi, B.A.M. Bader and A.K. Yousif, "Electrical Characteristics of Silicon p-n Junction Solar Cells Produced by Plasma-Assisted Matrix Etching Technique", Eng. Technol. J., 28 (2008).
[19] A.A.K. Hadi and O.A. Hamadi, "Optoelectronic Characteristics of As-doped Si Photodetectors Produced by LID Technique", Iraqi J. Appl. Phys. Lett., 1(2) (2008) 23-26.
[20] O.A. Hamadi, "Effect of Annealing on the Electrical Characteristics of CdO-Si Heterostructure Produced by Plasma-Induced Bonding Technique ", Iraqi J. Appl. Phys., 4(3) (2008) 34-37.
[21] O.A. Hamadi, "The Fundamentals of Plasma-Assisted CVD Technique Employed in Thin Films Production", Iraqi J. Appl. Phys. Lett., 1(2) (2008) 3-8.
[22] A.K. Yousif and O.A. Hamadi, "Plasma-Induced Etching of Silicon Surfaces", Bulg. J. Phys., 35(3) (2008) 191-197.
[23] O.A. Hamadi, "Characteristics of CdO-Si Heterostructure Produced by Plasma-Induced Bonding Technique", Proc. IMechE, Part L, J. Mater.: Design and Applications, 222 (2008) 65-71, DOI: 10.1243/14644207JMDA56.
[24] O.A. Hamadi, D.N. Raouf and N.A.-K. Alrubaiey, "Effect of Self-Absorption on the Output Power of CW CO_2 Laser", Iraqi J. Appl. Phys. Lett., 2(1) (2009) 31-34.
[25] O.A. Hamadi, "Profiling of Antimony Diffusivity in Silicon Substrates using Laser-Induced Diffusion Technique", Iraqi J. Appl. Phys. Lett., 3(1) (2010) 23-26.
[26] O.A. Hamadi, N.J. Shakir and F.H. Hussain, "Magnetic Field and Temperature Dependent Measurements of Hall Coefficient in Thermal Evaporated Tin-Doped Cadmium Oxide Thin Films", Bulg. J. Phys., 37(4) (2010) 223-231.
[27] O.A. Hammadi and M.S Edan, "Temperature Dependencies of Refractive Index and Optical Elasticity Coefficient on Lens Induced in Nd:YAG Crystal", Iraqi J. Appl. Phys., 8(1) (2012) 35-41.
[28] O.A. Hammadi, M.K. Khalaf, F.J. Kadhim and B.T. Chiad, "Operation Characteristics of a Closed-Field Unbalanced Dual-Magnetrons Plasma Sputtering System", Bulg. J. Phys., 41(1) (2014) 24-33.

 © ALL RIGHTS RESERVED

[29] O.A. Hammadi and N.I. Naji, "Effect of Acidic Environment on the Spectral Properties of Hibiscus sabdariffa Organic Dye used in Dye-Sensitized Solar Cells", Iraqi J. Appl. Phys., 10(2) (2014) 27-31.
[30] M.K. Khalaf, F.J. Kadhim and O.A. Hammadi, "Effect of Adding Nitrogen to the Gas Mixture on Plasma Characteristics of a Closed-Field Unbalanced DC Magnetron Sputtering System", Iraqi J. Appl. Phys., 10(1) (2014) 27-31.
[31] O.A. Hammadi, "Photovoltaic Properties of Thermally-Grown Selenium-Doped Silicon Photodiodes for Infrared Detection Applications", Phot. Sen., 5(2) (2015) 152-158, DOI: 10.1007/s13320-015-0241-4.
[32] O.A. Hammadi, M.K. Khalaf and F.J. Kadhim, "Fabrication of UV Photodetector from Nickel Oxide Nanoparticles Deposited on Silicon Substrate by Closed-Field Unbalanced Dual Magnetron Sputtering Techniques", Opt. Quant. Electron., 47(12) (2015) 3805-3813, DOI: 10.1007/s11082-015-0247-6
[33] O.A. Hammadi, "Characterization of SiC/Si Heterojunction Fabricated by Plasma-Induced Growth of Nanostructured Silicon Carbide Layer on Silicon Surface", Iraqi J. Appl. Phys., 12(2) (2016) 9-13.
[34] O.A. Hammadi, W.N. Raja, M.A. Saleh and W.A. Altun, "Magnetic Field Distribution of Closed-Field Unbalanced Dual Magnetrons Employed in Plasma Sputtering Systems", Iraqi J. Appl. Phys., 12(3) (2016) 35-42.
[35] O.A. Hammadi, W.N. Raja, M.A. Saleh and W.A. Altun, "Employment of Magnetron to Enhance Langmuir Probe Characteristics of Argon Glow Discharge Plasma in Sputtering System", Iraqi J. Appl. Phys., 12(4) (2016) 19-28.
[36] O.A. Hammadi, M.K. Khalaf and F.J. Kadhim, "Fabrication and Characterization of UV Photodetectors Based on Silicon Nitride Nanostructures Prepared by Magnetron Sputtering", Proc. IMechE, Part N, J. Nanomater. Nanoeng. Nanosys., 230(1) (2016) 32-36, DOI: 10.1177/1740349915610600
[37] O.A. Hammadi and N.E. Naji, "Electrical and spectral characterization of CdS/Si heterojunction prepared by plasma-induced bonding", Opt. Quant. Electron., 48(8) (2016) 375-381, DOI: 10.1007/s11082-016-0647-2
[38] O.A. Hammadi, "Characteristics of Heat-Annealed Silicon Homojunction Infrared Photodetector Fabricated by Plasma-Assisted Technique", Phot. Sen., 6(4) (2016) 345-350, DOI: 10.1007/s13320-016-0338-4
[39] O.A. Hammadi, M.K. Khalaf and F.J. Kadhim, "Silicon Nitride Nanostructures Prepared by Reactive Sputtering Using Closed-Field Unbalanced Dual Magnetrons", Proc. IMechE, Part L, J. Mater.: Design and Applications, 231(5) (2017) 479-487, DOI: 10.1177/1464420715601151
[40] O.A. Hammadi and N.E. Naji, "Fabrication and Characterization of Polycrystalline Nickel Cobaltite Nanostructures Prepared by Plasma Sputtering as Gas Sensor", Phot. Sen., 8(1) (2018) 43-47, DOI: 10.1007/s13320-017-0460-y
[41] O.A. Hammadi, "Production of Nanopowders from Physical Vapor Deposited Films on Nonmetallic Substrates by Conjunctional Freezing-Assisted Ultrasonic Extraction Method", Proc. IMechE, Part N, J. Nanomater. Nanoeng. Nanosys., 232(4) (2018) 135-140, DOI: 10.1177/2397791418807347
[42] O.A. Hammadi, "Nanostructured CdSnSe Thin Films Prepared by DC Plasma Sputtering of Thermally Casted Targets", Iraqi J. Appl. Phys., 14(4) (2018) 33-36.
[43] O.A. Hammadi, "Fabrication of High-Quality Microchannels for Biomedical Applications Using Third-Harmonic Radiation of Nd:YAG Laser", J. Laser Sci. Eng., 10(2) (2018) 61-64.
[44] F.J. Al-Maliki, O.A. Hammadi and E.A. Al-Oubidy, "Optimization of Rutile/Anatase Ratio in Titanium Dioxide Nanostructures prepared by DC Magnetron Sputtering Technique", Iraqi J. Sci., 60 (2019) 91-98.
[45] O.A. Hammadi, "Conjunctional Freezing-Assisted Ultrasonic Extraction of Silicon Dioxide Nanopowders from Thin Films Prepared by Physical Vapor Deposition Technique", Iraqi J. Appl. Phys., 15(4) (2019) 23-28.
[46] O.A. Hammadi, "Synthesis and Characterization of Polycrystalline Carbon Nitride Nanoparticles by Fast Glow Discharge-Induced Reaction of Methane and Ammonia", Adv. in Sci. Eng. Med., 11(5) (2019) 346-350, DOI: https://doi.org/10.1166/asem.2019.2365
[47] O.A. Hammadi, F.J. Kadhim and E.A. Al-Oubidy, "Photocatalytic Activity of Nitrogen-Doped Titanium Dioxide Nanostructures Synthesized by DC Reactive Magnetron Sputtering Technique", Nonlinear Optics, Quantum Optics, 51(1-2) (2019) 67-78.

IRAQI JOURNAL OF APPLIED PHYSICS
Vol. 16, No. 2, April-June 2020, pp. 37-42

Characterization of Highly-Pure Silicon Dioxide Nanoparticles as Scattering Centers for Random Gain Media

Hayder G. Fahad
Oday A. Hammadi

Department of Physics, College of Education, Al-Iraqia University, Baghdad, IRAQ

In this work, silicon dioxide thin films were prepared and deposited on glass substrates by dc reactive magnetron sputtering technique. The film material was extracted from the substrates as powder by conjunctional freezing-assisted ultrasonic extraction method. The structural characterization of the extracted powder confirmed the formation of nanostructures as the particle size was ranging in 19-34 nm. They also confirmed the high purity of these nanostructures as no other compound than silicon dioxide was observed in the final samples. The extracted nanopowder was employed as scattering centers in Rhodamine B dye solution and the spectral measurements showed that the relative enhancement in fluorescence of the dye solution containing silicon dioxide nanoparticles exceeds 25%, which highly encourages considering these results to prepare random gain media. These results can effectively be used to design and fabricate random gain media with low production cost, high spectral quality and good reliability for wavelength narrowing and tuning.

***Keywords*:** Random gain media; Random laser; Nanoparticles; Rhodamine B dye
Received: 7 May 2020; **Revised:** 29 May 2020; **Accepted:** 5 June 2020

1. Introduction

Random lasers have received much attention as a new development of laser physics and technology [1,2]. The random laser is essentially built on insulating and semiconducting media [3]. It is also characterized by its small size, simplicity, low cost and applicability [4,5]. It was observed in a variety of organic and inorganic gain media including powders of solid-state luminescent and laser crystals [6,7], and liquid laser dyes with scatterers [8].

Random gain media are strongly scattering media that amplify laser signal with some striking similarities to the conventional lasers based on a gain medium inside an optical resonator to provide optical feedback [9]. Examples for such similarities are the threshold for lasing action and the frequency narrowing mechanism. However, random laser is characterized by being an "open resonator", i.e., it does not need an external optical cavity [10]. Evidently, the optical properties of random lasers are different from these of the conventional lasers as the propagation of pump and fluorescence light is diffusive in random laser [11]. In contrast with the cavity systems, scattering is actually advantageous as the required feedback is provided by multiple scattering using the so-called "scatterers" or "the tiny cavities" [12,13]. Consequently, the threshold in random laser is lowered by a stronger scattering [14].

High density of scatterers, interference between the scattered waves occurs when there is high density of scatterers [15]. Since the transferring waves are exactly on the same distance, they maintain the same essential phase relationship even through the path is formed by a large number of scattering events [16]. If the scattered waves are in phase with each other, constructive interference occurs and thus forming closed paths for the light in the scattering media [17]. These closed paths provide the coherent feedback mechanism [18]. Upon the excitation of the random amplification media, the gain grows enormously and exceeds the loss. The intensity increases extremely fast yielding a strong pulse in all directions [19]. Due to the high intensity of the random lasing, the population inversion is emptied so quickly resulting in a short sharp peak (short pulse in the florescence emission) [20]. With the continuation of the exciting pumping beam, the population inversion is successfully built and emptied leading to a series of spikes within the emission. Such random laser has high and narrow gain emitted light and the photons at the highest peak of the emission will be amplified much more than its long paths inside the medium [21]. Therefore the feed mechanism responsible for random laser action is a “feed-forward mechanism” as compared to the “feed-back mechanism” in the ordinary laser [22,23]. The scatterers within the laser medium contribute in trapping light photons due to multiple scattering. So, the light path inside these media will be long (long time interval) and this is one reason for the decrease of the threshold intensity [24,25].

Rhodamine B (RB) dye is a common, typical material as active medium for dye laser. It belongs to the xanthene group and emits laser in the visible range. The lasing emission of RB dye is also dependent on the type of solvent used to form the dye solution [26]. For example, the central lasing wavelength is increased by about 43 nm when

 © ALL RIGHTS RESERVED

replacing ethanol by ethylene glycol. In general, the maximum lasing emission is ranging within 579-637 nm [27,28].

In this work, silicon dioxide nanoparticles were prepared by dc reactive magnetron sputtering technique and their structural characteristics were investigated for random gain media and their applications.

2. Experimental Part

A p-type silicon wafer of 10 cm in diameter and 300 µm in thickness was used as the target to be sputtered and maintained carefully on the cathode. It was cleaned by HF acid, ethanol and distilled water, dried and then used for preparation process. Highly pure argon and oxygen gases were used as discharge and reactive gases, respectively. This process used to prepare silicon dioxide nanoparticles.

The operation conditions of the sputtering system include total gas pressure, inter-electrode distance, gas mixing ratio and gas flow rate. Varying discharge voltage was almost possible during the operation. In addition, turning the cooling system off would raise the temperature of electrodes to 40-45 °C with circulating water, while stopping the circulation of water would raise electrode temperature more (up to 150 °C). Therefore, the temperatures of discharge electrodes could be controlled during operation. More details on the optimization of operation conditions of this system can be found elsewhere [29-35].

The optimum conditions to prepare silicon dioxide nanostructures were inter-electrode distance of 4 cm, Ar:O_2 gas mixing ratio of 50:50, total gas pressure of 0.08 mbar, discharge voltage of 2.5 kV, discharge current of 35 mA, anode temperature of 27 °C (room temperature) and cathode temperature of about 40 °C.

The thin film samples prepared in this work were transferred to the conjunctional freezing-assisted ultrasonic extraction chamber to extract film material as nanopowders [36,37]. This was carried out at ultrasonic frequency of 32.0 MHz for six hours. These nanopowders were characterized in order to determine their structural characteristics. The measurements and characterization tests include Fourier-transform infrared spectroscopy (FTIR), x-ray diffraction (XRD), scanning electron microscopy (SEM) and energy dispersive x-ray (EDX) spectroscopy.

The Rhodamine B (RB) laser dye solution was prepared by dissolving the required amount of the dye in the solvents (water and ethanol). This amount of the dye (W) was weighed using a precise digital balance of 10^{-3}g sensitivity and can be calculated using the following equation [38]:

$$W = \frac{MW.V.C}{1000} \quad (1)$$

Where M_W is the molecular weight of the dye (g/mol), V is the volume of the solvent (ml) and C is the molar concentration (mol/liter)

The spectroscopic characteristics (absorption spectra) of the dye solution were measured by a UV-visible spectrophotometer (K-MAC Spectra Academy SV-2100) in the range 200-900 nm with an optical resolution of about 0.2 nm, while the fluorescence was measured by a fluorescence spectrophotometer (F96 instrument from Shanghai LengGuang Tech.) in the emission wavelength range of 250-900 nm with a xenon CW lamp as an excitation source.

3. Results and Discussion

In order to confirm the formation of silicon dioxide molecules in the prepared samples, the FTIR spectrum of the powder sample extracted from the deposited thin films was recorded as shown in Fig. (1). The bonds around 458.05, 794.44 and 1072.87 cm^{-1} are ascribed to the vibrational modes of SiO_2 molecule, which is based on the O-Si-O bonding configuration [39]. This configuration has three different modes of vibration; bending, symmetric and asymmetric stretching. As no peaks belonging to other bonds were observed on this spectrum, this confirms the high structural purity of the prepared samples, which highlights the advantage of dc reactive sputtering technique with good control of operation conditions.

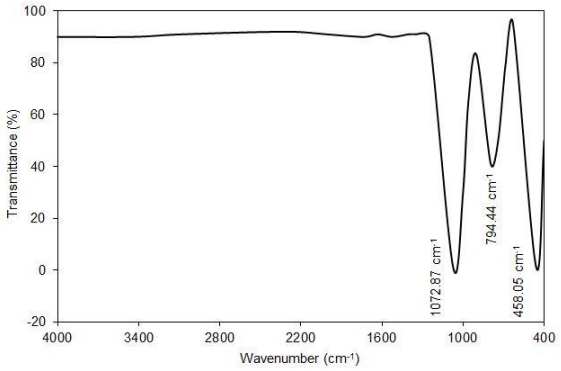

Fig. (1) The FTIR spectrum of the SiO_2 nanoparticles prepared in this work

Figure (2) shows the XRD pattern of the SiO_2 samples prepared in this work. It is clearly observed that the prepared samples are amorphous, which is an initial evidence for the formation of nanostructures. Therefore, calculations of the structural parameters were not performed as no specific peak could be individually analyzed. However, this pattern is completely identical to that of silica glass to prove that no other material was formed in the final sample.

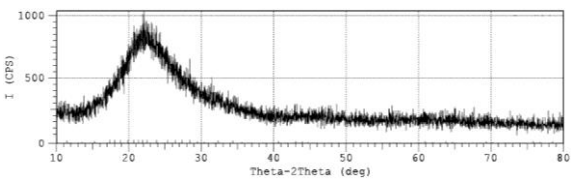

Fig. (2) The XRD pattern of SiO_2 nanoparticles prepared in this work

 ISSN 1813 – 2065 © ALL RIGHTS RESERVED

Figure (3) shows the SEM image for SiO_2 nanoparticles prepared in this work. The minimum particle size was 19.16 nm. As an advantage of sputtering technique in nanostructure fabrication, the aggregation over the prepared nanoparticles is relatively low. As well, the difference in particle size is not high too make the size distribution critical for certain applications requiring high uniformity of particle size, such as multiple scattering media.

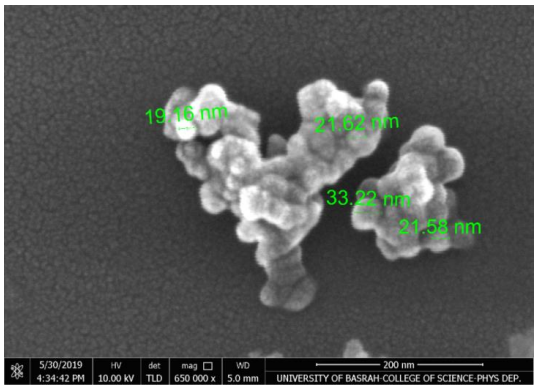

Fig. (3) The SEM image of SiO_2 nanoparticles prepared in this work

In order to detect and quantify the elemental composition of the prepared nanoparticles, the EDX spectroscopy was performed using the same SEM instrument. It is clear from Fig. (4) that the prepared nanoparticles are fundamentally made from silicon dioxide as the spectrum of the final sample contains peaks belonging silicon and oxygen only. This result supports the structural purity of the synthesized nanoparticles as a requirement for spectroscopic consideration of random gain medium. The weight percentage contents of silicon and oxygen are 31.03 and 58.84 wt. %, respectively, which confirms the stoichiometry of the chemical reaction leading to form silicon dioxide (SiO_2) molecules.

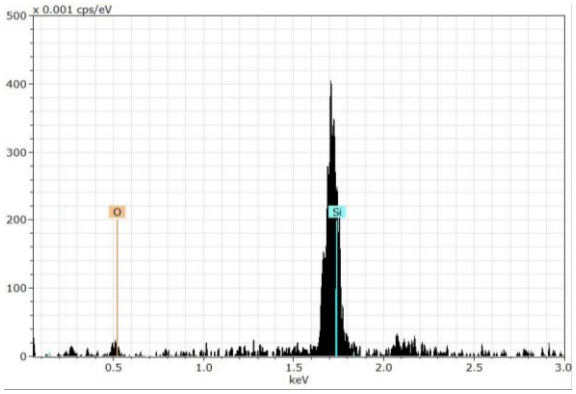

Fig. (4) The EDS results of SiO_2 nanoparticles prepared in this work

The absorption spectra of the Rhodamine B dye with different concentrations dissolved in water, were recorded in the spectral range 200-900 nm, as shown in Fig. (5). In general, the dye solution has low absorbance at wavelength range below 475 nm. Obviously, with increasing the concentration of the dye in the solution, the absorbance regularly increases too within the wavelength range of 475-590 nm with a maximum at 555 nm. For dye concentration of 10^{-5} M, the absorbance at 555 nm is about 800% higher than that for dye concentration of 10^{-6} M. At wavelength region longer than 590 nm, the absorbance decreases to the minimum regardless the concentration of dye. As the highest absorbance was obtained for the dye concentration of 10^{-5} M, the spectroscopic measurements to introduce the effect of adding SiO_2 nanoparticles to the dye solution samples were carried out using this concentration only.

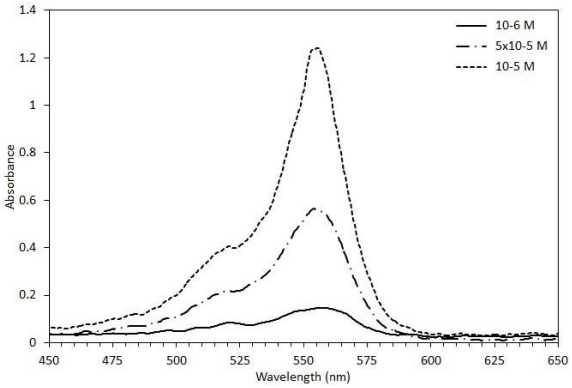

Fig. (5) Absorption spectra of Rhodamine B dye dissolved in water recorded at different concentrations

Figure (6) shows the absorption spectra of 10^{-5} M Rhodamine B dye solution with different amounts of SiO_2 nanoparticles (2, 4 and 6 mg). The highest absorbance was measured when 6 mg of SiO_2 nanoparticles added to the dye solution. This is attributed to the decrease in scattering mean free path, and hence traverse mean free path, of SiO_2 nanoparticles in the dye solution. Also, the absorption spectra were noticeably narrowed with consequent increase in the intensity, which is attributed to the contribution of SiO_2 nanoparticles to trap the emitted photon and hence to increase the photon flux (amplification) within narrow spectral range 540-565 nm. A shift towards longer wavelengths (~4 nm) was observed as the amount of SiO_2 nanoparticles was increased from 2 to 6 mg in the dye solution. Accordingly, the peak of absorption spectrum was shifted from 555 to 559 nm. Theoretically, increasing the amount of nanoparticles would lead to increase the absorbance; however, the effect of saturation makes a limitation on the amount of nanoparticles that can be added to the dye solution.

 © ALL RIGHTS RESERVED

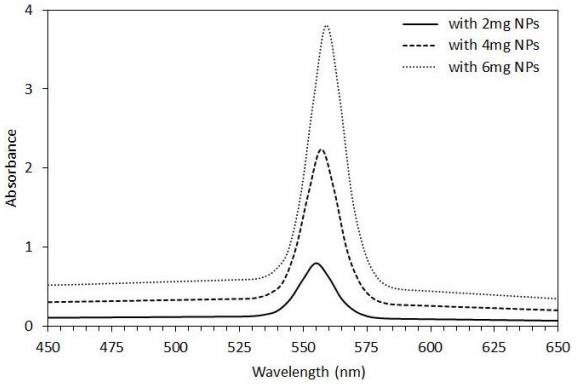

Fig. (6) Absorption spectra of Rhodamine B dye dissolved in water with different amounts of SiO_2 nanoparticles

The assessment of nanoparticles in dye solution can be determined by measuring the fluorescence spectra as the contributions of nanoparticles is observed by further increase in fluorescence intensity when compared to the fluorescence of laser dye. Figure (7) shows that the fluorescence intensity increases with increasing the amount of SiO_2 nanoparticles added to the laser dye solution. The fluorescence peak is centered at 578 nm, which is 18 nm away from the absorption peak. As the amount of nanoparticles reaches 6 mg, the fluorescence intensity is increased by more than 25% than that of laser dye nanoparticles. Inset figure apparently shows the variation of fluorescence intensity with amount of SiO_2 nanoparticles in the dye solution.

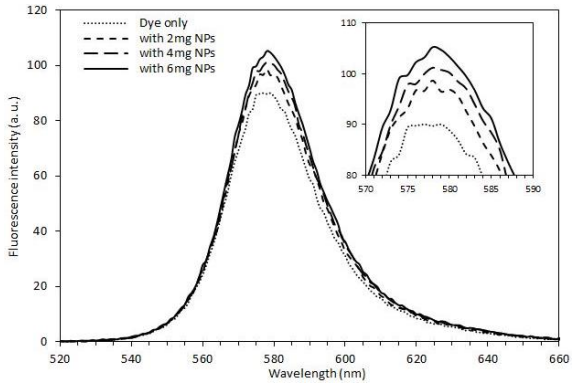

Fig. (7) Absorption spectra of Rhodamine B dye dissolved in water with different amounts of SiO_2 nanoparticles

Figure (8) shows both absorbance and fluorescence spectra of the laser dye solution containing 6 mg SiO_2 nanoparticles in the spectral range of 470-670 nm. The absorption peak was centered at 555-559 nm while the fluorescence peak was centered at 578 nm with a shift of 23-18 nm. This shift is slightly larger (~6 nm) than that measured for the RB dye only, which may be attributed to the existence of SiO_2 nanoparticles in the dye solution. This enhancement can be clearly observed in Fig. (9), which shows the relative enhancement in fluorescence intensity due to adding SiO_2 nanoparticles.

Light can be typically amplified in a random gain medium and this amplification effect is proportional to the scattering mean free path of such medium as [40]:

$$l_s = 1/n_s \sigma_s \quad (2)$$

where n_s is the number of scatterers and σ_s is the scattering cross-section of the individual scatterer

Due to anisotropy in scattering, the scattering mean free path is not sufficient to describe this effect. Therefore, the average distance that the light photons travel before their direction of propagation is randomized is alternatively considered. This distance is known as transport mean free path l_t and given by the following relation [41]:

$$l_t = l_s / (1-g) \quad (3)$$

where $g = \langle \cos\theta \rangle$ is the average cosine of scattering angle θ (so-called the anisotropy parameter). For isotropic scattering (e.g., Rayleigh scattering from particle of size $<< \lambda$), $g = 0$ or $l_t = l_s$, hence [41]:

$$l_t = 0.7\lambda/2\pi W \quad (4)$$

where λ is the excitation wavelength and W is the spectral scattering width of the ray reflected from the sample

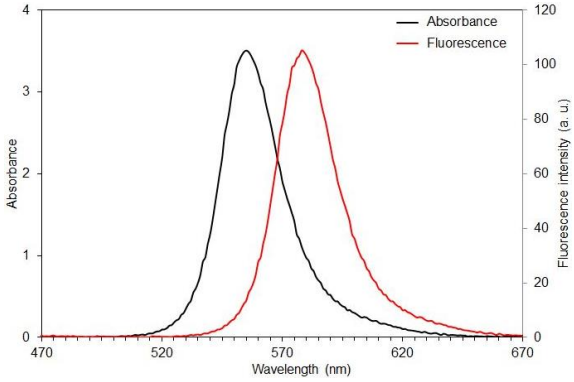

Fig. (8) Absorbance and fluorescence spectra of RB laser dye solution containing 6mg SiO_2 nanoparticles

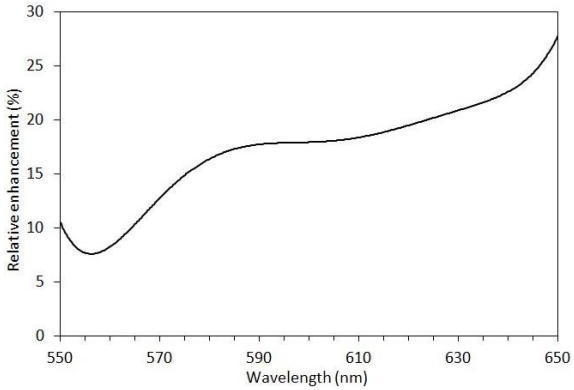

Fig. (9) Relative enhancement in fluorescence due to adding SiO_2 NPs (6 mg) to RB dye solution (10^{-5} M)

As shown in table (1), the traverse mean free path (l_t) decreases with increasing the amount of SiO_2 nanoparticles in the dye solution. This means that the emitted photons traverse very short distances before changing their directions towards other scatterers,

 ISSN 1813 – 2065 © ALL RIGHTS RESERVED

which give massive rise to the amplification of the emitted light.

Table (1) Effect of SiO_2 NPs amount on scattering parameters

Amount of SiO_2 (mg)	Excitation Wavelength, λ (nm)	Traverse Mean Free Path, l_t (nm)	Spectral Scattering Width, W (mrad)
2	555	2.0995398	58.87653751
4	555	1.0497699	117.753075
6	555	0.6998466	176.6296125

Nanostructures, in general, are described with very high surface roughness and hence very large number of single particles. Therefore, the value of scattering mean free path (l_s) is minimized according to Eq. (2) [42]. The transport mean free path (l_t) is accordingly minimized and the light is amplified within very small distance as traversing through random gain medium. The amplification effect is subsequently maximized [43]. An increase of fluorescence intensity of Rhodamine B dye was observed after adding SiO_2 nanoparticles to the dye solution.

4. Conclusion

In concluding remarks, highly-pure silicon dioxide nanoparticles were prepared by closed-field unbalanced dc magnetron sputtering technique to be employed as scattering centers in Rhodamine B dye solution water with 10^{-5} M concentration to act as a random gain medium. The highest increase in fluorescence intensity was reasonably measured as an amount of 6 mg of the SiO_2 nanoparticles were added to the dye solution. These results can effectively be used to design and fabricate random gain media with low production cost, high spectral quality and good reliability for wavelength narrowing and tuning.

References

[1] G. Zacharakis, N.A. Papadogiannis and T.G. Papazoglou, "Random Lasing Following Tow-Photon Excitation of Highly Scattering Gain Media", Appl. Phys. Lett., 81 (2002) 2511-2513.
[2] B.K. Nasser and M.A. Hameed, "Structural Characteristics of Silicon Nitride Nanostructures Synthesized by DC Reactive Magnetron Sputtering", Iraqi J. Appl. Phys., 15(4) (2019) 33-36.
[3] D. Anglos, A. Stassinopoulos, R.N. Das, G. Acharakis, M. Psyllaki, R. Jakubiakk, R.A. Vaia, E.P. Giannelis and S.H. Anastasiadis, "Random Laser Action in Organic-Inorganic Nanocomposites", J. Opt. Soc. Amer. B, 21 (2004) 208-213.
[4] D.S. Wiersma, "The physics and applications of random lasers", Nature Phys., 4 (2008) 359-365.
[5] A.M. Brito-Silva et al., "Random Laser Action in Dye Solutions Containing Stöber Silica Nanoparticles," Appl. Phys., 108 (2010) 033508.
[6] R. Frank and A. Lubatsch, "Scalar Wave Propagation in Random, Amplifying Media: Influence of Localization Effects on Length and Time Scales and Threshold Behavior",
[7] J.X. Zhu, D.J. Pine and D.A. Weitz, "Internal reflection of diffusive light in random media", Phys. Rev. A, 44(6) (1991) 3948-3959.
[8] P.E. Wolf and G. Maret, "Weak localization and coherent backscattering of photons in disordered media", Phys. Rev. Lett., 55 (1985) 2696-2699.
[9] D.S. Wiersma, M.P. van Albada and A. Lagendijk, "Random Laser", Nature, 373 (1995) 203.
[10] H. Ramachandran, "Mirrorless lasers", Pramana J. Phys., 58(2) (2002) 313.
[11] C.W.J. Beenakker, "Photon Statistics of a Random laser", in **Diffuse Waves in Complex Media**, ed. J.-P. Fouque, Kluwer academic Pub. (Netherlands) (1999) 137-164.
[12] C.F. Bohren and D.R. Huffman, **"Absorption and scattering of light by small particles"**, John-Wiley & Sons (NY) (1983) 130-132.
[13] A. Lagendijk, A. Bart van Tiggelen, "Resonant multiple scattering of light", Phys. Rep., 270 (1996) 143-215.
[14] A. Ishimaru, **"Wave propagation and scattering in random media"**, Academic Press (NY) (1978) 175-183.
[15] M. Wittmann and A. Penzkofer, "Concentration-dependent absorption and emission behaviour of sulforhodamine B in ethylene glycol", Chem. Phys., 172 (1993) 339-348.
[16] Y. Kuga and A. Ishimaru, "Retroreflectance from a dense distribution of spherical particles", J. Opt. Soc. A, 1 (1984) 831-836.
[17] M.B. van der Mark, M.P. van Albada and A. Lagendijk, "light scattering in strongly scattering media: multiple scattering and weak localization", Phys. Rev. B, 37 (1988) 3575-3592.
[18] R.M. Balachandran and N.M. Lawandy, "Theory of laser action in scattering gain media", Opt. Lett., 22 (1999) 319.
[19] R.M. Balachandran, N.M. Lawandy and J.A. Moon, "Theory of laser action in scattering gain media", Opt. Lett., 22(5) (1997) 319.
[20] W. Falkenstein and A. Apenzkofer, "Theoretical Investigation of Amplified Spontaneous Emission with Picosecond Light Pulses in Dye Solution", Opt. Quant. Electron., 10 (1978) 399.
[21] J. Andreasen et al., "Modes of random lasers", Adv. in Opt. Phot., 3 (2011) 88-127.
[22] P. Sebbah and C. Vanneste, "Random laser in the localized regime", Phys. Rev. B, 66 (2002) 144-202.
[23] S. John and G. Pang, "Theory of Lasing in a Multiple Scattering Medium", Phys. Rev. A, 54(4) (1996) 3642.
[24] G. Zacharakis et al., "Investigation of the laser like behavior of polymeric scattering gain media under sub picosecond laser excitation", Appl. Opt., 38(28) (1999) 6087.
[25] N.M. Lawandy et al., "Laser action in strongly scattering media", Nature, 368 (1994) 436.

 © ALL RIGHTS RESERVED

[26] G.J. Mohr, "Fibre-Optic and Nanoparticle-Based Fluorescence Sensing Using Indicator Dyes: Pitfalls, Self- Referencing, Application, and Future Trends", in: Resch-Genger U. (eds) Standardization and Quality Assurance in Fluorescence Measurements I. Springer Series on Fluorescence, vol. 5. Springer, Berlin, Heidelberg (2008) 347-372.
[27] Rhodamine B, data sheet, LambdaPhysik, Lambdachrome®, Laser Dyes, 2000, p. 173.
[28] Rhodamine 610, data sheet, Exciton, www.exciton.com
[29] O.A. Hammadi et al., "Operation Characteristics of a Closed-Field Unbalanced Dual-Magnetrons Plasma Sputtering System", Bulg. J. Phys., 41(1) (2014) 24-33.
[30] M.A Hameed and Z.M. Jabbar, "Optimization of Preparation Conditions to Control Structural Characteristics of Silicon Dioxide Nanostructures Prepared by Magnetron Plasma Sputtering", Silicon, 10 (2018) 1411-1418. DOI: 10.1007/s12633-017-9618-x
[31] M.A. Hameed and Z.M. Jabbar, "Preparation and Characterization of Silicon Dioxide Nanostructures by DC Reactive Closed-Field Unbalanced Magnetron Sputtering", Iraqi J. Appl. Phys., 12(4) (2016) 13-18.
[32] E.A. Al-Oubidy and F.J. Al-Maliki, "Effect of Gas Mixing Ratio on Energy Band Gap of Mixed-Phase Titanium Dioxide Nanostructures Prepared by Reactive Magnetron Sputtering Technique", Iraqi J. Appl. Phys., 14(4) (2018) 19-23
[33] F.J. Al-Maliki and E.A. Al-Oubidy, "Effect of gas mixing ratio on structural characteristics of titanium dioxide nanostructures synthesized by DC reactive magnetron sputtering", Physica B: Cond. Matter, 555 (2019) 18–20.
[34] O.A. Hammadi, F.J. Al-Maliki and E.A. Al-Oubidy, "Synthesis and Modification of Photocatalytic activity of TiO2 Nanostructures by Doping with Nitrogen using DC reactive magnetron sputtering", Nonlinear Optics, Quantum Optics, 51 (1-2) (2019) 67-78
[35] F.J. Al-Maliki, O.A. Hammadi and E.A. Al-Oubidy, "Optimization of Rutile/Anatase Ratio in Titanium Dioxide Nanostructures prepared by DC Magnetron Sputtering Technique", Iraqi J. Sci., Special Issue on 4th Conf. for Low Dimensional Materials and Applications (2019) 91-98.
[36] O.A. Hammadi, "Production of Nanopowders from Physical Vapor Deposited Films on Nonmetallic Substrates by Conjunctional Freezing-Assisted Ultrasonic Extraction Method", Proc. IMechE, Part N, J. Nanomater. Nanoeng. Nanosys., 232(4) (2018) 135-140.
[37] O.A. Hammadi, "Effects of Extraction Parameters on Particle Size of Titanium Dioxide Nanopowders Prepared by Physical Vapor Deposition Technique", Plasmonics, 15 (2020) doi: 10.1007/s11468-020-01205-8
[38] G. Wypych, **"Handbook of Solvents"**, Ch. 2: Fundamental Principles Governing Solvents Use, ChemTec Pub. (NY) (2001) p. 43.
[39] V.P. Tolstoy, I.V. Chernyshova and V.A. Skryshevsky, **"Handbook of Infrared Spectroscopy of Ultrathin Films"**, John Wiley & Sons, Inc. (NJ) (2003) p. 420
[40] A.K. Pradhan and S.N. Nahar, **"Atomic Astrophysics and Spectroscopy"**, Cambridge University Press (UK) (2011) 213-214.
[41] A. Corney, **"Atomic and Laser Spectroscopy"**, Oxford University Press (NY) (1977) 241, 244.
[42] E.A. Al-Oubidy and F.J. Al-Maliki, "Photocatalytic activity of anatase titanium dioxide nanostructures prepared by reactive magnetron sputtering technique", Opt. Quantum Electron., 51(1) (2019) 23.
[43] F.J. Al-Maliki et al., "Photocatalytic activity of Ag-doped TiO_2 nanostructures synthesized by DC reactive magnetron co-sputtering technique", Opt. Quantum Electron., 52 (2020) 188.

 ISSN 1813 – 2065 © ALL RIGHTS RESERVED

THE IRAQI JOURNAL OF APPLIED PHYSICS
EDITORIAL BOARD

COPYRIGHT RELEASE FORM
IRAQI JOURNAL OF APPLIED PHYSICS (IJAP)

We, the undersigned, the author/authors of the article titled

……
……
……
……
……
……
……

that is submitted to the Iraqi Journal of Applied Physics (IJAP) for publication, declare that we have neither taken part or full text from any published work by others, nor presented or published it elsewhere in any other journal. We also declare transferring copyrights and conduct of this article to the Iraqi Journal of Applied Physics (IJAP) after accepting it for publication.

The authors will keep the following rights:

1. Possession of the article such as patent rights.
2. Free of charge use of the article or part of it in any future work by the authors such as books and lecture notes after informing IJAP editorial board.
3. Republishing the article for any personal purposes of the authors after taking journal permission.

To be signed by all authors:

Signature:……..date: ……
Printed name: ……

Signature:……..date: ……
Printed name: ……

Signature:……..date: ……
Printed name: ……

Correspondence
address:……...
……
Address:……
……
Telephone:……..……..email: ……

Note: Complete and sign this form and mail it to the below address with your finally revised manuscript

The Iraqi Journal of Applied Physics
www.iraqiphysicsjournal.com
Email: info@iraqiphysicsjournal.com
Email: editor_ijap@yahoo.co.uk
Email: irq_appl_phys@yahoo.com

IRAQI JOURNAL OF APPLIED PHYSICS

Volume (16), Issue (2), April-June 2020

CONTENTS